Regulation of the mRNA silencing activity of Bicaudal-C

THÈSE Nᴼ 6606 (2015)

PRÉSENTÉE LE 8 MAI 2015
À LA FACULTÉ DES SCIENCES DE LA VIE
UNITÉ DU PROF. CONSTAM
PROGRAMME DOCTORAL EN APPROCHES MOLÉCULAIRES DU VIVANT

ÉCOLE POLYTECHNIQUE FÉDÉRALE DE LAUSANNE

POUR L'OBTENTION DU GRADE DE DOCTEUR ÈS SCIENCES

PAR

Florian Urs BERNET

acceptée sur proposition du jury:

Prof. P. Gönczy, président du jury
Prof. D. Constam, directeur de thèse
Prof. O. Bonny, rapporteur
Prof. J. Hülsken, rapporteur
Prof. W. Kühn, rapporteur

EPFL

ÉCOLE POLYTECHNIQUE
FÉDÉRALE DE LAUSANNE

Suisse
2015

Summary

Cilia dysfunction is a common factor underlying left-right axis malformation and the pathogenesis of virtually all known renal cystic diseases. Mutations in the RNA-binding protein Bicaudal-C (Bicc1) provoke cystic kidneys reminiscent of polycystic kidney disease (PKD), and ectopic Wnt/β-catenin signaling during left-right axis development. Renal cysts in these mice have been linked to defective miRNA-mediated silencing of specific mRNAs, including adenylate cyclase 6 (AC6) and protein kinase A inhibitor (PKIα), but little is known about how Bicc1 activities are regulated. Prompted by the overlapping phenotypes of mice lacking Bicc1 or Inversin (Invs), the protein defective in patients with nephronophthisis type II, we investigated a potential epistatic relationship. We found that Invs acts as an inhibitor of Bicc1 induced silencing and that Invs is required for Bicc1 localization to the 'Invs compartment' in the proximal cilium. Molecular analysis demonstrated that Invs interacts with the Bicc1 KH domains required for mRNA binding. The Bicc1/Invs complex prevented the recruitment of target mRNA and their incorporation into miRNA-induced silencing complexes (miRISC). To test whether Bicc1 activity is regulated *in vivo*, we monitored Bicc1 targets in *inv/inv* mutant mouse kidneys lacking Invs. While AC6, the RNA helicase Ddx5 (a novel Bicc1 target) and PKA signaling were dramatically downregulated in *inv/inv* mutant kidneys, these effects were suppressed in *Bicc1$^{-/-}$; inv/inv* double mutants, demonstrating that loss of Invs leads to ectopic activation of Bicc1.

In autosomal dominant polycystic kidney disease (ADPKD), fluid-filled cysts develop in both kidneys due to defective calcium-permeable mechanosensory complexes of polycystin-1 and -2 encoded by *PKD1* and *PKD2*. Studies in zebrafish suggest that Pkd2/Ca^{2+} signaling stimulates calmodulin kinase 2 (CaMK2). To further elucidate a role for Ca^{2+} in Bicc1 regulation, we mutated specific residues that are predicted to be phosphorylated by CaMK2. We found that CaMK2 phosphorylated Bicc1 on T724 and S805 and enabled miRISC assembly, at least in part by stimulating Bicc1 binding to nascent miRNAs. In addition, elevated Ca^{2+} concentrations prevented *in vitro* binding of Bicc1 to Invs. Based on these data we suggest a dual role for Ca^{2+} in regulating Bicc1. Elevated intracellular Ca^{2+} levels may induce the dissociation of a Bicc1/Invs complex and activate CaMK2 to enable Bicc1 mediated silencing of target mRNAs.

Keywords: Bicaudal-C, Inversin, CaMK2, Primary cilium, KH-domain, Calcium, AC6, Ddx5, polycystic kidney disease

Zusammenfassung

Ziliendysfunktion spielt eine entscheidende Rolle in randomisierter Organlateralität und in der Pathogenese praktisch aller zystischer Nierenerkrankungen. Mutationen im RNA-bindenden Protein Bicaudal-C (Bicc1) verursachen polyzystische Nieren (PKD) und aktivieren ein ektopisches Wnt/β-catenin Signal während der Entstehung der Rechts-Links-Asymmetrie. Die Nierenzysten dieser Mäuse sind zum Teil auf einen Defekt in der Hemmung der Translation von Adenlyte Zyklase 6 (AC6) und Protein Kinase Inhibitor α (PKIα) durch spezifische miRNAs zurückzuführen. Jedoch ist bisher nicht bekannt wie Bicc1 reguliert wird. Aufgrund eines weitgehend übereinstimmenden Phänotyps zwischen $Bicc1^{-/-}$ und *inv/inv* Mäusen untersuchten wir eine potenzielle epistatische Wechselwirkung. Unsere Studie identifiziert Invs als Bicc1 Inhibitor, welcher die Lokalisierung von Bicc1 im proximalen Teil des Ziliums dem sogannten `Invs Kompartiment` reguliert. Molekularbiologische Analysen zeigten zudem, dass Invs mit den RNA bindenden KH-Domänen von Bicc1 interagiert und dadurch deren Bindung an Ziel-RNA und Inkorperation in miRNA-Induced-Silencing-Complex (miRISC) blockiert. Um die Funktion von Bicc1 *in vivo* zu charakterisieren, untersuchten wir die Translation von Ziel-RNAs in *inv/inv* Mausnieren. Die Expression von AC6 und Ddx5 war stark vermindert, was zu einer Herunterregulation der PKA Signal-Kaskade führte.

Bei der autosomal-dominanten polyzystischen Nierenkrankheit (ADPKD) treten Zysten in allen Segmenten des Nephrons auf. Der Krankheitsverlauf kann sich über mehrere Jahrzehnte erstrecken was zu einer massiven Vergrösserung der Niere und schlussendlich zum völligen Verlust der filtrativen Nierenfunktion führt. Molekular Ursache sind Mutationen im *PKD1* oder *PKD2* Gen, welche zu einem weitgehenden Funktionsverlust der codierten Proteine Polycystin-1 und 2 (PC1 und PC2) führen. Diese Mutationen resultieren in einer Dysfunktion des Kalzium-permeablen, mechano-sensorischen PC1/PC2 Komplex. Wie der Flusssensor und die Kalziumantwort die Zystenbildung verhindert ist bislang nicht ausreichend ergründet. Im Zebrafisch-Pronephron wird vermutet, dass der Einstrom von Kalzium die Calmodulin-Kinase 2 (CaMK2) stimuliert. Um eine CaMK2 induzierte Phosphorylierung von Bicc1 zu untersuchen wurden prognostizierte Ziel- Aminosäuren antiphosphomimetisch substituiert. CaMK2 phosphorylierte die Aminosäuren T724 and S805 und ermöglicht dadurch die Bindung von Bicc1 mit spezifischen miRNAs und die Assoziation mit dem miRISC Komplex. Hingegen wurde die Bindung zwischen Bicc1 und Invs durch hohe Kalzium Konzentrationen verhindert.

Die Ergebnisse dieser Arbeit suggerieren, dass Kalzium eine duale Rolle in der Regulation von Bicc1 einnehmen kann. Einerseits hemmt es die Interaktion von Bicc1 mit Invs, andererseit führt eine erhöhte Kalziumkonzentration zur aktiven Form von CaMK2 und zur anschliessenden Phosphorylierung und Aktivierung von Bicc1.

Schlüsselwörter: Bicaudal-C, Inversin, CaMK2, Primärzilium, KH-Domäne, Kalzium, AC6, Ddx5, Polyzystische Niere

Acknowledgements

Table of contents

1. Abbreviations

A	Alanine
Ac tub	α –acetylated tubulin
ADPKD	Autosomal dominant polycystic kidney disease
Anks6	ankyrin repeat and SAM domain-containing protein
ARPKD	Autosomal recessive polycystic kidney disease
BBS	Bardlet-Biedl Syndrome
Bicc1	Bicaudal-C
CaMK2	Calmodulin kinase 2
CFTR	Cystic fibrosis transmembrane conductance regulator
CREB	cAMP-response element –binding protein
CREMs	CRE modulator proteins
DBA	Dolichous Biflorus Agglutinin
Dvl	Dishevelled
EMT	Epithelial-mesenchymal transition
ESRD	End stage renal disease
Hh	Hedgehog
IFT	Intraflagellar transport
Invs	Inversin
KH	K homology
LTL	Lotus Tetragonolobus lectin
MDCK	Madine-Darby canine kidney cells
MEF	Mouse embryonic fibroblasts
MET	Mesenchymal-epithelial transition
mIMCD	Murine inner medullary collecting duct
MM	Metanephric mesenchyme
NMDAR	N-methyl-D-aspartate receptor
NPHP	Nephrocystin
PC	Polycystin
PCP	planar cell polarity
PKD	Polycystic kidney disease
REF	Response to mechanical stimuli
RyR	Ryanodine receptor
S	Serine
SAM	Sterile alpha motive
T	Threonine
THP	Tamm-Horsfall protein
UB	Ureteric bud
VPV2R	Vasopressin V2 receptor
WT	Wild type

2. Introduction

2.1 The kidney

The kidney is a highly structured and complex organ that is involved in various processes, including waste elimination. Water and vital nutrients are reabsorbed into the circulation system, and redundant and harmful substances are filtered and excreted via the urine. As early as 1832, it was described by Bowman on purely morphological observations that only water and salts are excreted in the glomeruli, and that the other components of the urine are secreted by the renal tubules. A few years later, Ludwig introduced a physical and mechanical theory that the blood was filtered in the glomerular capillaries simply by hydrostatic pressure and that this filtrate was subsequently concentrated in the tubules by the diffusion of water and various solutes. However at this point the tubules where thought to have only a passive function and that their activity could be simply explained by the relative osmotic pressure and protein content of the tubular urine and peritubular blood. These observations were the start of an extensive study of the kidney function and anatomy (Smith 1951). Today the kidneys main functions still include filtering waste products like metabolites and xenobiotics from the circulation system and maintaining electrolyte and pH balance of body fluid by secretion and reabsorption. Furthermore they are involved in bone mineralization, produce the hormone erythropoietin to stimulate the production of erythrocytes, and also arterial blood pressure is partly regulated by the endopeptidase renin which is synthesized in the kidney (Sands and Verlander 2004).

2.1.1 The kidney physiology and anatomy

The two kidneys have a bean shaped appearance and are localized in the retroperitoneal space of the abdomen. An adult kidney is approximately 10 cm long, 5 cm wide and weights around 120-200 g. Anatomically, it can be divided into three segments, on the apical side the cortex, the middle segment medulla, and the innermost part is called renal pelvis (Fig. 1A). The renal pelvis gives rise to the ureter, which exits the kidney at the hilum. The functional unit of the kidney is the nephron, which is composed of the glomeruli and the connecting renal tubule. Each human kidney composes of approximately one million nephrons, which are assembled in early postnatal life (Bertram et al. 2011). The nephron serves
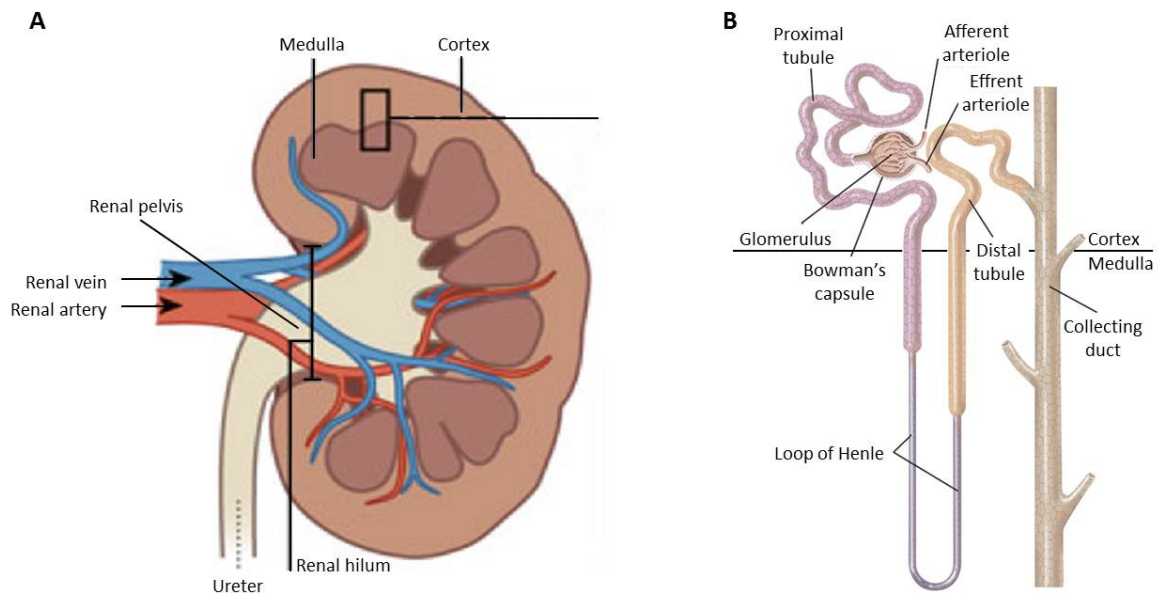
Figure 1. Kidney structure (A) *Sectional anatomy of the kidney (adapted from Lammert and Zeeb 2014)* **(B)** *Scheme of a nephron, the functional unit of the kidney. The glomeruli and the renal tubule perform filtration of the blood, reabsorpition, and secretion (adapted from O'Brien and McMahon 2014).*

as the blood filtering mechanism of the human body. The glomeruli located in the renal cortex are perfused by around 4'000 – 5'000 liters of blood per day. As blood pumps through the capillaries the pressure pushes water and small solutes through a three-layered filter. Blood cells and essential plasma proteins are retained based on their size (< 70 kDa) and charge resulting in a virtually protein free ultrafiltrate that eventually becomes urine (Lammert and Zeeb 2014). Solutes such as salts, carbohydrates, and amino acids are allowed to pass into the nephron where the filtrate subsequently enters the renal tubule for further modifications. The average glomerular filtration rate is around 150 liters of primary urine per day. The renal tubule itself consist of three major segments: the proximal tubule, the loop of Henle, and the distal tubule, each can be divided even further by molecular and morphological criteria into subdomains. After the collection of the ultrafiltrate in the Bowman's capsule primary urine is transported via the proximal tubule followed by the loop of Henle into the medulla, where it makes a hairpin turn and returns back to the cortex before arriving at the distal tubules (Fig. 1B). From there the remaining filtrate enters the collecting duct which transports the urine through the entire medulla to release it into the ureter. Along the nephron most of the water is reabsorbed and the terminal urine is concentrated to approximately two liters a day.

All segments of the nephron have a specialized role in the physiological action of the kidney to ensure that essential components are returned to the blood; that water, salt, and pH homeostasis are

maintained, and that waste products are excreted (Liu et al. 2005). The main segment for the reabsorption of water, sodium, and bicarbonate is the proximal tubule. Water is both transported para-cellularly via leaky cell-cell contacts as well as trans-cellularly via aquaporin 1. Under normal physiological conditions 100% of the filtered glucose and amino acids are reabsorbed in the proximal tubules. In addition, the proximal tubules secrete endogenous and exogenous metabolites such as, antibiotics and organic bases. The descending loop of Henle concentrates the urine further by reabsorbing water. The ascending loop of Henle is water impermeable but actively transports the ions sodium, potassium, and chloride through the cell layer. The regulation of salt and water excretion occurs in the principal cells of the collection duct. Water is passively reabsorbed via aquaporin 2 after stimulation with vasopressin. In addition, the acid-base metabolism is regulated by the collecting duct, whereas intercalated cells type A secrete H^+ ions into the urine and type B cells actively secrete bicarbonate. These processes are individually regulated and are essential for acid-base homeostasis. For example in acidic conditions, the secretion of protons into the urine will be increased to adjust acid-base imbalances.

2.1.2 Major steps in kidney organogenesis

Kidney organogenesis has been extensively studied in several animal models, including amphibians, fish and mice for different reasons. The processes required for renal development have common roles in other tissues, like branching morphogenesis, stem cell maintenance and differentiation, cell migration, oriented cell division, as well as interactions between cells and the extracellular matrix (reviewed in Carroll and Das 2013; O'Brien and McMahon 2014). On the other hand several processes are unique to the kidney and not found in other organs for instance mesenchymal-epithelial transition (MET) and the differentiation of highly specialized structures such as the glomerulus.

The urogenital system of mammals is derived entirely from the intermediate mesoderm of the developing embryo and progresses through three major stages in a cranial to caudal sequence (Fig. 2A). The first two stages, the pronephric and mesonephric kidney, are primitive tubular structures that are transient and only minimally functional. However, the pronephric tubules form functioning kidneys in fish and in amphibian larvae. The adult kidney, the metanephros, arises by inductive interaction between an epithelial component, the nephric duct (also called Wolffian duct), and the surrounding metanephric mesenchyme (MM). The MM serves a dual role; it harbors the progenitor cells for the nephrons and secretes signaling molecules including Gdnf and Fgf10. These signals bind to receptors on the caudal end of the nephric duct inducing the outgrowth of structure called ureteric bud (UB). The UB undergoes
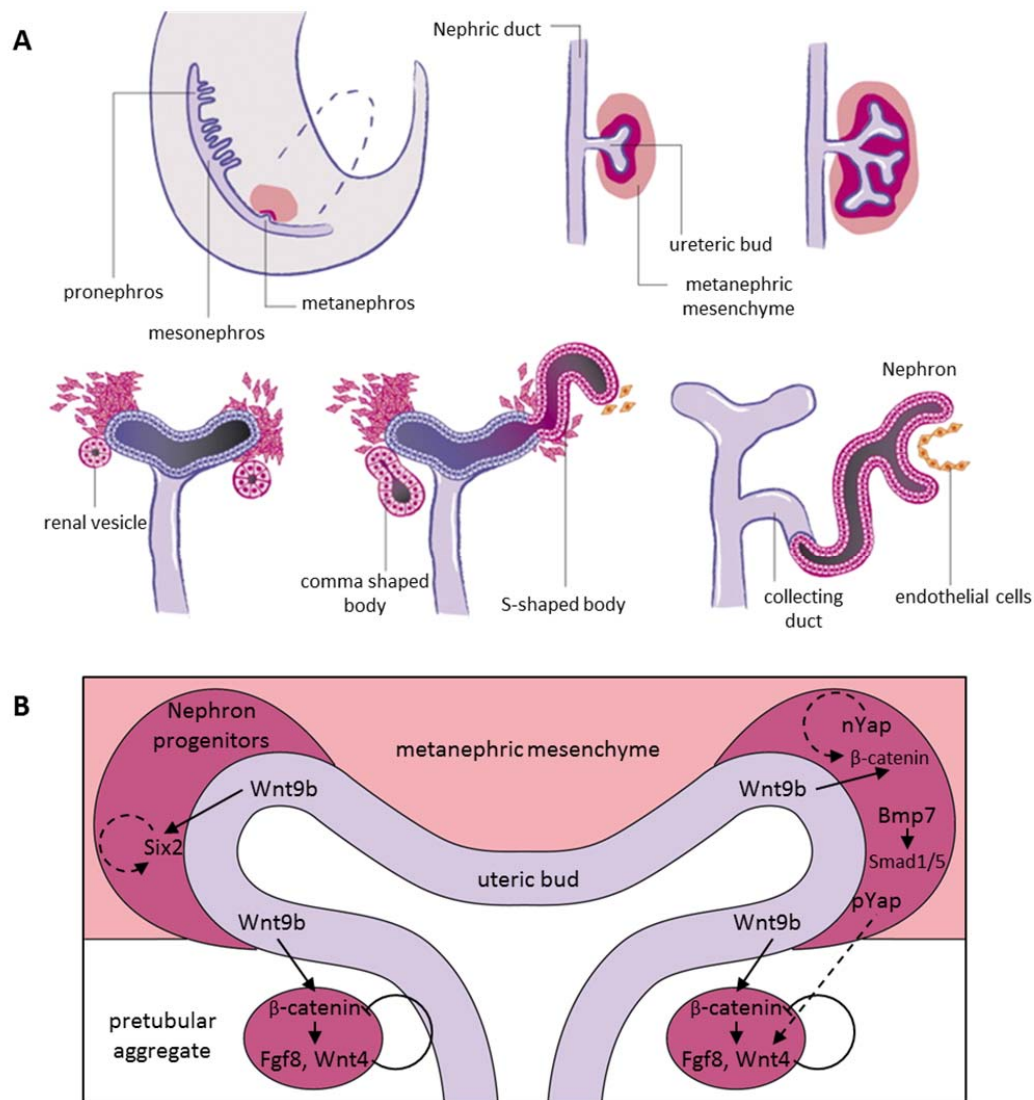
Figure 2. Major steps in kindey morphogenesis (A) *The metanephros becomes the permanent kidney and is formed by branching of the ureteric bud from the nephric duct into the metanephric mesenchyme in a process of reciprocal interactions. The ureteric branches give rise to the collecting duct system and induce MET of the sourrounding mesenchyme, creating renal vesicles and then comma and S-shaped structures and finally nephrons that fuse with the collecting duct (adopted from Uhlenhaut and Treier 2008).* ***(B)*** *Interaction of the ureteric tip with the surrounding mesenchyme. Canonical and noncanonical Wnt signaling play important roles in MET and subsequent formation of the renal vesicle.*

repeated branching within the MM and eventually generates the network of collecting duct system and the ureter. Although the mesenchyme is crucial for UB growth and branching, nephronogenesis reciprocally is induced by signals secreted from the ureteric epithelium. These signals initiate the continuous induction of nephrons at the ureteric tips which eventually undergo several morphological transformations. For the series of events the activation and inhibition of different signaling cascades are

required, in which the Wnt proteins play a prominent role. Nephronogenesis starts with the condensation and cap formation of the mesenchyme around the ureteric bud tip (Fig. 2B). Wnt9b is released from the ureteric tip to induce renal vesicle formation by stabilizing β-catenin in the nephric progenitors (Carroll et al. 2005). The accumulation of cytoplasmic β-catenin activates a molecular cascade involving Fgf8, Lhx1, and a second Wnt member, Wnt4 (Perantoni et al. 2005; Park et al. 2007). Activated Wnt4 in the pretubular aggregates directs MET and completes the transition to the epithelial renal vesicle (Stark et al. 1994; Kispert et al. 1998). However, high levels of β-catenin inhibit MET and consequently progression of the nephrogenic program. Termination of Wnt/β-catenin signaling is likely to be crucial for completion of MET and Wnt4 response is probably modulated to switch from canonical to non-canonical Wnt signaling (Tanigawa et al. 2011). Subsequently the renal vesicle derivatives undergo several morphological changes during the proximal distal patterning. Polarized expression of several Notch pathway components are thought to drive the patterning through the different morphological stages from the renal vesicle, the comma shaped body to the S-shaped body (Cheng et al. 2007). Also a Wnt4 and Lef1 gradient have been observed in the renal vesicle suggesting that Wnt signaling may contribute to early renal vesicle polarity (Mugford et al. 2009).

Only a small fraction of cells in the MM commit to active nephronogenesis at each round of ureteric branching, this raises the question how canonical Wnt signaling is restricted to the pool of cells undergoing MET (reviewed in O'Brien and McMahon 2014). Six2 expressed in the MM inhibits Wnt9b nephron induction by binding to Fgf8 and Wnt4 enhancers and thereby blocking the activation of these genes (Park et al. 2007). However Six2 alone is not able to inhibit progenitor differentiation, since isolated mesenchyme undergoes apoptosis within 48 hours. A positive role for Wnt9b in maintaining the progenitors by direct transcriptional regulation of progenitor target genes has been suggested (Karner et al. 2011). Recent studies also reveal a role for the Hippo pathway by modulating β-catenin activity and for Bmp7 in maintaining the nephron progenitor population (Reginensi et al. 2013; Tomita et al. 2013).

2.2. The cilium

Cilia are evolutionarily conserved organelles that are protruding the cell surface of virtually all cell types in the human body (Ishikawa and Marshall 2011). History of the cilium commences with the observation of Leeuwenhoek that tiny cellular projections propelled single cells and with this he described the first cellular organelles (described in Wallingford and Mitchell 2011). The first evidence of vertebrate cilia came from Steinbruch in the early 19th century who reported fluid flow across the surface of tadpoles. In

the late 19th century Zimmerman discovered the primary cilium, which he suggested to have a sensory role (Zimmermann 1898). Those findings were largely ignored until the introduction of transmission electron microscopy in the 1950s which allowed the identification of the ultrastructure of the primary cilium (Bernhard and De Harven 1956). Later, Barnes introduced the structural concept of motile cilia in the first study of a particular cell type and cilium (Barnes 1961). Today cilia are typically distinguished into primary or non-motile and motile cilia, which differ in their microtubule organization (See 2.2.1 ciliary structure and assembly). The primary cilium has been considered as vestigial and quiescent structure with unknown functions. It was just two decades ago, and around 100 years after the initial description by Zimmermann that primary cilia were established as a sensory organelle. The discovery that the oak ridge polycystic kidney (ORPK) mouse, a model for autosomal recessive polycystic kidney disease, harbors mutation in the ciliary gene *ift88* revealed the cilium as a clinically relevant organelle (Schrick et al. 1995; Pazour et al. 2000).

Subsequent data introduced the primary cilium on renal epithelial cells as mechanosensors, which respond to fluid by initiating an intracellular calcium signal (Praetorius and Spring 2003). A link between kidney cyst formation and ciliary dysfunction was further provided in various genetic mouse models as well as in genetic screening of patients with cystic kidney disorders. Many of the corresponding proteins identified localize to the cilium or the basal body. This led to the ciliary hypothesis of polycystic kidney disease in which mechanosensory cilia are crucial for the etiology cyst formation (Berbari et al. 2009). Apart from its mechanosensory role, primary cilia have important functions in sensing external and environmental cues as in photoreception and olfaction.

Motile cilia, on the contrary, have been examined extensively. They are generally present in large numbers at the apical surfaces of an epithelial cell for examples at ependymal cells lining the brain ventricle or the epithelia of the trachea (Ishikawa and Marshall 2011) (Fig. 3). These cilia beat in an orchestrated wave-like manner important for cerebrospinal fluid movement in the brain, and to clear mucus from the lung, respectively. Genetic defects of motile cilia structure causes primary ciliary dyskinesia also known as the Kartagener's syndrome. The disease is characterized by impaired mucociliary clearance and recurrent respiratory infections, male infertility due to abnormal sperm motility and organ laterality defects in approximately 50% of the cases (Popatia et al. 2014; Kurkowiak et al. 2015).

To date, the cilia proteome contains more than 1'000 different proteins. In mammals, single loss of many of these proteins prevents normal ciliary function leading to cystic and non-cystic pathology in the kidney, brain, pancreas, and liver as well as developmental patterning defects. These disorders may be

summarized as ciliopathies (Yuan and Sun 2013). Thus the cilium is a highly complex organelle orchestrated by numerous proteins, which plays a pivotal role in normal tissue homeostasis.

2.2.1 Ciliary structure and assembly

The core structure or axoneme of the cilium is constructed from nine parallel doublet microtubules, which are arranged in a circular fashion on the periphery of the cilium (Fig. 3). It is surrounded by a ciliary membrane that is continuous with the plasma membrane but functionally it is separated by a diffusion barrier (Rohatgi and Snell 2010). The axoneme emerges from the basal body that serves as a microtubule organizing center just underneath the cell membrane. The latter is attached to the cell membrane via transitional fiber proteins. Together they are thought to regulate protein entry and exit to the ciliary compartment (Pazour and Bloodgood 2008). Historically cilia have been classified into two categories, the primary and motile cilia. The two types differ in their axonemal microtubule organization (Ishikawa and Marshall 2011; Hoey et al. 2012). Motile cilia consist of the nine fold microtubule doublet symmetry, which surround an additional pair of microtubules in the center of the axoneme (referred to as '9+2' axoneme). This central pair is connected to radial spokes and dynein arm with the outer doublets to drive their bending motion (Porter and Sale 2000). The primary cilia lack the central pair of microtubules and have a '9+0' arrangement making them immotile with a purely sensory character. Recently a third category of cilia has been described, the nodal cilia which is localized in the ventral node of a gastrulating embryo. Nodal cilia, as primary cilia, are unique to each cell and display '9+0' axoneme structure, but they possess dynein arms which enables them to move in a propeller like fashion (Nonaka et al. 1998). Thus generating a leftward flow across the node required for the specification of the left-right body axis in mammals (Nonaka 2009). The ciliary '9+0' structure in the left-right organizing center is not evolutionarily conserved in mammals. Electron microscopy of motile cilia in the Kupffer's vesicle of zebrafish revealed a '9+2' axoneme (Kramer-Zucker et al. 2005). The Henson's node in rabbits displays cilia with three different ultra-structures; '9+0', '9+2' and a novel '9+4' axoneme, which are arranged in a salt and pepper like fashion (Feistel and Blum 2006).

Ciliogenesis is regulated by the cell cycle and is typically induced during the G1 growth phase. The mother centriole migrates to the apical cell surface and acquires accessory structures and appendages (basal feet) to form the basal body (Fisch and Dupuis-Williams 2011; Kim and Dynlacht 2013). Multi-ciliated cells only assemble cilia upon terminal differentiation; multiple basal bodies are rapidly generated using the pre-existing centriole as template (Fisch and Dupuis-Williams 2011). The basal body associates with membrane vesicles which will subsequently fuse with the plasma membrane to give rise
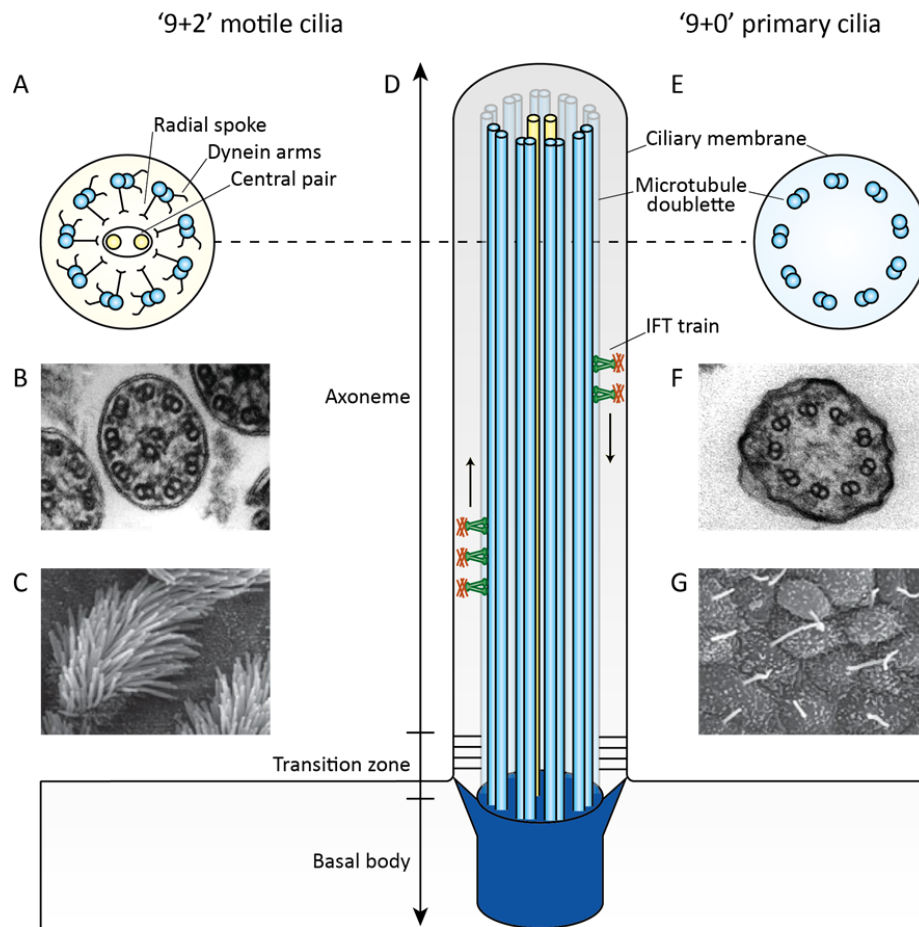
***Figure 3. Structural overview of motile (left side) and primary (right side) cilia with reference to the axonemal architecture. (A,E)** Cross-section diagram of motile cilium with a typical '9+2' configuration and components responsible for motility (A) and a non-motile primary cilium lacking the central microtubule pair (E, '9+0' configuration). **(B,C)** Transverse transmission electron microscopy of an axoneme (B) and scanning electron micoscopy micrograph (C) from a conventional motile cilia of mouse tracheal epithelium. **(D)** Schematic diagram of a motile cilium togthther with IFT complexes. **(F,G)** Transverse transmission electron microscopy (F) and scanning electron micoscopy micrograph (G) of a mouse nodal cilia. Images in B & F are are courtesy of (Takeda and Narita 2012) and images C & G are courtesy of (Ishikawa and Marshall 2011).*

and establish the ciliary membrane compartment. Once the basal body has docked to the plasma membrane the ciliary axoneme assembles and protrudes into the extracellular space. Initial growth is believed to involve the transition zone; however elongation is restricted to the distal tip of the cilium. Since cilia are already compartmentalized from the cytoplasm at the time of ciliogenesis and also lack their own translational machinery, material utilized for construction has to be transported from the cell body. The selective import and transport of proteins destined for the cilium are performed by the intraflagellar transport (IFT) machinery (Kozminski et al. 1993; Pedersen and Rosenbaum 2008). The

mechanism was first described in the green algae *Chlamydomonas*, which still remains the best-studied model of IFT-mediated ciliogenesis. IFT is a highly conserved process essential not only for assembly but also for maintenance of almost all cilia and flagella. The transport of large protein complexes (IFT particles) from the cytoplasm to the ciliary tip follows the axonemal microtubules in a bidirectional manner. Anterograde trafficking (from the base to the tip) is catalyzed by the kinesin II motor complex, Kif3A. At the cap IFT particles are remodeled, cargo such as the sonic hedgehog component Gli or new tubulin are unloaded and ciliary turnover products are taken up. The return to the base or the retrograde movement of the IFT trains is mediated by dynein 2, a different motor protein.

2.2.2 The primary cilium as signaling platform

The cilium acts as a cellular antenna for a variety of cell signaling events that profoundly condition cell growth, morphology, adhesion, and provides a specialized site for additional signaling receptors. The signaling cascades that are coordinated by the primary cilium include sonic hedgehog (Hh), Notch, Wnt/planar cell polarity (PCP), and Calcium signaling (Tran et al. 2014a). Wnt/PCP and calcium signaling are explained in section 2.3 and 2.4 in detail. Proper signaling is normally tightly coupled to correct translocation of receptors and downstream signaling molecules in and out of the cilium. Defects in many of the signal transduction pathways may be associated with ciliopathies. Among the main signaling pathways the relationship between Hh signaling and the primary cilium is best understood and one of its striking features is its reliance on the primary cilium for signaling transduction (Goetz and Anderson 2010). Hh signaling is evolutionarily conserved but genetic screens in *Drosophila* had not revealed a connection to IFT proteins. It came as a surprise when a correlation between the function of IFT particles and sonic Hh was established in vertebrates (Huangfu et al. 2003). The Hh pathway has a crucial role in development and normal tissue homeostasis as well as in cell fate determination, cell proliferation, and differentiation (Ingham et al. 2011). Briefly, in the absence of the Hh ligand, the receptor Patched resides in the cilium and inhibits the accumulation of the signal transducer Smoothend. As a result, Gli3 is proteolytically processed into its transcriptional repressor form. Upon Hh binding, Patched translocates to the cytoplasm thereby relieving its inhibition on Smoothend. Activated Smoothend accumulates in the ciliary membrane and promotes the movement of the Gli2/3 transcription factors to the ciliary tip. Accumulation of Gli2/3 proteins at the tip associates with their activation and expression of Hh target genes (reviewed in Nozawa et al. 2013). Increased Hh signaling has also been associated with renal cystogenesis. Several mouse models for renal cysts show elevated Gli proteins and/or increased expression of sonic Hh target genes. Mutation of Gli2 transcription factor causes nephronophthisis in

human and mice with upregulation of Gli1, a direct target of the Hh signaling cascade (Attanasio et al. 2007). In addition deletion of the IFT complex components Ift140 and Thm1 during embryogenesis resulted in renal cystic disease associated with increased expression of Gli transcripts in affected kidneys (Jonassen et al. 2012; Tran et al. 2014b).

2.3 Autosomal dominant polycystic kidney disease

The potentially lethal autosomal dominant polycystic kidney disease (ADPKD) is the most prevalent inherited monogenetic disorder. It typically affects adults and occurs with a prevalence estimated to be between 1:400 -1000 (Harris and Torres 2014). The patients exhibit massive renal enlargement deriving from the progressive formation of fluid-filled cyst that my lead to kidney failure (Torres et al. 2007). In a healthy person both kidneys account for around 1% of the total body weight, whereas in a patient with end stage renal disease (ESRD) the total weight of the kidneys was measured 22kg which was 20% if his body weight (Ekser and Rigotti 2010). ADPKD is a systemic disease; the extra-renal manifestations include cysts in liver and pancreas, and defects in the vasculature such as intracranial aneurysms and cardiac valve abnormalities (Torres et al. 2007). Hypertension is a very common symptom of ADPKD patients but also hematuria, renal colic, and urinary tract infections have been observed. ADPKD is predominantly caused by germline mutation in two genes polycystin 1 (*PKD1*) and polycystin 2 (*PKD2*), which encode for PC1 and PC2 (Hughes et al. 1995; Mochizuki et al. 1996; Qian et al. 1996; Watnick et al. 1998; Wu et al. 1998). Further genetic heterogeneity has been suggested with positional cloning approaches which identified more than 20 genes causing polycystic kidney disease (PKD). In patients identified via the renal clinic, *PKD1* accounts for approximately 78% of ADPKD and *PKD2* for about 13%, no mutations in either of the two genes were detected in approximately 9% of the cases (Rossetti et al. 2007; Audrezet et al. 2012). Although the clinical features associated with loss of PC1 and PC2 proteins overlap completely, mutations in *PKD1* manifest in a more severe pathogenesis of ADPKD characterized by larger kidneys and earlier onset of ESRD (Harris and Torres 2014). The mean age of renal failure in individual with *PKD1* mutations is around 58 years compared with an average age of 79 years for *PKD2*.

2.3.1 Structure and role of Polycystin 1 and 2

The *PKD1* and *PKD2* corresponding proteins, PC1 (450 kDa) and PC2 (110 kDa) are transmembrane glycoproteins that are able to form a functional complex. The overall expression of PC1 and PC2 is

overlapping and temporarily regulated. The highest levels are found in renal fetal tissue of the developing embryo, whereas only low detectable levels are present in the adult tissue (Chauvet et al. 2002). Apart from the kidney they follow the same expression pattern in a variety of other somatic tissues including liver, heart, and endocrine glands, for example pancreatic islets and the adrenal glands (Peters et al. 1999). Polycystin proteins exert important effects on calcium homeostasis and formation of focal adhesions. PC1 can be found in the basolateral plasma membrane domain of polarized epithelial cells, where it participates in adherence junctions and focal adhesion complexes (Ibraghimov-Beskrovnaya et al. 1997; Huan and van Adelsberg 1999). PC2 protein is concentrated in the endoplasmatic reticulum where it appears to play a role in regulating Ca^{2+} release (Cai et al. 1999). Perhaps the most important role for polycystins is the regulation of calcium levels in the primary cilium.

Like many other proteins implicated in renal cystic diseases PC1 and PC2 are located in the primary cilium (Pazour et al. 2002; Yoder et al. 2002), and are thought to play an important role in regulating the ciliary microenvironment. PC2 is a non-selective cationic ion channel capable of transporting calcium ions (Ca^{2+}). In the cilium, PC2 Ca^{2+} channel activity depends on the direct interaction with PC1 via their C-terminal tails (Hanaoka et al. 2000; Gonzalez-Perrett et al. 2001). The binding of PC1 to PC2 is thought to stabilize the channel function and direct trafficking to the cilium (Babich et al. 2004; Xu et al. 2007). In renal tubular epithelial cells the cilium projects into the lumen and the PC1/PC2 complex is thought to function as a flow detector. PC1 is suggested to act as a mechanosensor to detect urinary flow while PC2 responds to this stimulus by generating a Ca^{2+} influx into the cytoplasm (Praetorius and Spring 2003; Liu et al. 2005). A recent study by Jin et al. used a single cell imaging technique to demonstrate that fluid-shear stress initiates Ca^{2+} influx into the cilioplasm with a subsequent cytosolic calcium response (Jin et al. 2014). Importantly the flow induced Ca^{2+} signaling depends on the ciliary PC2 channel activity (Fig. 4). Another study questions whether altered ciliary calcium concentrations have a global cytoplasmic effect. In contrast, they argue that two different polycystins, PC1-like1 and PC2-like2, act to regulate the cilia calcium compartment instead of PC1 and PC2 (Delling et al. 2013). The polycystin proteins interact with a long list of proteins and are thereby able to modulate diverse signaling pathways. The regulation of the pathways may be broadly summarized into three general themes: Ca^{2+} signaling, negative growth regulation and differentiation (Chapin and Caplan 2010).
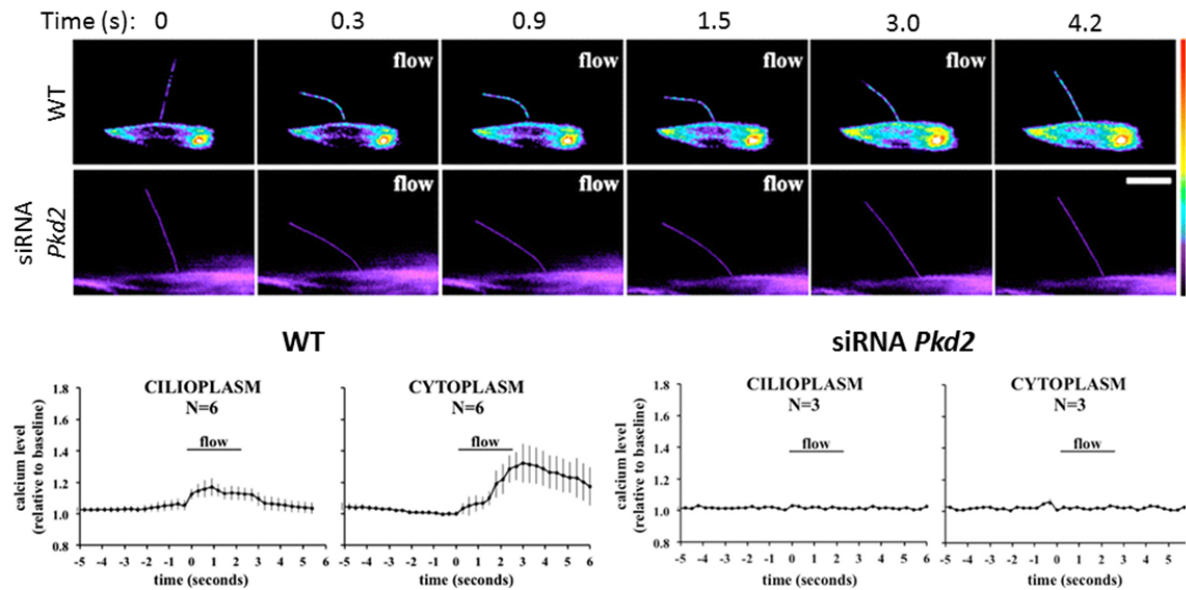
Figure 4. Flow-induces calcium signaling. *Live imaging of single cells of the LLC-PK proximal tubule kidney cell line transfected with CTS-G-CaMP3. This fluorescent sensor comprises a conserved cilia targeting sequence (CTS) that mediates localization to the cilioplasm and cytoplasm to visualize calcium signaling in the two compartments. Fluid shear stress on transfected LLC-PK bends the cilium and induces an increase in ciliary calcium levels. The increase of calcium in the cilioplasm is followed by an increase in cytosolic calcium. Cotransfection with siRNA against Pkd2 abolished ciliary or cytosolic calcium changes in response to fluid-shear, indicating that PC2 is involved in flow-induced intracellular calcium increase. Bottom graphs show quantification of calcium induced fluorescence. All pictures courtesy of (Jin et al. 2014).*

2.3.2 ADPKD pathogenesis

Studies on kidneys from adult patients with ADPKD indicate that cysts are formed equally and focally primarily from collecting ducts and to lesser extent from the other nephron segments (Paul and Vanden Heuvel 2014). Microdissections of those kidneys suggest that cysts are derived from only 1 to 2% of the nephrons and that they originate from clonal growth of a single cells lining the tubules (Grantham et al. 2008). Cystic epithelial cells are characterized by incomplete differentiation and sustained cell proliferation provoking the tubular wall to expand and form a pocket. Interestingly, when the cavity expands to around 2 mm diameter the cyst buds from the parent tubule to become a fluid-filled sac lined by a single epithelial cell layer (Grantham et al. 1987). These isolated cysts progressively expand in size by a combination of epithelial cell proliferation and transepithelial fluid secretion (Fig. 5).

In ADPKD the initiation of cystogenesis in the kidney is caused by mutations in either *PKD1* or *PKD2*. Although every kidney cell in an ADPKD patient carries the same germline mutation in one, or the other of the two alleles for the polycystin genes, only a small subset of cells becomes cystic. Moreover the severity of the ADPKD phenotype varies considerably among family members. To explain these phenomena the theory of a second hit was proposed (Pei 2001). This model states that kidney cyst formation begins upon loss of function of both alleles of *PKD1* or *PKD2* within an epithelial cell. The initial mutation would be germline whereas the second hit would be somatic. In support of this 2-hit model, combinations of germline and somatic mutations in either of the polycystins were detected in individual cysts of patients with ADPKD (Qian et al. 1996; Watnick et al. 2000). Further evidence came from a study in mice which demonstrated that in *Pkd2*^{+/-} mice somatic loss of *Pkd2* in the second normal allele correlates with focal cyst development in the kidney (Wu et al. 1998). In those mice PC2 was absent in all cyst lining cells, suggesting that somatic loss of *Pkd2* is sufficient for cystogenesis. However the 2-hit model does not fully explain recent observation in humans and mice suffering ADPKD. Dosage reduction of PC1 and PC2 due to hypomorphic alleles indicates that cysts can develop even if the protein is not completely absent. Although hypomorphic alleles appeared to be less potent and were relatively mildly pathogenic (reviewed in Eccles and Stayner 2014). These results suggest that the polycystin proteins are crucial to maintain the differentiated phenotype of the tubular epithelium. Reduction of the PC1 or PC2 below a critical threshold may result in a phenotypic switch by increased cell proliferation and the inability to sustain planar cell polarity (PCP).

Mechanisms on cysts formation and progression have been extensively studied in animal models. Kidneys of mice with homozygous mutations for *Pkd1* or *Pkd2* develop normally until E14.5. Cystic dilations were first noted in the maturing kidney by E15.5 and most of the mice died perinatally due to sever cystic disease and vascular defects (Ko and Park 2013). These results are consistent with the expression pattern of murine PC1 and PC2, which peaks at E15.5 in the UB derivatives and suggests that they are not required for nephronogenesis, but for the subsequent elongation of tubular segments (reviewed in Paul and Vanden Heuvel 2014). Of interest, a study by Piontek et al. using an inducible *Pkd1* mouse model demonstrated that inactivation of *Pkd1* before P13 results in severe PKD within 3 weeks, consistent with a rapid renal phenotype (Piontek et al. 2007). Later inactivation of Pkd1 induced a late cystic phenotype at approximately 6 months of age. Comparably, cystic growth rates in the human fetus are exuberant and exceed 2300% per year (12% / year in adults), in contrast after birth the cyst expansion in the same kidneys proceeded at much slower rate (Grantham et al. 2010). These observations argue that the slow onset of ADPKD in matured kidney cannot be justified by the 2-hit
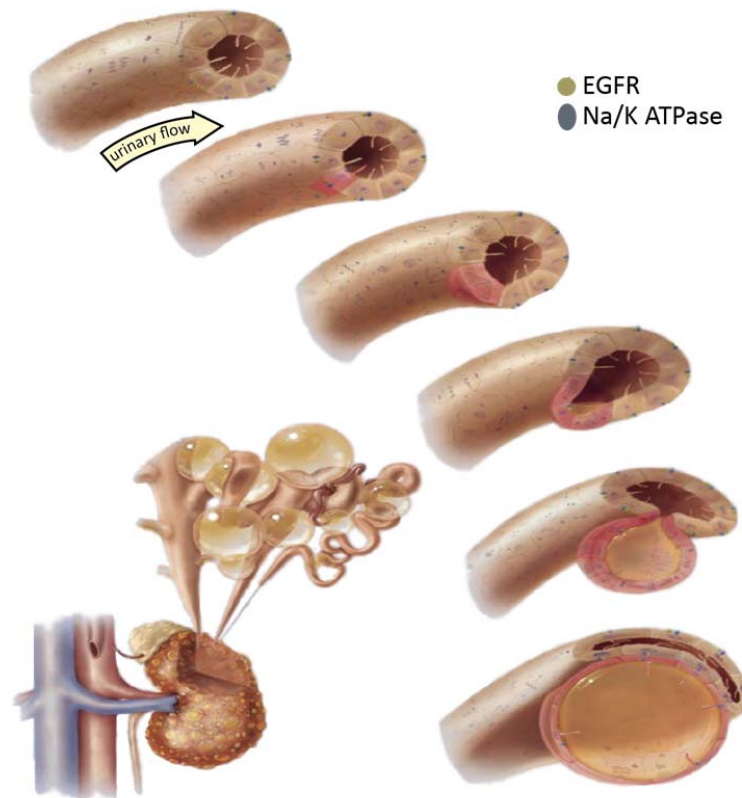
Figure 5. Renal cystogenesis at the level of the nephron. *Cystic kidneys show mislocalization of the tyrosine kinase receptor EGFR and of Na+/K+ ATPase pump, leading to increased cell proliferation and aberrant ion transport and fluid secretion. The direction of oriented cell divisions also becomes randomized, thus promoting tubular dilatation rather than nephron elongation. Cysts ballon out and bud off from the renal tubules. Collectively, these effects lead to the formation of a cyst-filled kidney with reduced functional capacity. Figure adopted from (Abdul-Majeed and Nauli 2011).*

hypothesis. A third-hit model was proposed, which builds upon the second hit hypothesis. It states that the cell may not convert into a cystogenic state just because it carries a germline mutation and a somatic inactivation of the normal allele, but it also requires a third hit that leads to cell proliferation and cyst growth. Recent studies support this idea, in adult mice elimination of PC1 or Kif3a (protein required for ciliogenesis) using gene inducible knock out causes late onset of focal cystic disease. However, subsequent renal injury by either nephrotoxins or ischemia in those mice induced rapid cystogenesis instead of normal tissue repair (Patel et al. 2008; Takakura et al. 2009). The model emerging from these findings is that polycystins and cilia in general are required to turn off proliferative signaling in renal epithelial cells after stress induced insults. In an identical way, they are necessary to negatively regulate proliferation after renal maturation is complete. For the adult kidney homeostasis and day to day operations they seem dispensable and no longer required to suppress proliferation.

The formation of fluid-filled cysts constitutes a stark contrast to the compact arrangement of tubules in a healthy kidney. At a cellular level this transformation is predicted to be facilitated by two pathological processes, increased fluid secretion into the cyst lumen and inappropriately increased cell proliferation by the epithelium lining the cyst in order to organize themselves in way to create a spherical structure (Mochizuki et al. 2013). Elevated secretion is expected to increase hydrostatic pressure inside the cyst and to stimulate expansion, whereas the increase in cyst surface area is a consequence of ectopic cell proliferation. Expansion of cyst fluid volume may be explained as the conversion of the cyst-lining cells from an ion-absorptive to an ion-secretory epithelium. The influx is regulated by the chloride channel cystic fibrosis transmembrane conductance regulator (CFTR) and is directly proportional to its quantity found in the cyst lining cell (Sullivan et al. 1998). Since the chloride channel, CFTR is activated by cytosolic cAMP; excessive fluid secretion may be under the control of elevated cAMP.

2.3.3 ADPKD as ciliopathy

Cilia dysfunction has emerged as common factor underlying the pathogenesis of ADPKD together with virtually all diseases provoking renal cysts. The concept of ciliopathy describes that proteins altered in these single-gene disorders function and localize to the cilium-basal body complex, which acts as nature's universal cellular detection mechanism (reviewed in Hildebrandt et al. 2011). The syndromic cystic disease includes the dominant disorder ADPKD and the recessive disorders autosomal recessive PKD (ARPKD), nephronophthisis, Joubert syndrome, Senior-Loken syndrome, Meckel syndrome, Bardet-Biedel syndrome (BBS), and orofacial digital syndrome. The different disorders display a high degree of phenotypic overlap. Apart from the development of renal cyst, a number of pathologies are observed in at least two or more of those syndromes including liver fibrosis, retinal defects, central nervous system/neural tube abnormalities, and developmental delay (Luciano and Dahl 2014). A surprising discovery is that mutation of the same recessive gene may cause different disorders. Very similar to the observation in the Pkd1 inducible knock-out mice in which cyst occurrence and progression depends on the development status or physical integrity of the kidney (See 2.3.1 ADPKD pathogenesis and Piontek et al. 2007), mutations in NPHP6/CEP290 were detected in patients with either Joubert or Senior-Loken syndrome (Hildebrandt et al. 2011). These variabilities may be related to allelic effects. Truncating mutations that act during development cause a severe phenotype, whereas cases with at least one missense mutation or a hypomorphic allele are associated with a mild, late onset phenotype as seen in the Senior-Loken syndrome (Helou et al. 2007; Hildebrandt et al. 2011).
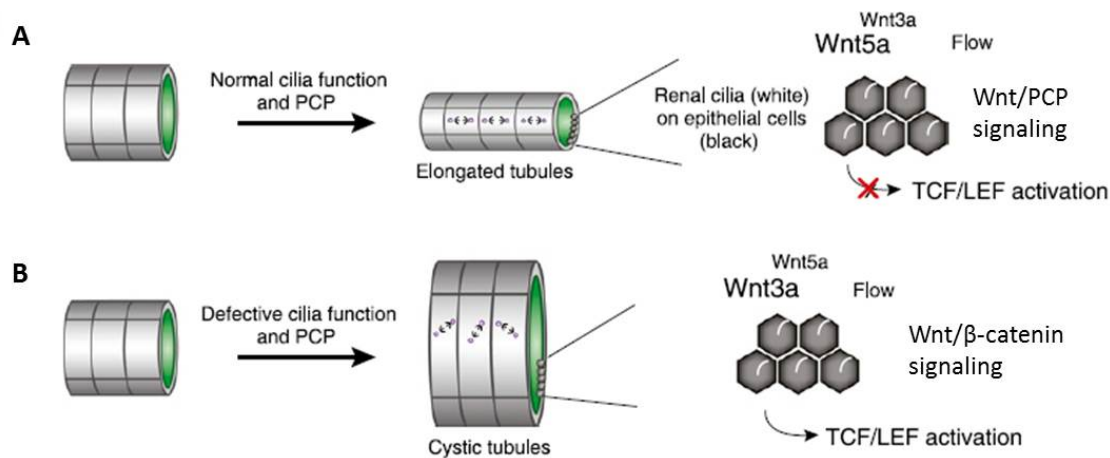
Figure 6. Wnt signaling during kidney development and homeostasis is important for convergent extension. *(A) PCP/Wnt signaling is directly involved in the establishment of normal tubular architecture in various ways, including directional cell division, preservation of cellular spatial orientation, and convergent extension. During development tubular cells undergo massive cell proliferation and tubular lengthening occurs without any increase in tubular diameter. Tubular flow is thought to instruct the PCP machinery to define the tubular axis. (B) Cilia integrity is essential for sensing tubular flow. Loss of proteins required for cilia formation or defective PCP signaling may result in missoriented cell divisions, exacerbated canonical Wnt signaling and eventually cystic tubules. Image is courtesy of (Oh and Katsanis 2013).*

These different diseases provide important insights into the mechanisms of cystogenesis, in particular the role of cilia/basal body in this process and the associated signaling pathways that require a functional cilium. The primary cilia act as a complex signaling center and have been linked to key cellular events such as cell fate/differentiation, polarity, and signaling pathways (Berbari et al. 2009). In particular the Wnt signaling pathway plays not only an important role in the development and maintenance of the kidney, but also in cystogenesis (Fig. 6). Possible effectors of PKD as well as NPHP proteins include Wnt signaling pathways and unopposed canonical Wnt signaling during renal development causes PKD (Saadi-Kheddouci et al. 2001).

2.3.4 Wnt signaling and the cilium

A myriad of developmental and adult life processes are regulated by the Wnt signaling cascade, some of the prominent ones include organogenesis from worms to humans, stem cell differentiation, primary embryonic axis formation, and nervous system patterning (Niehrs 2012). Defective Wnt signaling is implicated in various diseases such as cancers, cystic kidney and neurodegenerative diseases. The

majority of colorectal cancers involve hyperactivation of β-catenin causing constitutive activation of Wnt signaling (Polakis 2012). The Wnts form a large family of secreted glycoproteins that couple with various membrane bound receptors to activate different downstream pathways that have been classified as either canonical (β-catenin dependent) or non-canonical pathways (β-catenin independent). The human and most mammalian genomes encode for 19 Wnt transcripts. Several Wnt molecules are also found in the Cnidaria (sea anemone *Nematostella vectensis*) and even sponges contain a few Wnt genes whereas single cell organisms lack them completely, emphasizing that the Wnt signaling cascade has been an important instrument in the evolutionary origin of multicellular animals (Clevers and Nusse 2012).

2.3.4.1 Canonical Wnt signaling

The co-transcriptional regulator β-catenin plays a key role in the signaling output of the canonical Wnt cascade (Fig. 7) .In the absence of canonical Wnt molecule, levels of cytosolic β-catenin are kept low by proteasomal degradation promoted by a destruction complex. The β-catenin destruction complex consists of the scaffold protein Axin, which interacts with the tumor suppressor protein APC and the two constitutively active kinases CK1α and GSK3β. In the absence of Wnt activation the complex engages with β-catenin to sequentially phosphorylate it by CK1α and GSK3β at a series of residues. As a consequence, the phosphorylated β-catenin is ubiquitinated and targeted for degradation by the proteasome (Aberle et al. 1997). The canonical Wnt signaling pathway initiates when the ligand binds to the receptor complexes Frizzled and LRP5/6, which recruit cytoplasmic Dishevelled (Dvl) to form a platform for the β-catenin destruction complex. The resulting Wnt signalosome formation inhibits the GSK3β kinase activity. Free β-catenin accumulates in the cytoplasm and translocates into the nucleus, where it activates target genes by binding TCF/LEF transcription factors. The precise mechanism of how GSK3β is inhibited upon canonical Wnt signaling is still debated and several models have been proposed. The first one suggests that the Wnt signalosome, comprising Wnt and is co-receptors as well as the axin destruction complex bound to β-catenin, sequesters inside multivesicular endosomes thereby preventing GSK3β enzymatic activity on newly synthesized β-catenin (Taelman et al. 2010; Vinyoles et al. 2014). Another mechanism is based on the observation that Wnt-induced LRP5/6 phosphorylation titrates away the destruction complex which is still able to capture β-catenin, however ubiquitination and subsequent degradation is inhibited (Li et al. 2012). The study of Li et al, does not support the GSK3β sequestration into multivesicular endosomes during the initial Wnt activation, but cannot exclude it as later event. Moreover, GSK3β is inhibited by LRP5/6 itself, binding causes the axin destruction complex to separate from β-catenin and the signalosome (Kim et al. 2013). It is likely that these processes coexist and depend on the extent of Wnt stimulation.

2.3.4.2 Wnt/Planar cell polarity signaling

Planar cell polarity (PCP) refers to polarization of cells along the plane of an epithelium perpendicular to the apical-basal axis. PCP was initially introduced to describe the spatial organization of polarized structures such as Drosophila wing hairs or stereocilia in the inner ear (Seifert and Mlodzik 2007). Apart from the apical basal polarity, cells in most developing tissues require positional information to generate polarized structures for example by regulating directional cell movement or oriented cell division (Fig. 6) (Schnell and Carroll 2014). It has been proposed that the global orienting cue for PCP establishment is provided by noncanonical Wnt signals (Fig. 7). In the noncanonical Wnt/PCP pathway, Wnt ligand binds to Frizzled thus retaining Dvl at the plasma membrane and stimulating the small GTPase Rho and Rac thereby activating the further downstream kinases JNK and Rho to organize the actin cytoskeleton (Kikuchi et al. 2009). Indeed, inhibition of Rac1 impaired the polarized positioning of basal bodies in node cilia resulting in left-right asymmetry defects (Hashimoto et al. 2010). Mutations of Wnt/PCP signaling genes in mammals, zebrafish, and frogs lead to phenotypes in neural tube closure and in the kidney tubules (see 2.1.2 Major steps in kidney organogenesis and Goggolidou 2014). Despite the connection between Wnt and PCP, the mechanism leading to a global asymmetry of core PCP proteins within a tissue is still poorly understood. Therefore it is important to keep in mind that Wnt/PCP signaling is not the only pathway that directs and contributes to the orientation of cells. An asymmetric localization of 'core PCP' proteins along a field of cells is considered to be sufficient for the initiation of a local cellular spatial organization through cell-cell contacts. The core proteins consist of Vangl and Prickle which accumulate at the distal side of the cells, whereas Frizzled, Diego, and Dvl segregate to proximal side. The core PCP member Celsr is localized to both sides. Cellular asymmetry is maintained by intracellular feedback interactions leading to mutual inhibition between distal and proximal core proteins and intercellular contact between distal Vangl and proximal Frizzled (Chen et al. 2008; Strutt et al. 2011). How the core proteins initially acquire their asymmetric localization is very controversial but a morphogen gradient of noncanonical Wnt has been suggested to be the underlying mechanism (Gao 2012). The Fat/Dachsous cascade has also been implicated to provide cues for the arrangement of cells, but its relationship with PCP signaling has to be elucidated (Thomas and Strutt 2012). It is also possible that cilia can influence planar cell polarization independently of PCP signaling. A conditional mutation of Ift88 in the inner ear, which is critical for the formation of the kinocilium but not for the stereocilia, resulted in the disorganization of planar-polarized stereocilia. The asymmetric localization of PCP core proteins was not affected in those cells, suggesting that loss of the kinocilium controls polarized cell behavior independently or downstream of PCP signaling (Jones et al. 2008). Apart from the role in Wnt signaling, cilia themselves are regulated by the PCP pathway. The multi-ciliated epidermis of *Xenopus*

laevis relies on Dvl and Vangl2 function to properly orient basal bodies, which in turn controls ciliary beating (Park et al. 2008; Mitchell et al. 2009). Moreover PCP signaling is also required for left-right patterning due to its role in the planar polarization of motile cilia at the node (Hashimoto et al. 2010).

2.3.4.3 The kidney, Wnt signaling and the primary cilium

Several lines of evidence revealed that Wnt signaling in the kidney is coupled to the ciliary axoneme and basal body. An important aspect of kidney morphogenesis is to control the appropriate diameter of the renal tubules while they increase in length (Fig. 6). This process is controlled by oriented cell division and convergent extension of the epithelial cells along the proximal-distal axis of the tubule (Lienkamp et al. 2012). Defects in either of the two mechanisms will lead to the formation of cysts in the kidney. Both oriented cell division as well as convergent extension is regulated by the noncanonical Wnt/PCP pathway, whose signaling is thought to be associated with the primary cilium. So far more than 30 reports have documented ectopic canonical and noncanonical Wnt signaling in ciliary mutants associated with kidney, pancreas, gastrulation, and convergent extension defects (reviewed in Oh and Katsanis 2013). Members of both the canonical Wnt and Wnt/PCP pathway are located in the cilium. The core PCP protein Vangl2 resides in the cilium together with Frizzled, Dvl1 and 3, and the destruction complex members GSK3β and APC, whereas β-catenin and Dvl2 have been located at the basal body (Ross et al. 2005; Thoma et al. 2007; Corbit et al. 2008; Park et al. 2008; Luyten et al. 2010). The ciliary location of Wnt members suggests that the primary cilium is an important factor in the canonical and noncanonical Wnt signaling cascades. The first direct link between cilia and Wnt signaling was observed in a study with Bardlet-Biedl Syndrome (BBS) proteins 1, 4, and 6 which specifically localize to the basal body (Gerdes et al. 2007). Knockdown of those genes, associated with the ciliopathy BBS, resulted in a hyperactive β-catenin Wnt response and impaired noncanonical Wnt signaling. Mouse and zebrafish BBS models manifest convergent extension defects, symptoms that are reminiscent of a defective PCP pathway (Ross et al. 2005). Consistent with this idea, activation of PCP/Wnt signaling by overexpression of membrane bound Dvl rescued the convergent extension phenotype of the Bbs 1, 4, and 6 morphants (Gerdes et al. 2007). Likewise, the disruption of the primary cilia in mice harboring mutations in *kif3a* (gene transcribing a kinesin motor protein essential for ciliogenesis), *ift88*, or *odf1* led to enhanced β-catenin dependent Wnt signaling at embryonic day 9 (Corbit et al. 2008; Lancaster et al. 2011). In the kidney increased β-catenin levels were reported in mice mutant of Kif3a or two IFT proteins (Ift20 and Ift140), which are also associated with cystic kidneys (Lin et al. 2003; Jonassen et al. 2008; Jonassen et al. 2012).
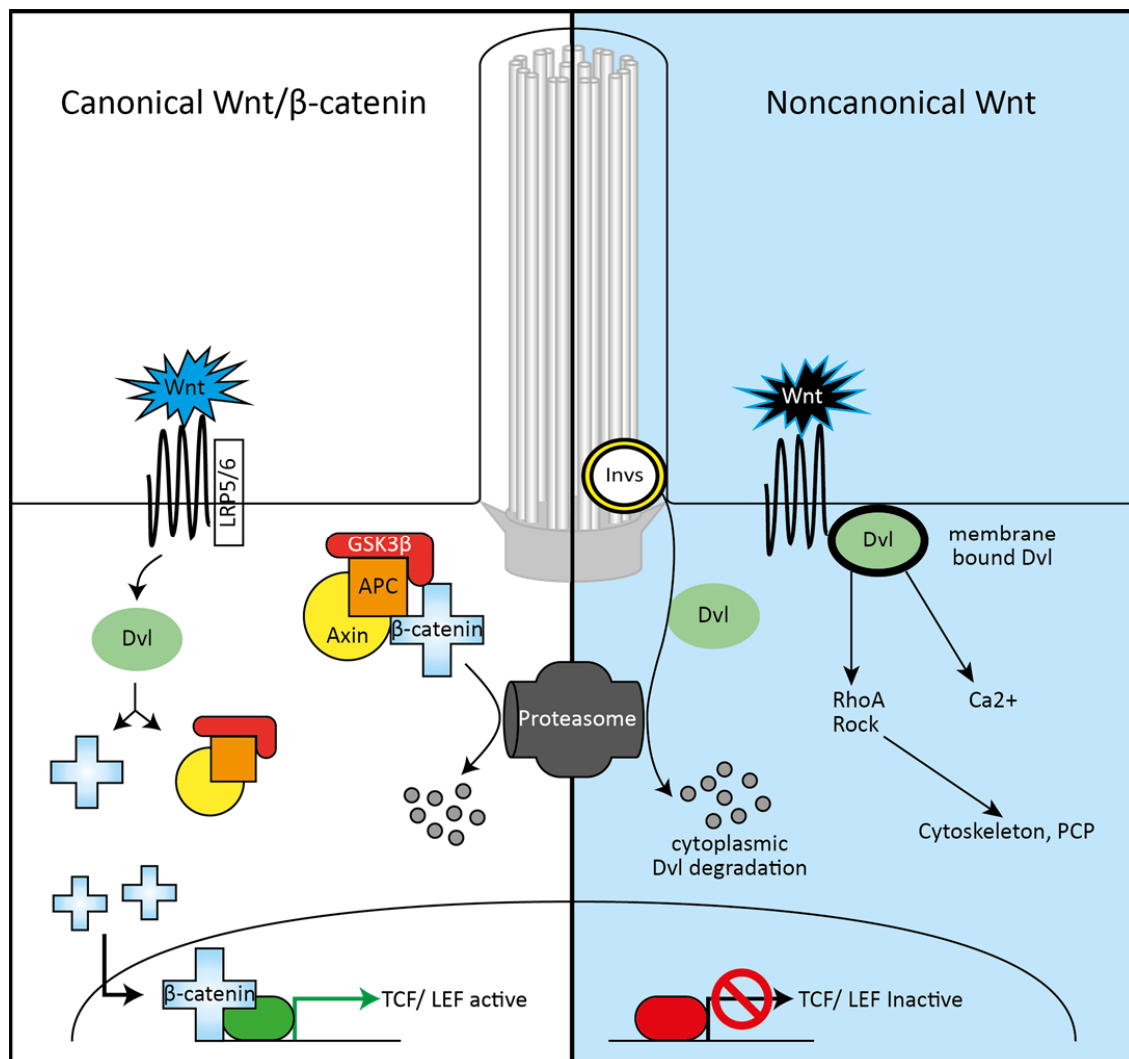
Figure 7. Wnt signaling and the cilium. *The cilium might act as a switch between canonical and noncanonical Wnt signaling pathways. In the Wnt/β-catenin pathway (left) a Wnt ligand binds to the co-receptor Frizzled/LRP to guide Dvl to the signalosome. This interaction inhibits the activity of the Axin destruction complex and leads to the stabilization and accumulation of β-catenin. β-catenin translocates to the nucleus to activate TCF/LEF target gene expression. In the non-canonical pathway (right side), a different Wnt ligand binds to Frizzled receptor independently of LRP. This activates the membrane form of Dvl which regulates downstream signaling pathways such as PCP and Ca^{2+}. Inversin at the base of the cilium is thought to act as a switch by promoting cytoplasmic Dvl for degradation and recruiting membrane bound Dvl to the Frizzled receptor.*

A possible connection between the cilium and Wnt signaling pathway may be the protein Inversin (Invs or NPHP2), which localizes to a defined ciliary compartment. Experiments in *Xenopus laevis* suggest that Invs, which is a paralog of the core PCP protein Diego, regulates the balance between canonical and Wnt/PCP signaling. Invs promotes PCP signaling and simultaneously targets cytoplasmic Dvl for degradation and thereby antagonizing canonical Wnt signaling (Simons et al. 2005). The function of Invs

will be discussed in greater detail in section *2.4 'The role of Inversin'*. Two additional ciliary proteins NPHP3 and 4, both implicated in nephronophthisis and like Invs belonging to the family of Nephrocystins (NPHP) can suppress canonical Wnt signaling (Bergmann et al. 2008; Burckle et al. 2011). These studies suggest that the cilia or cilia-associated proteins constrain the canonical Wnt signaling cascade and thereby promoting Wnt/PCP signaling (Fig. 7).

It seems that the regulation of the canonical Wnt pathway by the cilium is rather cell type specific than global , since the Ift88 cilia disruptive mouse mutant does not exhibit widespread defects in β-catenin dependent developmental processes (Wallingford and Mitchell 2011). The genes and factors described also contribute to the genesis of cystic kidneys in addition to aberrant Wnt signaling. Thereby it has been hypothesized that cilia regulate the balance between the different Wnt signaling cascades to maintain kidney development and homeostasis. Interestingly hyper-activation of canonical Wnt signaling as well as loss of Wnt stimulation gives rise to renal cysts (Pinson et al. 2000; Saadi-Kheddouci et al. 2001). Providing evidence that the canonical and noncanonical Wnt signals must be finely tuned as ectopic Wnt signaling results in cystogenesis. Although defective Wnt signaling and cilia are not the only mechanisms leading to cystic kidneys they clearly have an important role.

There have been several reports arguing against a role of cilia in Wnt signaling (reviewed in Wallingford and Mitchell 2011; Oh and Katsanis 2013). For example studies in zebrafish and mice lacking *ift88* and mice that are absent of either Kif3a or Dync2h1 (retrograde trafficking) demonstrate that canonical Wnt signaling is similar in mutant animals compared to wild-type (WT) littermates (Huang and Schier 2009; Ocbina et al. 2009).

2.3.5 The ciliary and cellular calcium signaling in PKD

In ADPKD disturbed Ca^{2+} signaling is one of the first events and it directly affects several signaling pathways (Fig. 8). In particular, elevation of the second messenger cAMP in the kidney is a common feature in most if not all models of PKD, probably leading to an excess of PKA signaling (Yamaguchi et al. 1997; Belibi et al. 2004). A link between cellular Ca^{2+} alterations and cAMP concentrations was proposed via the activity of adenylyl cyclase (AC) and phosphodiesterases (PDE) (Wallace 2011). The primary cilium as a key signaling organelle also seems to regulate cellular Ca^{2+} homeostasis and thereby cAMP alterations in this context. In the cilium of renal epithelial cells, PC1 and PC2 constitute a mechanosensory calcium channel complex. Urinary flow induces bending of the primary initiating influx
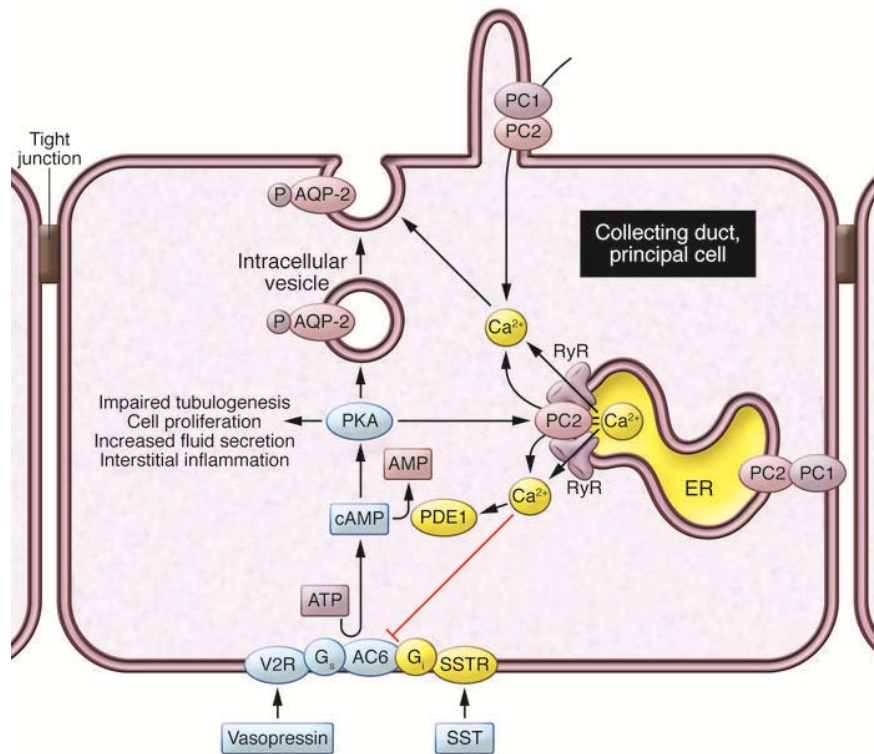
Figure 8. Ca^{2+}-dependent signaling pathways that are perturbed in PKD. *Altered Ca^{2+} and cAMP levels in kidney epithelial cells lead to a cystic phenotype (Harris and Torres 2014). Dysfunction occurs in the ciliary mechanosensory calcium channel complex PC1/PC2 which normally restrains cAMP signaling by PC2-mediated Ca^{2+} influx. Inhibition of PDE and activation of AC6 due to decreased Ca^{2+} causes abnormal accumulation of cAMP and activation of PKA. Disrupted Ca^{2+} cellular homeostasis also interferes with aquaporin-2 (AQP-2) targeting to the apical plasma membrane. Atypical PKA activation disrupts tubulogenesis, stimulates chloride and fluid secretion into the cyst lumen and activates propoliferative signaling pathways including MAPK, mTOR and β-catenin. Vasopressin and somastatin (SST) interaction with their receptors V2R, respectively SSTR stimulate cAMP production. Gs and Gi refer to guanosine nucleotide-binding proteins s and i. Yellow highlights proteins and molecules that are reduced in PKD; blue indicates factors that are increased in PKD. Picture is courtesy of (Harris and Torres 2014).*

of extracellular Ca^{2+} into the cilioplasm. Localization of the polycystins to the primary cilium is essential and necessary to initiate this first signaling cascade of intracellular calcium (Nauli et al. 2003). Subsequently ciliary calcium is transduced to the cytosol and amplified through the ryanodine receptor (RyR) to generate a more global Ca^{2+} signal. Novel live-cell imaging techniques with Ca^{2+} indicators allow the dissection of Ca^{2+} signaling in different subcellular compartment. When kidney cells were subjected to shear stress an increase in Ca^{2+} concentration was first visualized in the primary cilium then in the cytoplasm (Su et al. 2013; Jin et al. 2014). Knock down of PC2 abolished the Ca^{2+} response to fluid flow completely, whereas inhibition of the RyR suppressed only the increase in cytosolic Ca^{2+}. The initial signal

is only further amplified by Ca^{2+} release from the RyR but not by the calcium channel IP_3R which also resides in the endoplasmatic reticulum.

In ADPKD calcium homeostasis is disrupted, cultured renal epithelial cells derived from human ADPKD cysts as well as from *Pkd1* or *Pkd2* mutant mice exhibit a reduction in intracellular Ca^{2+} concentration compared to healthy tubular cells (Wallace 2011). It has been suggested that aberrant intracellular Ca^{2+} homeostasis accounts directly for the accumulation of cAMP. Dampened Ca^{2+} levels stimulates the calcium inhabitable AC6 and inhibits the calcium/calmodulin dependent phosphodiesterase (Choi et al. 2011). Elevated cAMP metabolism fuels cystic growth by cell proliferation and transepithelial fluid secretion, the two major processes in the expansion of renal cyst in ADPKD. Cyclic AMP activates downstream effectors such as the cAMP dependent protein kinase A (PKA). PKA is known to affect tubulogenesis and regulate tubular diameter by enhancing canonical Wnt signaling through the phosphorylation of GSK3β and thereby stabilizing β-catenin (Fig. 6&7) (Torres and Harris 2014). The driving force in fluid secretion into the renal cyst is the active transport of chloride from the basolateral to the apical side. Chloride enters the cell at the basolateral side through the Na^+-K^+-2Cl^- cotransporter and PKA-induced phosphorylation of the CFTR opens the channel to allow the flow of chloride ions into cyst lumen (Sullivan et al. 1998). Cyclic AMP/PKA signaling is intimately connected with cell proliferation which is necessary but not sufficient for cystogenesis (reviewed in Mekahli et al. 2013). However, the response to cAMP signaling can have completely opposite effects depending on the cell type. In normal kidney tissue, cAMP leads to a non-mitogenic response by inhibiting the mitogen-activated protein kinase (MAPK) activity via PKA mediated phosphorylation and has therefore an anti-proliferative function. In cystic cells however cAMP signaling is changed and is known to stimulate cell proliferation. Ca^{2+} restriction are associated with an elevation of B-Raf protein and in these conditions high levels of cAMP stimulate the MAPK signaling pathway.

2.3.6 Therapy for PKD

The identification of genes and signaling pathways led to a better understanding of the pathophysiologic mechanisms responsible for the development and progression of PKD and laid the foundation for the development of new potential therapies. The goal of those therapies is to delay or prevent cyst growth while treating the complications. The major treatment strategies currently being tested in clinical trials are designed to reduce cAMP levels or inhibit increased cell proliferation (Harris and Torres 2014). Vasopressin which acts on V2 receptors (VPV2R) stimulates cAMP generation in the collecting ducts, connecting tubules, and thick ascending loop of Henle, the major sites for cytogenesis (Mutig et al.

2007). The exclusive localization of VPV2R makes it a prime target, especially to minimize off target effects and improving tolerability. Pharmacological inhibition of VPV2R with receptor antagonist Tolvaptan attenuates the cAMP synthesis and cyst formation, but to reduce side effects, a better understanding how Ca^{2+} regulates cAMP signaling is needed (Torres et al. 2012). Another means to limit cellular cAMP levels is through the action of the drug Somastostatin, which acts on five GPC receptors (SSTR1-5) (Fig.8). Interaction with the receptors slows down cyst growth in both the kidney and the liver due to inhibition of AC and MAPK (Hogan et al. 2010). Finally, mTor inhibitors like rapamycin reduce cell proliferation and cyst growth in several orthologous and non-orthologues animal models. Rapamycin is extremely effective in reducing renal cystogenesis in the *bpk* mouse (ARPKD) and Polaris mutant mouse (ADPKD). These findings were also supported in a retrospective observational study where rapamycin limited native kidney enlargement in ADPKD patients after renal transplantation (Brown and Murcia 2003; Shillingford et al. 2006). However, the results of clinical trials have been disappointing, most probably because humans do not tolerate blood levels capable of inhibiting mTOR in the kidney (Canaud et al. 2010). In summary, many of the drugs and therapies were effective in animal models of PKD, but may be limited by toxicity. Combination therapies might be necessary to preserve the kidney function and to avoid adverse effects since effective treatment is likely to be long term possible lifelong.

2.4 The function of Inversin

Inversin (Invs) was first identified in positional cloning in the *inv/inv* (inversion of embryonic turning) mouse. An animal model created by fortuitous insertion of a tyrosine mini-gene between exon 2-12 of the Invs locus, however a truncated protein containing only the first 90 aa is still expressed in those mice (Mochizuki et al. 1998; Morgan et al. 1998). Invs comprises 16 N-terminal ankyrin repeats and a C-terminal region that binds calmodulin via two IQ domains in the absence of Ca^{2+}, but not in its presence (Yasuhiko et al. 2001; Morgan et al. 2002) (Fig. 9B). *inv/inv* mice exhibit visceral situs inversions, combined with cystic growth in kidneys and the pancreas, consequently they die within a few weeks after birth (Fig. 9A). Subsequently mutations in the human *INVS* gene were found to cause the autosomal recessive disease nephronophthisis type 2 (NPHP2) accompanied with enlarged cystic kidneys, abnormal left-right asymmetry as well as cardiac valvular and septal defects (Tory et al. 2009). Aberrant left-right axis formation has been attributed to a defect in the orientation of motile cilia in the posterior notochord. The partial misalignment of cilia in *inv/inv* mutant embryos slows down a cilia-propelled leftward flow of extracellular fluid across the ventral node that is required to correctly pattern the
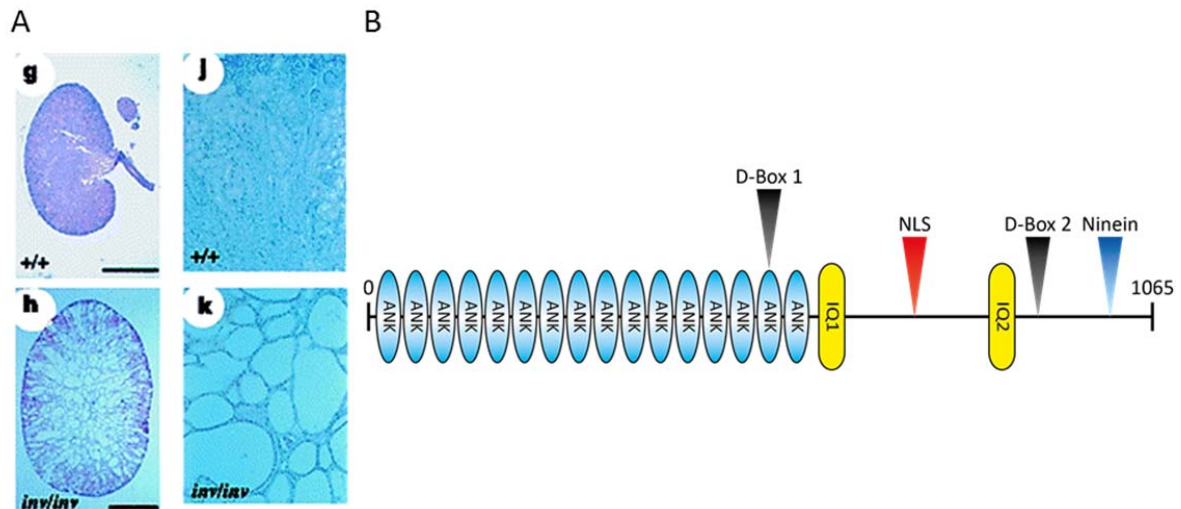
Figure 9. Loss of Invs results in massive cyst development. (A) Cross sections of newborn WT or inv/inv mutant mouse kidneys 5 days after birth. (B) Domain architecture of Inversin. The N-terminal half consists of 16 ankyrin repeats. Two calmodulin (IQ) binding domains and a nuclear localization sequence are found on the C-terminal half. The ninein-homology domain at the C-terminus together with IQ2 mediates ciliary targeting (Shiba et al. 2009). Two destruction boxes (D-Box) regulate the stability of Invs. Picture in A is courtesy of (Mochizuki et al. 1998).

visceral primordia during early somite stages (Okada et al. 2005). Studies in Xenopus and in zebrafish indicate that Invs promotes Dvl signaling in the Wnt/PCP pathway in a complex with Frizzled 8 at the plasma membrane, apparently by binding to and depleting the cytoplasmic pool of Dvl that mediates canonical Wnt/β-catenin signals (Simons et al. 2005; Lienkamp et al. 2010). In addition, the delay in tubular maturation and renal cytogenesis observed in *inv/inv* mice resembles the phenotype of mice with degradation-resistant β-catenin which extensively stimulate canonical Wnt signaling (Saadi-Kheddouci et al. 2001). However, subsequent work revealed that *inv/inv* mutant kidneys, similar to *Pkd1* and *Pkd2* mutants, completely switch off the expression of a transgenic reporter of canonical Wnt/β-catenin signaling (Sugiyama et al. 2011). The mechanism by which Invs controls the planar orientation of cilia thus remains unclear, but it was speculated that Invs directly affects planar cell polarity. The global domain architecture of Invs correlates with the core PCP protein Diego and likewise it interacts with two other PCP core proteins, Strabismus and Prickle (Simons et al. 2005).

Due to the lack of sufficiently specific antibodies, Watanabe and his colleges developed an Invs-GFP mouse to study the subcellular localization of Invs (Watanabe et al. 2003). Invs-GFP mice are inv mutant mice carrying a transgenic Invs-GFP full length fusion protein, which is able to rescue all the *inv* associated pathologies. The Invs-GFP protein localization was confined to the proximal segment of the

primary ciliary axoneme, immediately adjacent to the transition zone and the distinctive intraciliary segment was defined as Invs compartment. The C-terminal region of Invs is essential for the localization of Invs to the base of the primary cilium (Shiba et al. 2009). Additional subcellular localization for Invs have been proposed at the plasma membrane where it associates with N-cadherin and catenins. It also interacts with the tubulin network and is recruited to mitotic spindle fibers (Nurnberger et al. 2002; Nurnberger et al. 2004).

2.5 The role of Bicaudal-C

Bicaudal-C (Bicc1) encodes for an evolutionarily conserved RNA-binding protein consisting of RNA-binding K homology (KH) domains at the N-terminus and a C-terminal sterile alpha motif (SAM), separated by an intervening sequence (IVS) of unknown function (Fig. 10A) (Gamberi and Lasko 2012). SAM domains are modules present in most species and are thought to mediate protein-protein interactions and self-polymerization (Qiao and Bowie 2005). Bicaudal-C was first discovered in a *Drosophila* mutagenesis screen that identified a gene responsible for a 'double abdomen' phenotype in offspring of heterozygous females (Fig. 10B) (Mohler and Wieschaus 1986). BicC is required for anterior-posterior patterning by restricting oskar translation to the posterior pole (Saffman et al. 1998). *Caenorhabditis elegans* GLD-3 is a putative homolog of Bicc1 and is involved in the control of germline sex determination (Eckmann et al. 2002). In Xenopus and mouse, homologs were identified in a search for regulators of endodermal patterning (Wessely and De Robertis 2000). A link of Bicc1 to PKD was first suggested by the discovery that this locus is mutated in the *bpk* and *jcpk* mouse models of ARPKD and ADPKD respectively (Guay-Woodford et al. 1996; Cogswell et al. 2003) (Fig. 10C). In the *bpk* allele, a GC insertion in exon 22 of one of two splice variants leads to a frame shift and abnormal elongation of the C-terminus. *bpk* mice show apical missorting of EGFR, a characteristic feature of human ARPKD (Sweeney et al. 2001). In the chemically induced *jcpk* mutant allele, translation stops prematurely before the first KH domain. The link between PKD and Bicc1 was further confirmed in *Xenopus* where mutations in xBic-C are associated with dilated tubules and ducts, a phenotype reminiscent in all forms of human PKD and in zebrafish a model of PKD was validated that inhibits Bicc1 function (Tran et al. 2007; Bouvrette et al. 2010). More recently, a study of patients with renal disease identified two mutations in human *BICC1* gene; one nonsense mutation in the first KH domain and one missense in the SAM domain (Kraus et al. 2012).
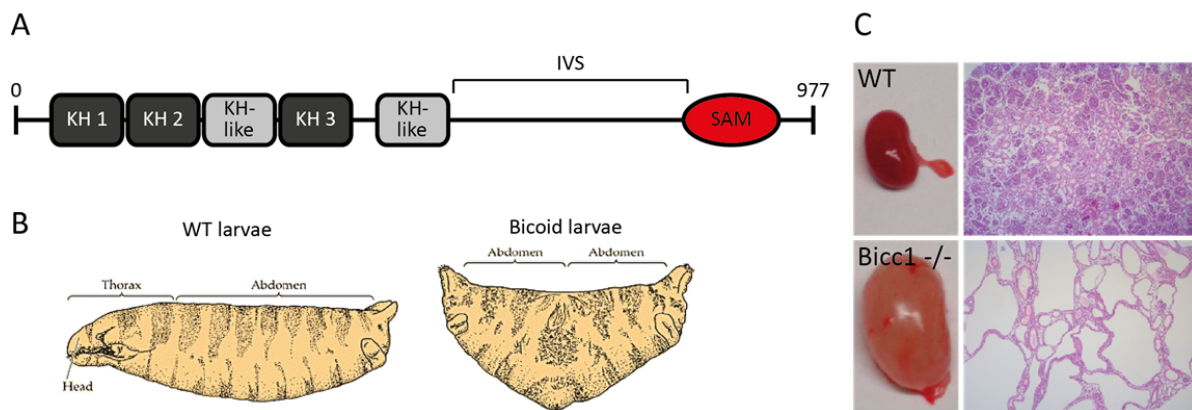
Figure 10. The RNA-binding protein Bicaudal-C. (A) *Bicc1 domain architecture. The Bicc1 N-terminus contains 3 RNA-binding KH domains and 2 KH-like domains. It is not clear whether the KH-like domains participate in RNA binding. A SAM domain is located at the C-terminus and is normally involved in protein-protein interactions and/or self-polymerization.* ***(B)*** *In Drosophila, dominant mutations of Bicaudal-C cause heterozygous females to produce double abdomen embryos.* ***(C)*** *Wild-type (WT) (top left) and Bicc1$^{-/-}$ mutant (bottom left) littermate kidneys at P8. Histological analysis of kidney section from control (right top) and Bicc1 mutant (right bottom) mice by haematoxylin-eosin staining. The Bicc1 $^{-/-}$ mutant kidney is dramatically enlarged compared to the WT kidney and at this stage of the disease glomeruli, tubules, and ducts can barely be recognized. Picture in C is courtesy of (Piazzon et al. 2012).*

Studies in various animal models suggest that Bicc1 regulates mRNA stability and translation (Tab.1). Repression of target mRNA requires generally the two distinct domains of Bicc1. The N-terminal KH domains are sufficient for specific binding to mRNA but insufficient for repression, conversely C-terminal SAM domain is needed for repression but fails to interact with the mRNA (Piazzon et al. 2012; Zhang et al. 2013). Bicc1 target mRNA binding is not well understood, but it is suggested that Bicc1 interacts with a conserved region on the mRNA to stabilize a stem-loop structure which facilitates miRNA binding. Bicc1 KH domains are able to mediate their own RNA binding in vitro, furthermore *Xenopus* xBic-C negatively regulates its own expression by association with its 5'UTR (Chicoine et al. 2007; Bouvrette et al. 2008). Bicc1 directly acts in the cAMP/PKA pathway; cAMP and the expression of its synthetic enzyme AC6 are upregulated in cystic kidneys of *Bicc1$^{-/-}$* knockout mice (Piazzon et al. 2012). In vitro, Bicc1 KH domains interacted independently with AC6 mRNA and the miR125a and AC6 mRNA was silenced by miR-125a only in the presence but not in the absence of full length Bicc1. By an analogous mechanism, Bicc1 also induced silencing of the protein kinase inhibiter alpha (PKIα) by miR-27a (Piazzon et al. 2012). A recent study reported that Bicc1 enhances the expression of Pkd2 in mouse kidneys apparently by inhibiting silencing by miR-17 (Tran et al. 2010). Interestingly, it was also proposed that loss of the ADPKD causal gene *Pkd1* downregulates Bicc1 expression *in vivo* and *in vitro* (Lian et al. 2014). Thus, the findings that

multiple genes regulated by Bicc1 are critical for normal kidney development and function, support the idea that translational control by Bicc1 plays a key role in nephronogenesis.

Targeted inactivation of mouse Bicc1 revealed an additional function in the ventral node during left-right axis formation. Node cells depend on Bicc1 expression for the planar positioning of motile cilia, which is reminiscent of Invs (Maisonneuve et al. 2009). Bicc1 also inhibited Dvl activity in luciferase reporter assays of canonical Wnt/β-catenin signaling similar to Invs, although without targeting Dvl for degradation.

Table1: Direct mRNA targets of Bicc1

Bicc1 target mRNA	Animal model	miRNA	Reference
Bicc1	Xenopus, mouse	-	(Chicoine et al. 2007) (Bouvrette et al. 2008)
AC6 PKIα	mouse	miR-125 respectively miR-27a	(Piazzon et al. 2012)
xCripto	Xenopus	-	(Zhang et al. 2013) (Zhang et al. 2014)
Coco, spin1, Dpy30, Ddx5, OAZ2, OCT-25, V ATPase B1, Smad4b, Nufip1, Wnk1	Xenopus	-	(Zhang et al. 2013)

3. Aim of the study

There is currently no treatment that can cure polycystic kidney disease, partly because the mechanisms causing PKD remain poorly understood. In our study we tried to shed light on the regulatory mechanisms that define the activity Bicc1. Mutations in *Bicc1* provoke cystic kidney diseases both in mouse and human. The following work will address two different aspects of Bicc1 regulation.

1. Loss of the RNA-binding protein Bicc1 randomizes visceral left-right patterning and induces fluid-filled cysts in kidneys and pancreas reminiscent of ADPKD. Visceral situs defects combined with renal and pancreatic cysts have also been linked to mutations in the calcium-dependent ankyrin repeat protein Invs. We therefore asked whether the two proteins act in a common pathway. To identify an epistatic relationship, we determined a potential interaction between Bicc1 and Invs and the pattern of Bicc1 localization in the kidney. Then we studied the effect of genetic *Invs* inactivation on Bicc1 target gene expression *in vitro* and *in vivo*.

2. Current research on ADPKD and other ciliopathies revolves around the central question of how polycystin-mediated calcium flux suppresses cysts. Recently it was suggested that PC2 activity is mediated primarily by CaMK2. In the second part we tried to establish a link between CaMK2 kinase activity and Bicc1 translational silencing. This work was originally started by Nathalie Piazzon a former postdoc from our group.

4. Results

4.1 Immunohistolological analysis of Bicc1 expression in mice

4.1.1 Expression of Bicc1 in the newborn mouse kidney

Bicc1-deficient mice are born with cysts in kidneys and pancreas as well as dilated liver bile ducts (Flaherty et al. 1995; Cogswell et al. 2003; Piazzon et al. 2012; Lian et al. 2014). Concordant with a function in renal morphogenesis, Bicc1 protein is expressed in new-born mouse kidney cortex (Piazzon et al. 2012; Lian et al. 2014). However, the subcellular distribution of Bicc1 in the kidney or other tissues has not been characterized. To validate the role of Bicc1 *in vivo*, we raised a polyclonal rabbit antibody against the C-terminal SAM domain. Specificity of anti-SAM antibody was confirmed in Western blot experiments by overexpressing HA-tagged or WT Bicc1 in HEK 293T cells and by Bicc1 RNAi in ciPTEC (conditionally immortalized proximal tubular epithelial cell) and mIMCD3 (murine inner medullary collecting duct) cells (Fig. 11A). The antibody also detected a band in kidney extracts of WT, but not of *Bicc1*$^{-/-}$ mutant mice. To better understand the kidney phenotype of *Bicc1*$^{-/-}$ mice, we analyzed the expression of Bicc1 in frozen sections of P0 (post-natal day zero) kidneys using the custom anti-SAM antibody. The novel antibody specifically reacted with tissues of WT but not *Bicc1*$^{-/-}$ mice (Fig. 11C, C'). Lotus tetragonolobus lectin (LTL) which is expressed in proximal tubules was used to mark cortical renal structures, whereas Tamm-Horsfall protein (THP) stained the thick ascending limb of Henle. Bicc1 exhibited medium cytoplasmic staining in epithelial cells of proximal tubules and ascending loop of Henle. Interestingly, one of the tissue cross-sections displayed a proximal tubule connected to an entire loop of Henle (Fig. 11C). In this structure, increased expression is observed in the descending loop Henle which is situated between the proximal tubule and the ascending loop of Henle (Fig. 11B). In addition, Bicc1 was observed in the parietal capsular epithelium of Bowman's capsule, and dual staining with dolichous biflorus agglutinin (DBA) revealed Bicc1 expression in collecting ducts (Fig. 12B, C). These data indicate that Bicc1 is present in all nephron segments as well as in the collecting duct system.
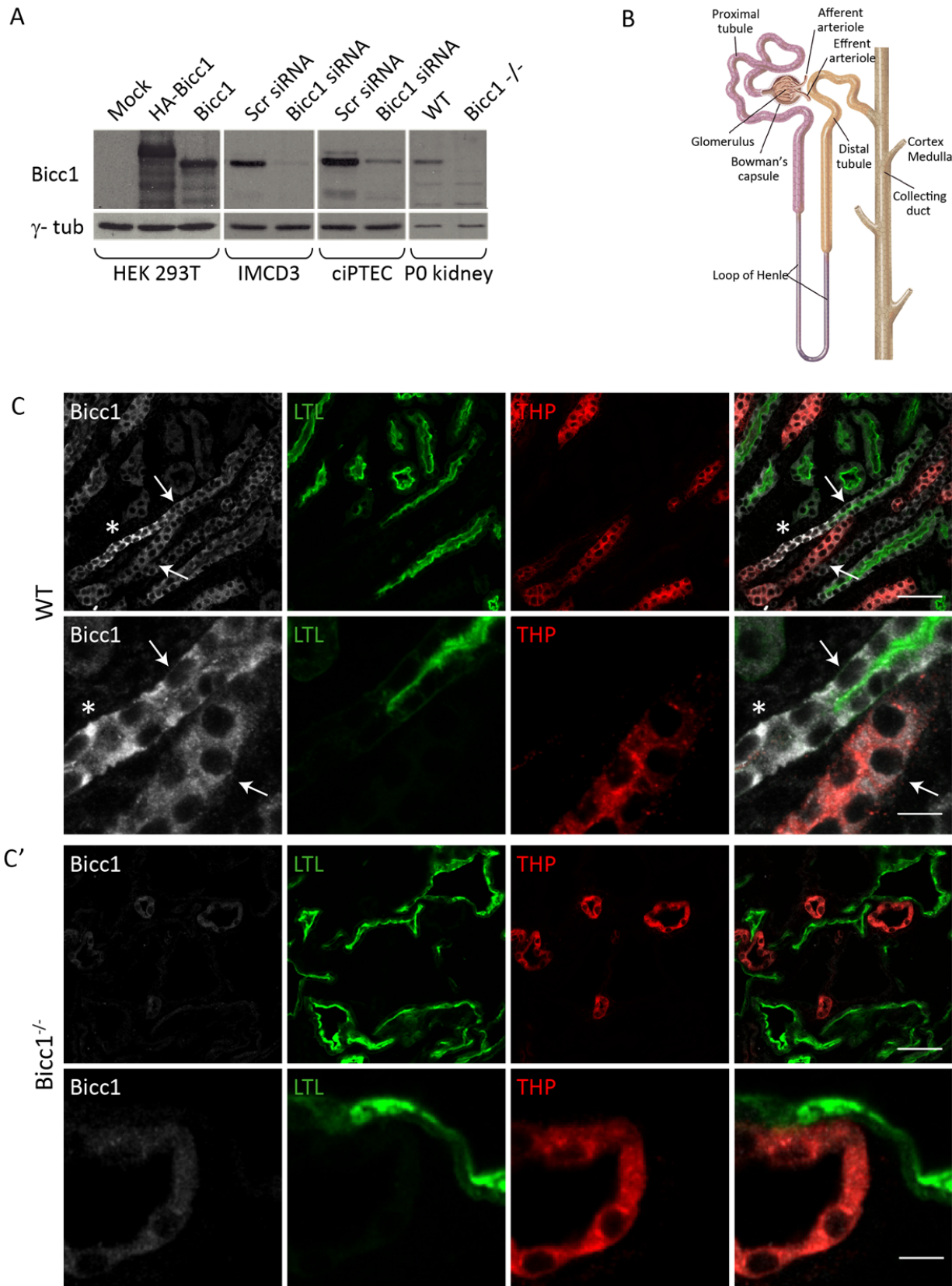
Figure 11. Bicc1 is expressed along the entire nephron. (A) *Characterization of a polyclonal anti-Bicc1 SAM domain antibody. Western blot of Bicc1 in HEK 293T cells expressing HA-tagged Bicc1, of endogenous Bicc1 in IMCD3 and ciPTEC cells and in extracts of WT and Bicc1$^{-/-}$ newborn kidneys. Panel A is courtesy of Nathalie Piazzon.* ***(B)*** *Schematic of a nephron.* ***(C, C')*** *Expression profiles of Bicc1 protein in newborn WT (C) and Bicc1$^{-/-}$ (C') kidneys. Regions of interest are shown at higher magnifications in the bottom row of C & C'. Frozen sections were co-stained with anti-SAM Bicc1 antibody (white), the proximal tubule marker Lotus Tetragonolobus lectin (LTL, green), and Tamm-Horsfall protein (THP, red) which marks the ascending loop of Henle. (C) Kidney cross-section of WT mice at stage P0 showing a proximal tubule connected to the loop of Henle. Intermediate levels of Bicc1 expression are observed in the proximal tubules (top arrow) and ascending loop of Henle (bottom arrow). The two segments are separated by the descending loop of Henle (*) which displayed elevated Bicc1 immunostaining. (C') Bicc1$^{-/-}$ kidneys were used to confirm antibody specificity. Scale bars: 50 µM (top row: C, C'), 10 µM (bottom row: C, C')*

4.1.2 Polycystic kidney disease phenotype in Bicc1$^{-/-}$ mice

The mutant *Bicc1* allele in *jcpk* mice expresses a shortened and abnormal transcript causing severe ADPKD, characterized by the development of cysts in all segments of the nephron (Flaherty et al. 1995). Similar to the *jcpk* mouse, two different mouse models of *Bicc1$^{-/-}$* developed severely enlarged kidneys at birth (P0), with cysts arising predominantly from the Bowman's capsule and proximal tubules (Tran et al. 2010; Piazzon et al. 2012). To identify the origin of renal tubular cysts at P0 in detail, segment-specific markers were analyzed. Immunofluorescent pictures of the entire kidneys were acquired by confocal microscopy with a motorized stage, which allowed creating a tiled scan of the whole specimen. Stitching of the multiple tiled images enabled the direct reconstruction of the whole kidney. In post-natal kidneys, cysts were derived from glomeruli and proximal tubules stained with LTL (Fig. 12A). To a lesser extent, cysts were also observed in the ascending limb of Henle and collecting ducts marked by THP, respectively DBA (Fig. 12B,C). THP and DBA positive cysts were usually smaller in size than the ones observed in proximal tubules. Several collecting ducts and ascending limb of Henle were still intact and displayed a normal shape. In the large central cysts disconnected LTL staining was observed in the epithelial cells suggesting that those structures are losing their proximal fate. Epithelial cells lining the cysts from all segments lost their cuboidal shape and adopted a more squamous appearance (Figs. 11A & 12).
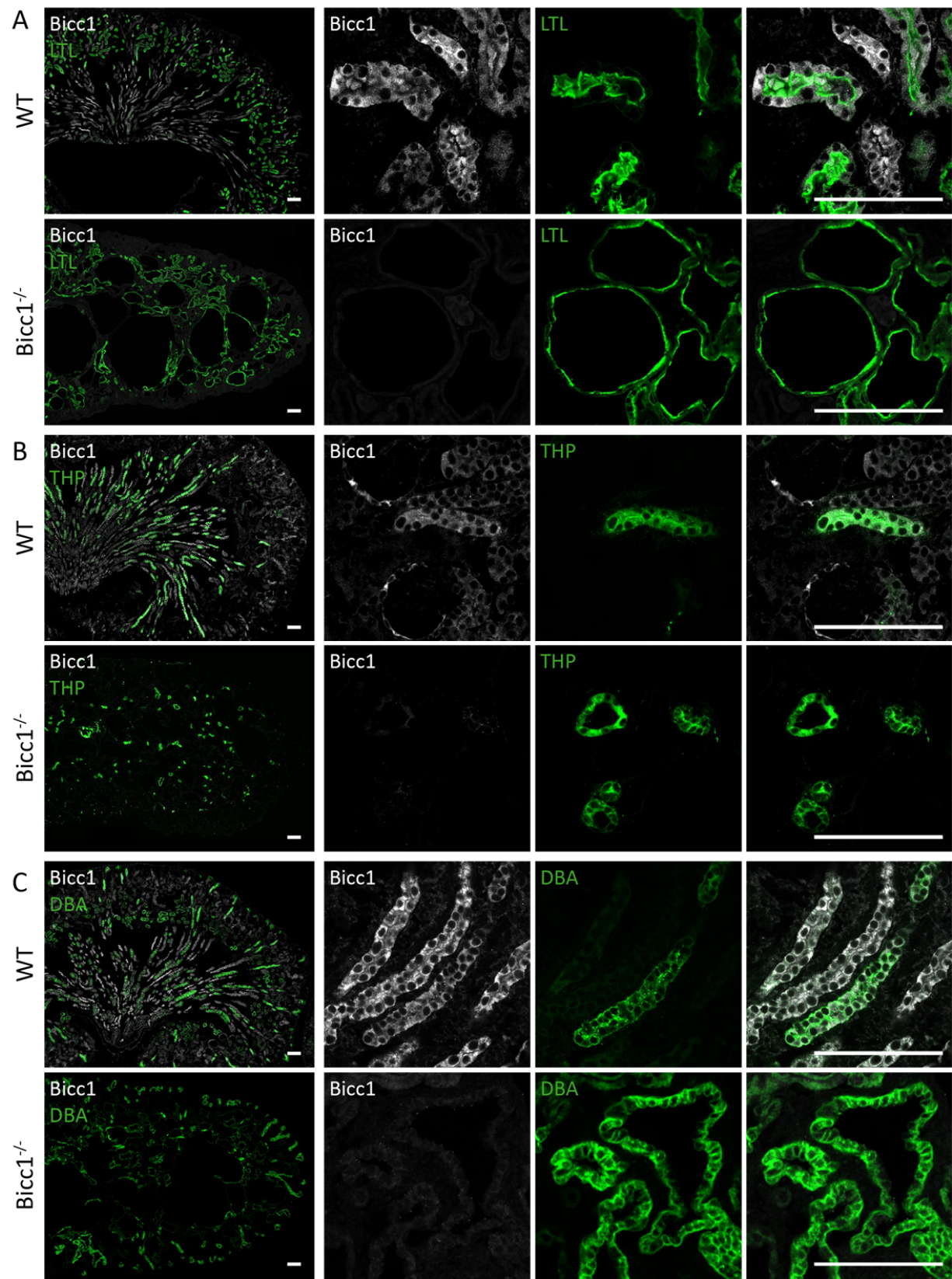
Figure 12. Cyst formation in Bicc1^{-/-} mutant kidneys. (A-C) *Frozen sections were immunofluoresently co-labeled with anti-SAM Bicc1 antibody (white), (A) LTL (green) a marker for proximal tubules, (B) THP (green) a marker for the ascending loop of Henle, and (C) DBA (green) which stains collecting ducts. Regions of interest are shown at higher magnification on the right. In addition to its expression in proximal tubules and ascending limb of Henle, Bicc1 is found in collecting ducts. The majority of cysts in Bicc1 ^{-/-} kidney develop in proximal tubules. In contrast, fewer cysts of modest size express markers of the ascending loop of Henle or collecting duct at this stage (P0). Scale bars: 100 µM.*

4.1.3 Bicc1 expression in adult kidneys

To validate Bicc1 expression in adult kidneys, we co-stained kidney cross sections of three month and one year old WT animals with LTL and THP. Immunofluorescent images of the entire kidney were acquired using confocal microscopy coupled to a motorized stage. In adult kidneys, Bicc1 staining was observed in the cortical and medullary regions, with a complete absence of expression in the renal pelvis (Fig. 13 A,B). Sections labelled with the proximal tubule marker LTL or with the thick ascending limb of Henle marker DBA were used to identify nephron segments. A similar staining pattern of Bicc1 was observed in three month (A) and one year old kidneys (B). Bicc1 exhibited relatively weak and diffuse cytoplasmic expression in proximal convoluted tubules (Fig. 13 A',B'). The strongest labeling was seen in the thick ascending limb of Henle. These results indicate that Bicc1 expression persists during kidney maturation and that Bicc1 is still present in all nephronic segments at adult stage.

4.1.4 Bicc1 is expressed in cholangiocytes

Extra-renal manifestations of PKD include bile duct dilations that potentially lead to ductal cysts in the liver similar to those observed in *Bicc1^{-/-}* mutant animals (Flaherty et al. 1995; Tran et al. 2010). To monitor Bicc1 expression in the liver, we stained frozen sections of P0 old livers by indirect immunofluorescence. Anti-SAM Bicc1 antibody reacted specifically with liver specimen of WT but not *Bicc1^{-/-}* animals (Fig. 13C). Co-labeling with cytokeratin-19, a marker for cholangiocytes, revealed exclusive expression of Bicc1 in the epithelial cells of bile ducts. Similar to renal tubular cells staining of cholangiocytes with Bicc1 revealed a non-homogenous distribution of numerous cytoplasmic puncta (Fig. 13C').

Intriguingly, Bicc1 expression in the kidney and liver is restricted to sites that become cystic in ADPKD patients and animal models of ADPKD, suggesting that Bicc1 likely acts locally within the nephron and cholangiocytes to prevent kidney cyst formation and bile duct dilation.
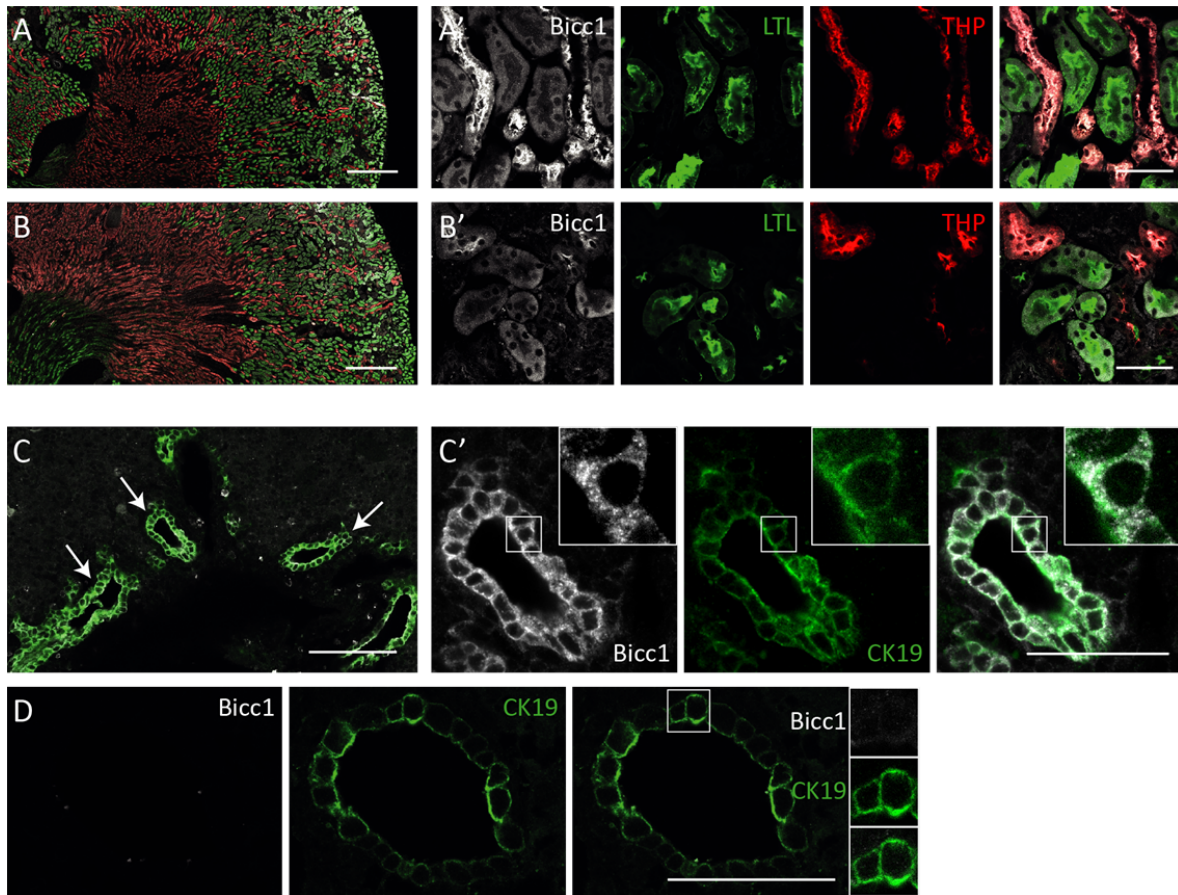
Figure 13. Bicc1 expression profiles in adult kidney and postnatal liver. *Co-immunofluorescent staining on frozen cross-sections of 3-month old **(A, A')** and 1-year old **(B, B')** WT kidneys with anti-Bicc1 SAM antibody, LTL (proximal tubules), and THP (ascending loop of Henle). Cortical regions are shown at higher magnification on the right (A', B'). Bicc1 expression in 3-month and 1-old kidneys was seen in similar regions. **(C, D)** Frozen section of liver portal tract at P0 of WT (C) and Bicc1$^{-/-}$ (D) mice labelled with anti-Bicc1 and anti-CK19 antibodies. Cytokeratin 19 (CK19) acts as a bile duct marker and stains an intermediate filament protein of epithelial tissues. CK19 co-staining reveals that Bicc1 expression in the liver is exclusive to cholangiocytes. Arrows: bile ducts. **(C')** Magnified view of a bile duct. Scale bars: 500 µm (A,B), 100 µm (C), 50 µm (A'-C', D).*

4.2 Regulation of the RNA binding protein Bicaudal- C by the ankyrin repeat protein Inversin

4.2.1 Bicc1 localizes to the primary cilium

The theory of ciliopathy describes a concept that the pathogenesis of a heterogeneous group of diseases relates to dysfunction of the primary cilium. Ciliopathies cover a large spectrum of often overlapping phenotypes ranging from relatively mild and tissue-restricted pathologies to severe defects in multiple organs. The clinical phenotypes include cystic kidney disease, retinal degeneration, mental retardation, obesity and diabetes. A common feature of those disorders is that the disease-relevant gene product functions at the level of the cilium-centrosome complex (Hildebrandt et al. 2011). We therefore asked whether a pool of endogenous Bicc1 may localize to cilia.

Primary cilia were visualized in mIMCD3 cells that were cultured at high confluency to promote the formation of cilia in a polarized epithelial monolayer. Under those conditions, Bicc1 localized to the primary cilium as shown by co-staining with the axonemal marker Arl13b (Fig. 14A). To test the specificity of the anti-SAM Bicc1 antibody we depleted Bicc1 by RNAi. Ciliary Bicc1 staining was lost completely and cytoplasmic staining was reduced (Fig. 14B). siRNA mediated knockdown of Bicc1 in mIMCD3 cells was further validated in Western blot experiments. In different mammalian cell lines as well as in the left-right organizing center of mouse embryos, primary cilia also harbor the protein Invs (Shiba et al. 2009; Sang et al. 2011). Given the phenotypic overlap between *inv/inv* and *Bicc1$^{-/-}$* mutant mice, we hypothesized that Invs may be required to recruit Bicc1 to the cilium or vice versa. mIMCD3 cells were transfected with siRNA against Invs and grown to a polarized epithelial cell layer. We found that Bicc1 failed to localize to the cilium in the absence of Invs shown by co-labeling with the ciliary marker acetylated tubulin (Fig. 14A). Depletion of Invs by RNAi was confirmed by quantitative real time PCR (qRT-PCR) (Fig. 14C). Ciliogenesis in polarized mIMCD3 cells was not affected by the transfection of siRNA against Bicc1 or Invs.
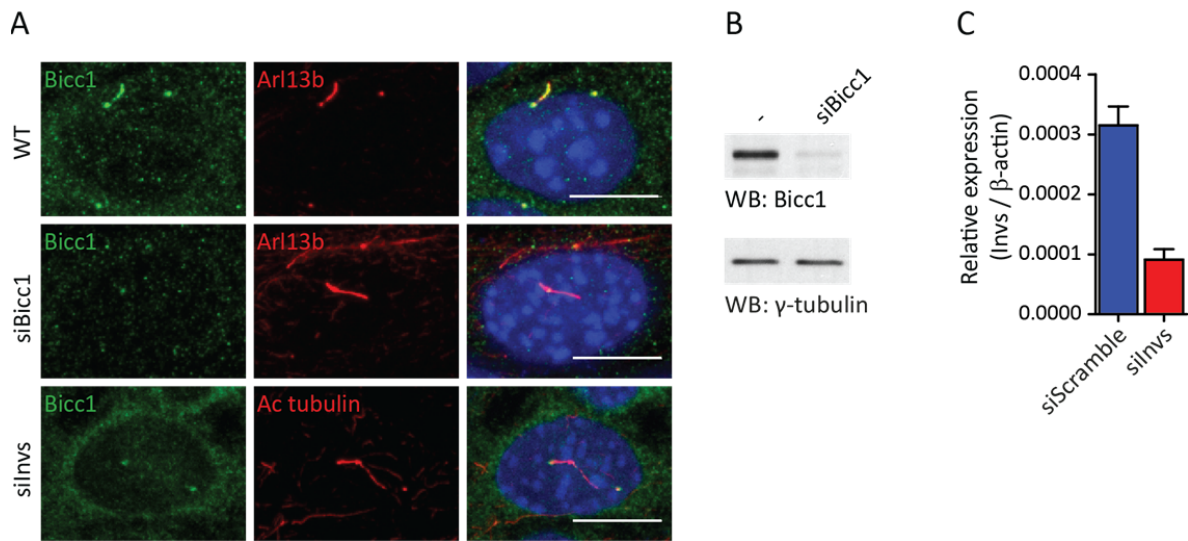
Figure 14. Endogenous Bicc1 in inner medullary collecting duct (IMCD)-3 cells localizes in part to the primary cilium. (A) Cilia in IMCD3 cells were immunostained for Arl13b and acetylated α-tubulin (red). Endogenous Bicc1 (green) is detected in the ciliary axoneme and in cytoplasmic puncta (top row). Bicc1 antibody staining was inhibited in cells transfected with siRNA against Bicc1, confirming specificity (middle row). Targeting of Bicc1 to the cilium was lost in Invs depleted cells (bottom row). (B,C) Efficiency of siRNA-mediated knockdown of Bicc1 (B) or Invs mRNA (C). Expression of Bicc1 was assessed in Western blot experiments. Depletion of the Invs gene was compared to non-targeting siRNA (siScramble) and validated using qRT-PCR in 4 independent experiments. Scale bars: 10 μm (A).

4.2.2 Inversin recruits Bicc1 to the cilium

To further characterize the subcellular localization of the Bicc1 protein *in vivo*, kidney sections of postnatal mice were stained with the axonemal cilia marker Arl13b. Immunofluorescent microscopic analysis revealed that Bicc1 localized to the cilium of tubule epithelial cells as indicated by its co-localization with Arl13b (Fig. 15A). Probing *Bicc1*$^{-/-}$ mutant kidneys with anti-SAM Bicc1 antibody resulted in low background staining in all subcellular compartments. Interestingly in WT animals, the Bicc1 ciliary signal in renal epithelial cells is confined to a proximal segment of the primary cilium. Many protein products of genes linked to cystic kidney diseases do not localize to the whole ciliary axoneme but to defined subregions or to basal bodies (Sang et al. 2011). The localization of Bicc1 in the proximal axoneme was reminiscent to the one observed for the Invs protein. The *inv/inv* mutant mouse displays *situs inversus* associated with multiple renal cyst, and mutations in the human *INVS* gene was later found to cause NPHP2 (Yokoyama et al. 1993; Mochizuki et al. 1998; Morgan et al. 1998; Otto et al. 2003). To determine whether Bicc1 localizes to the Invs compartment, we used the Invs-GFP transgenic mouse model. Expression of a GFP-tagged full-length Invs transgene in *inv/inv* mutants rescues all *inv*-associated

phenotypes and the mice are able to grow normally (Watanabe et al. 2003). Invs-GFP in those mice also correctly localized to a portion of the cilia shaft adjacent to the transition zone, a region termed as the 'Inversin compartment' (Shiba et al. 2009). Kidney sections of GFP-Invs mice were co-labelled with Bicc1 and the ciliary marker Arl13b. Invs-GFP primarily localized to the proximal part of the ciliary axoneme in tubular renal epithelial cells as previously observed in node cells (Watanabe et al. 2003). Furthermore, the Bicc1 staining perfectly overlapped with GFP signal, indicating that in the primary cilium Bicc1 is exclusively recruited to the Invs compartment (Fig. 15A). The sizes of the Invs and Bicc1 compartments as well as the ciliary length were measured from immunofluorescently labelled three dimensional images. While a strong size correlation was observed between the Invs compartment and the Bicc1 staining (Fig. 15B), the lengths of the Bicc1 and Invs segments did not correlate with the length of the ciliary axoneme (Fig. 15 C,D).

The mechanisms that establish the Invs compartment are currently unknown. Since two components, NPHP3 and NEK8 are known to be recruited in an Invs-dependent manner (Shiba et al. 2010), we studied whether Invs expression is similarly required for the intra-ciliary localization of Bicc1. Co-staining of *inv/inv* mutant kidney sections with anti-Bicc1 and anti-Arl13b antibodies revealed that specific localization of Bicc1 to the Invs compartment was completely lost, although cytoplasmic Bicc1 staining remained intact (Fig. 15A). Expression of the Invs-GFP transgene in *inv/inv* mutant mice rescued the Bicc1 ciliary phenotype. The mean intensity of the Bicc1 signal was quantified in each cilium of WT and *inv/inv* mutant renal epithelial cell and was significantly reduced *inv/inv* mutant cilia (Fig. 15E). However, a faint signal above background level could still be detected when compared to kidney sections not immunofluorescently labelled with anti-Bicc1 antibody. Lack of ciliogenesis could be ruled out as the underlying cause of cyst formation, since all genotypes demonstrated renal monocilia in epithelial cells. Also the length of the ciliary axoneme was similar in the different genotypes indicating that cilia-length control was unaffected (Fig. 15F). These results suggest that Bicc1 localizes to the proximal ciliary axoneme in an Invs-dependent fashion.
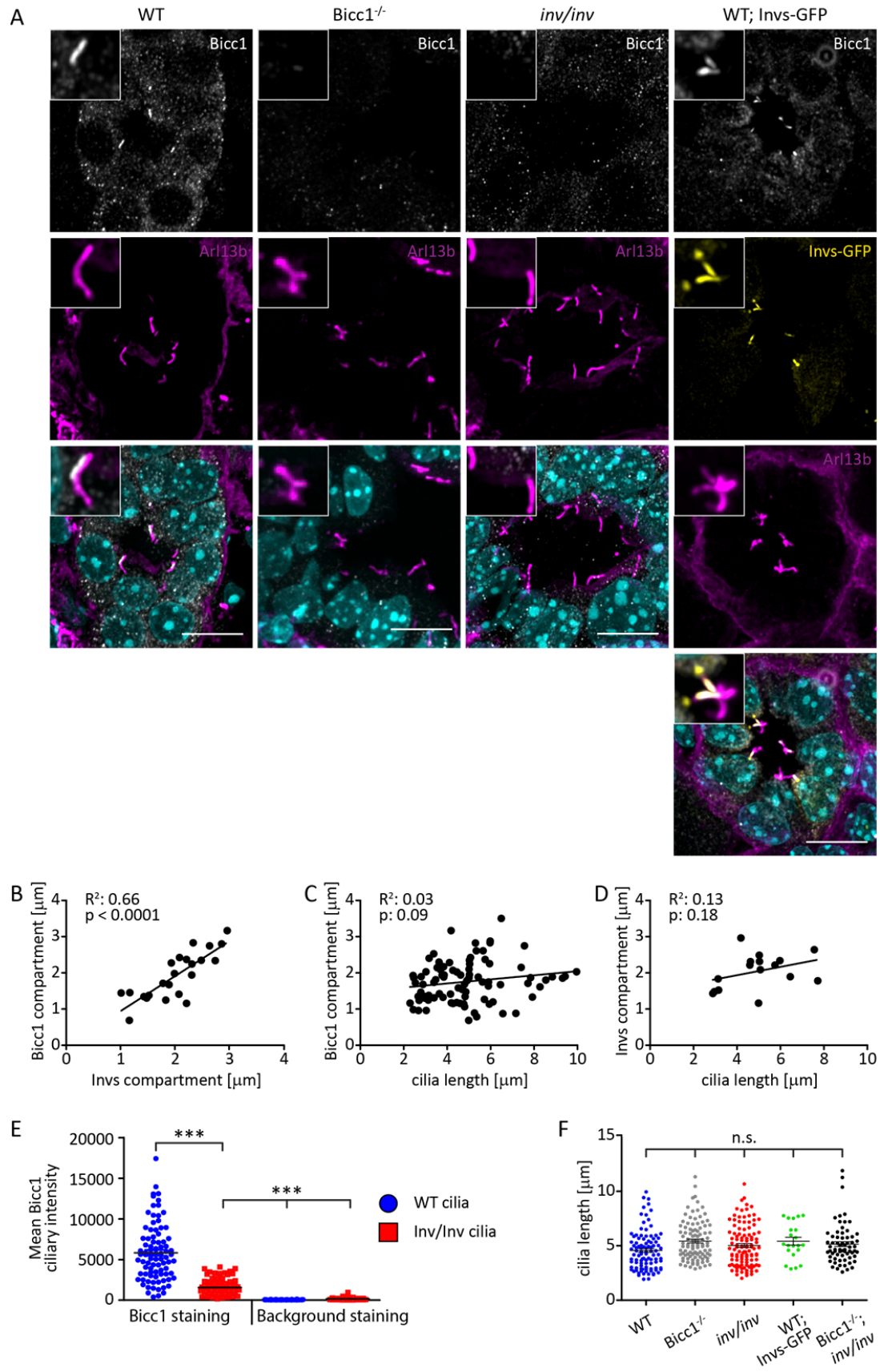
Figure 15. Bicc1 ciliary localization is regulated by Invs in vivo. (A) *Immunofluorescent staining of Bicc1 in renal tubules. Bicc1 (white) localizes in part to cilia (Arl13b, magenta) in WT renal epithelial cells (first row). Bicc1 antibody specificity was confirmed in Bicc1$^{-/-}$ animals (second row). Mutant inv/inv mice either completely lack or show reduced Bicc1 expression in ciliary axonemes (third row). In primary cilia of Invs-GFP transgenic mice, GFP fluorescence (yellow) defines the so-called Inversin compartment at the proximal region of the cilium (fourth row) (Watanabe et al. 2003). Co-staining of Arl13b revealed that Bicc1 co-localizes with Invs-GFP at the base of the cilium. (B-D)* *Linear regression analysis to determine the relationship between the Bicc1 and GFP-Invs compartments on the same cilium (B) or among the length of cilia and its corresponding compartments (C,D), each represented by a circle. The length of the cilium and the different compartments were assessed by IMARIS software. The black line represents linear regression. A positive correlation was only observed between the lengths of Bicc1 and GFP-Invs, but not between the compartments and the cilium itself (P< 0.0001). (E)* *The mean intensity of Bicc1 was measured for each cilium in WT vs inv/inv mutant kidneys (n=3 animals). Ciliary staining of kidney sections without anti-Bicc1 SAM primary antibody served as background control (right side). Bicc1 expression is reduced in the ciliary axoneme of inv/inv mice, but is not completely absent when compared to the background control staining. ***P< 0.0001 (one-way ANOVA). (F)* *Each circle represents a cilium of a renal epithelial cell, and its length was assessed by IMARIS software. Mean cilia lengths are constant, irrespective of the genotypes (n=3 animals per genotype). Scale bars: 50 µm (A).*

4.2.3 Bicc1 and Invs form a complex

To validate an interaction between Bicc1 and Invs, and investigate potential mechanism possible at the level of canonical Wnt/β-catenin signaling, we first analyzed *in vitro* co-localization. Immunostaining of Flag-tagged Invs transfected cells revealed a punctate distribution similar to the one previously described for HA-tagged Bicc1 (Maisonneuve et al. 2009), although less than 10% of cells stained positive in mIMCD3 cells. By comparison, control cells transfected with GFP alone showed 50% of transfection efficiency, suggesting that Invs may fail to stably accumulate under the conditions examined. Invs stability is controlled by two destruction boxes (D-boxes) which are usually found in regulatory proteins with short half-lives (Simons et al. 2005; Barford 2011). D-Boxes bind to the multimeric anaphase promoting complex, a protein involved in cell cycle progression that selectively targets proteins for proteasomal degradation. Treatment with the proteasomal inhibitor MG-132, which blocks the degradation of ubiquitin-conjugated proteins in mammalian cells, increased Invs protein levels approximately 6-fold in HEK 293T cells (Fig. 16A,B). A drawback of MG-132 is its ability to stimulate apoptosis. A substantial fraction of the cells induced apoptosis and died when treated for 24 hours with 10μM MG-132. 12-hour treatment increased the survival rate drastically but a reduction of protein expression (3-4-fold) was the consequence when compared to 24h MG-132 induction (Fig. 16A,B). Do to those disadvantages we abstained from using MG-132 and examined co-localization in the 10% of cells expressing Flag-Invs. mIMCD3 cells and Madine-Darby canine kidney cells (MDCK) seeded at low density were transfected with HA-Bicc1 and Flag-Invs and their subcellular distribution was examined by indirect immunofluorescence in unpolarized cells (Fig. 16C,D). We detected co-localization in cytoplasmic foci in both cell types or in cytoplasmic scaffolds in MDCK cells. Ciliary targeting could not be examined since subconfluent mIMCD3 and MDCK cells do not undergo ciliogenesis at this point.
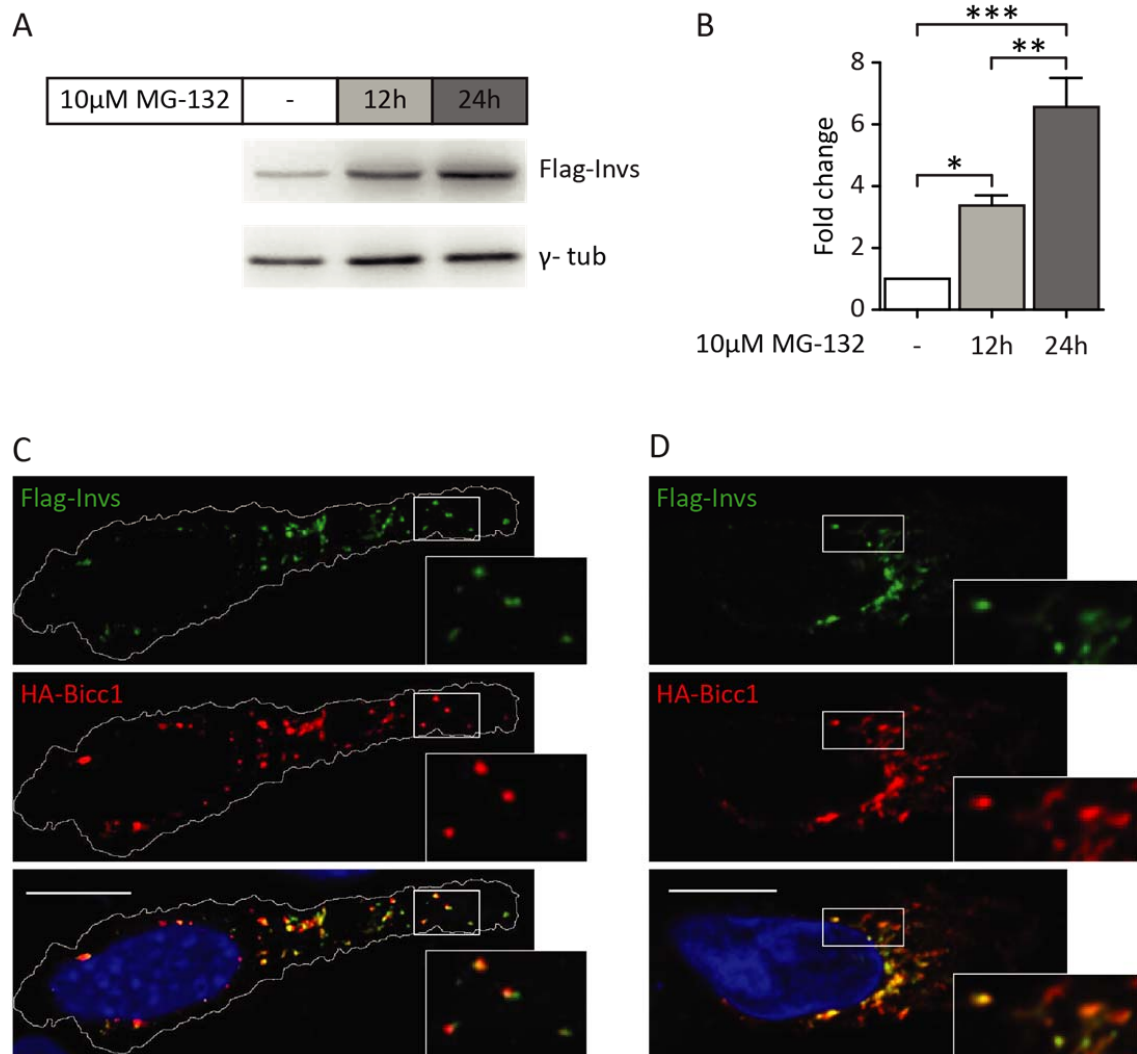
Figure 16. Bicc1 and Invs co-localize in vitro *(A) Western blot of Flag-Invs expression in transiently transfected HEK 293T cells treated with or without the proteasome inhibitor MG-132 (10 µM). MG-132 treatment increases Invs expression levels while reducing cell viability. (B) Quantification of Invs protein expression normalized to γ-tubulin loading control. Invs protein levels increased 3- to 6-fold when treated for 12 or 24 hours, respectively. *P< 0.05; **P< 0.01; ***P< 0.001 (One-way Anova). (C, D) Flag-Invs (green) and HA-Bicc1 (red) were overexpressed in mIMCD3 cells C) or in Madine-Darby canine kidney cells (MDCK; D). Co-localization of the two proteins is observed in cytoplasmic foci (C, D) and cytoplasmic scaffolds (D).*

4.2.4 Bicc1 and Invs interaction is mediated by the KH domains

To further explore whether Invs participates in direct molecular interaction with Bicc1, tagged proteins were co-expressed in HEK 293T kidney cells. Binding of Flag-tagged Invs with HA-Bicc1 was demonstrated in co-immunoprecipitation assays (Fig. 17B). In the reverse experiment, the epitope tagged Invs was co-precipitated with HA-Bicc1. To test a direct interaction between the two proteins, we used a yeast two-hybrid assay in which Invs was fused to the Gal4 activation domain and human BICC1 to the Gal4 binding domain. Invs interacted strongly with Bicc1, in good agreement with the binding observed in co-immunoprecipitation assays (Fig. 17C). GST-pull down experiments were used to identify the subunit within Bicc1 that mediates the interaction with Invs. Flag-Invs was transfected in HEK 293T, and its retention was assessed on glutathion-sepharose beads coated with recombinant GST-KH, GST-IVS, or GST-SAM fusion proteins as baits (Fig. 17A). While full length Flag-Invs weakly bound to GST-KH beads, it failed to interact with beads coated with GST alone, GST-IVS, or GST-SAM (Fig. 17D). This interaction was verified in yeast two-hybrid mating assay, by fusing the human BICC1 KH domains to the Gal4 binding domain and Invs to the Gal4 activation domain (Fig. 17E). Taken together these data identify a direct interaction between Invs and Bicc1 and suggest that the binding is mediated by the Bicc1 KH domains.
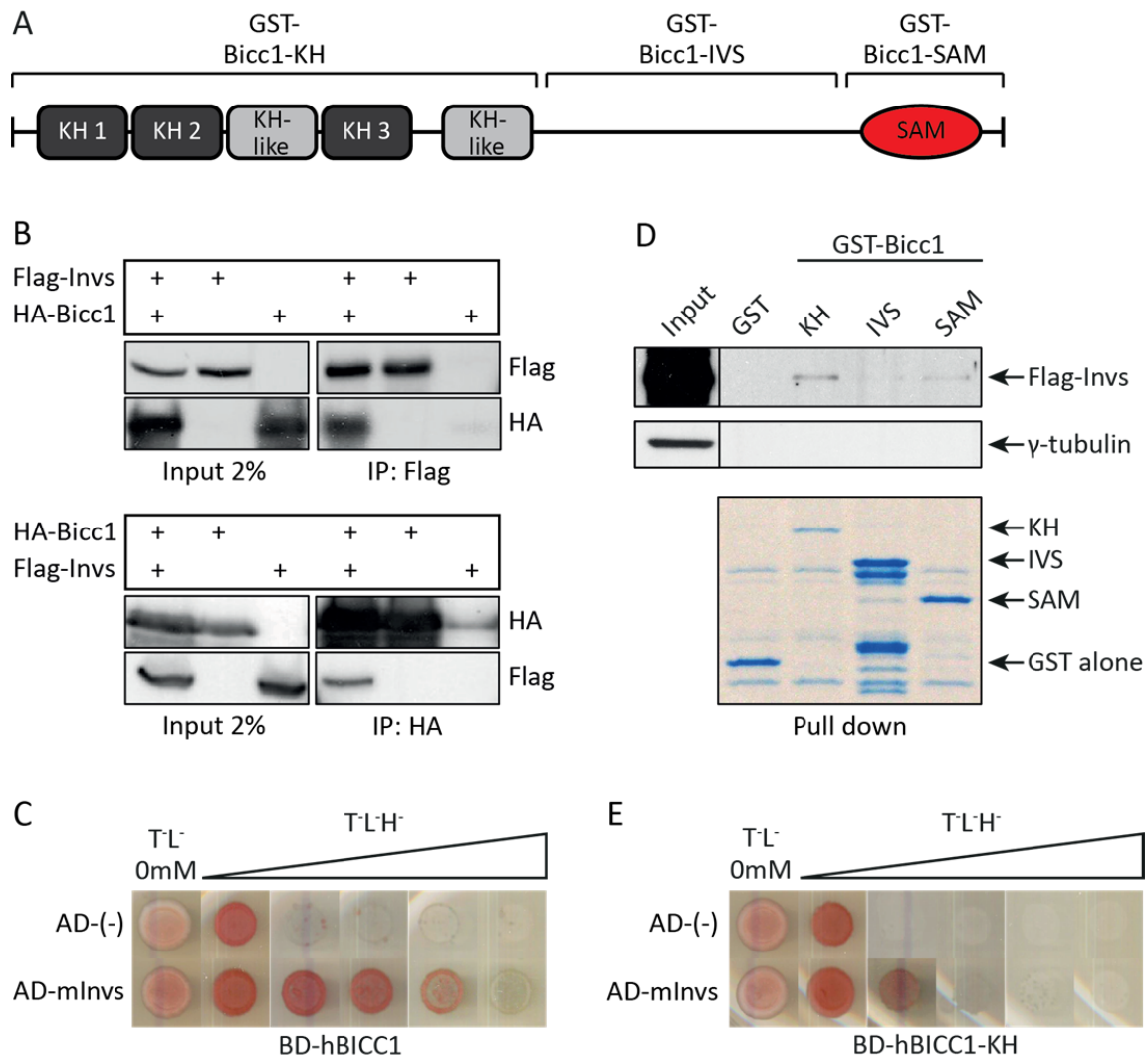
Figure 17. Bicc1 and Invs form a complex mediated by Bicc1 KH domains (A) *Schematic representation of Bicc1 and its truncated fragments fused to Glutathione-S-transferase (GST)* **(B)** *Co-immunoprecipitation of Flag-Invs with HA-Bicc1 in HEK 293T (top) and vice versa (bottom) reveals an interaction between the two proteins.* **(C)** *Yeast two-hybrid analysis of the interaction between hBICC1 fused to the Gal4 binding domain (Gal4-BD) and mInvs fused to the Gal4 activation domain (Gal4-AD). A control was performed with non-fused Gal4-AD. Cells were grown on solid glucose medium containing 3-Amino-1,2,4-triazol (3AT) at a 1, 2, 5, 10, 20 mM concentration, but lacking tryptophan and leucine (−TL) or tryptophan, leucine and histidine (−TLH), respectively. 3AT is competitive inhibitor of the HIS3 reporter gene product, and the presence of colonies is indicative of a protein–protein interaction.* **(D)** *The KH domains, the IVS, and the SAM domain of mouse Bicc1 were fused to GST to assess Flag-Invs binding in pull down assays (top panel). Glutathione sepharose beads coated with recombinant GST alone (control) or GST-Bicc1 truncated polypeptides were incubated with HEK 293T cell extracts. Bicc1-KH domains are sufficient to pull down Flag-Invs (A, top panel). Lack of interaction with γ-tubulin indicates specificity of the assay (middle panel). The coomassie-stained gel of the GST-fusion proteins used in this pull-down assay is shown below. 10% of total cell extracts were loaded as input.* **(E)** *Interaction between the HsBICC1 KH domains fused to Gal4-BD domain and mInvs fused the Gal4-AD in yeast two-hybrid assays. The yeast two-hybrid analysis was performed as in (C).*

45

4.2.5 Invs inhibits Bicc1 induced silencing activity

The KH domain is an evolutionary conserved sequence motif that is typically found in multiple copies on the same protein and is implicated in RNA recognition (Valverde et al. 2008). KH domain-containing proteins are involved in different aspects of RNA metabolism, including RNA stability and translation. Bicc1 has been shown to bind its own RNA via the KH domains, and *Drosophila* Bic-C regulates its own expression by binding specific segments of the 5'UTR (Chicoine et al. 2007; Bouvrette et al. 2008). More recently, it was described that Bicc1 interacts with AC6 and PKIα mRNAs and with precursors of specific cognate miRNAs (pre-miR125, respectively pre-miR27) to enable their incorporation into miRNA-induced silencing complexes (miRISC) with Argonaute (AGO) and TNRC6 (Piazzon et al. 2012). The interaction of KH domains with Invs raised the question of influence on RNA binding and silencing activity, and we hypothesized that Invs regulates Bicc1 activity. To test this, we first monitored the effect of Invs on 3'UTR luciferase reporters of PKIα mRNA in HEK 293T cells. Expression of Bicc1 alone inhibited the reporter mRNA as expected. Conversely, co-expression with Invs inhibited the Bicc1 induced silencing of the PKIα luciferase reporter (Fig. 18A). Subsequently, we assessed whether Invs blocks the interaction of Bicc1 with target mRNA in HEK 293T cells. RT-PCR analysis revealed that HA-tagged Bicc1 co-immunoprecipitates endogenous AC6 and PKIα mRNA and their cognate miRNAs miR-125, respectively miR-27 as well as its own mRNA, whereas binding to β-actin control mRNA was below detection limits (Fig. 18B). In contrast, co-expression of Flag-Invs abolished the interaction with target mRNAs and miRNAs.

Bicc1 similar to Invs is able to inhibit the canonical Wnt/β-catenin signaling pathway at the level of Dvl, although without promoting cytoplasmic Dvl1 degradation (Simons et al. 2005; Maisonneuve et al. 2009). To further examine the Bicc1/Invs interaction we tested its effect on a TCF/LEF-1 dependent luciferase reporter construct (TOPflash). Both Bicc1 and Invs inhibited the Dvl-2 induced canonical Wnt signaling activity, and when co-expressed they demonstrated an additive effect, suggesting that they act in a parallel rather than a common pathway (Fig. 18C). To conclude, Invs binds Bicc1 KH domains and thereby inhibits Bicc1-induced silencing on target mRNAs *in vitro*.
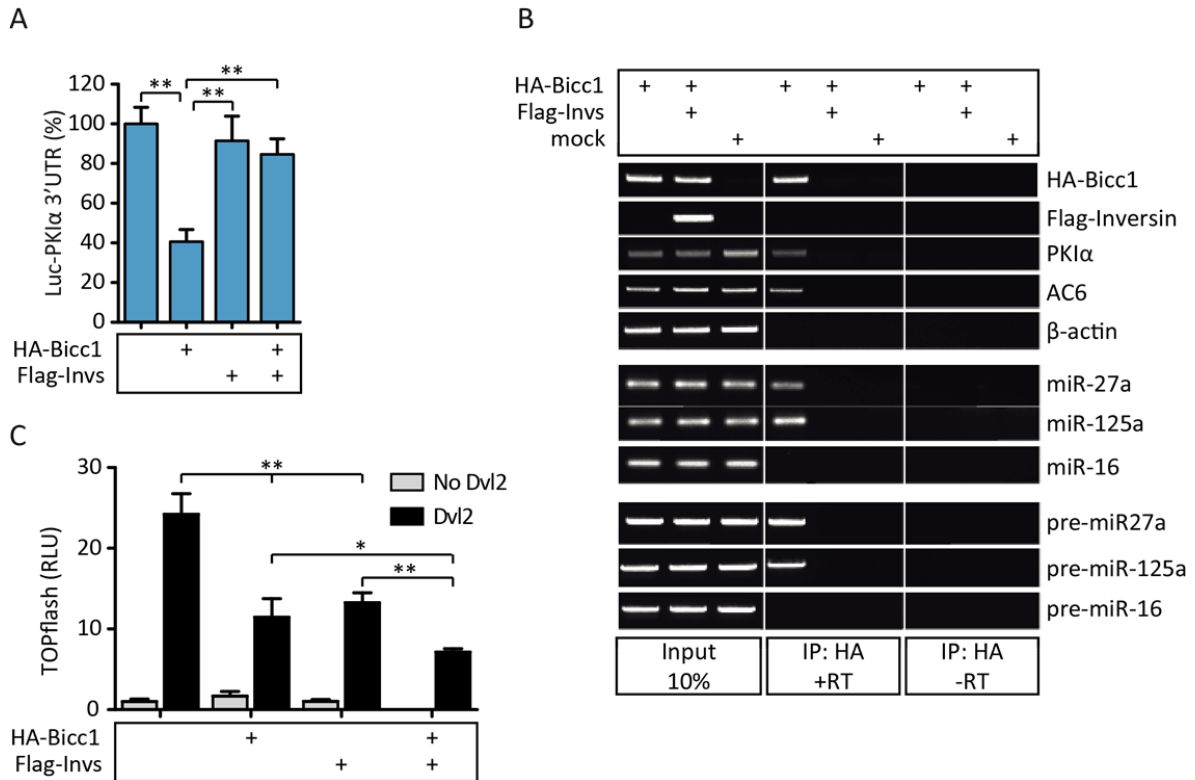
Figure 18. Invs inhibits Bicc1-mediated gene silencing by blocking its association with RNA (A) *Activity of luciferase reporter containing the PKIα 3'UTR in HEK 293T cells co-transfected with HA-Bicc1 and/or Flag-Invs. ß-galactosidase was used as control for normalization. **P< 0.01 (student t-test). **(B)** RNA co-immunoprecipitation. RT-PCR analysis of PKIα and AC6 mRNA and of associated miRNA in immunoprecipitates of HA-tagged Bicc1 in HEK 293T cells. Binding of HA-Bicc1 to target mRNA and miRNA was abolished when coexpressed with Flag-Invs. **(C)** Both Bicc1 and Invs diminish Dvl2-induced activation of the canonical Wnt TCF/LEF-1 dependent luciferase reporter (TOPflash) in HEK 293T cells. Combined expression leads to a further suppression of luciferase activity. Reporter activity was normalized to ß-galactosidase expression. *P< 0.05; **P< 0.01 (student t-test).*

4.2.6 Bicc1 targets are downregulated in inv/inv kidneys

Given the protein-protein interactions described above, we wished to validate whether Invs negatively regulates Bicc1 activity *in vivo*. AC6 and PKIα expression have previously been shown to be upregulated in cystic kidneys of *Bicc1*^{-/-} knockout mice (Piazzon et al. 2012). Ddx5, Atp6v1b1, and Dpy30 were identified as xBic-C targets in *Xenopus*, by RNA-coimmunoprecipitation of xBic-C followed by deep sequencing (Zhang et al. 2013). xBic-C mediated repression was then validated in animal cap assays by injecting target 3'UTR luciferase reporters and xBic-C mRNA into *Xenopus* embryos. Protein expression of some of these previously reported Bicc1 targets was analyzed in post-natal kidney extracts of *inv/inv*
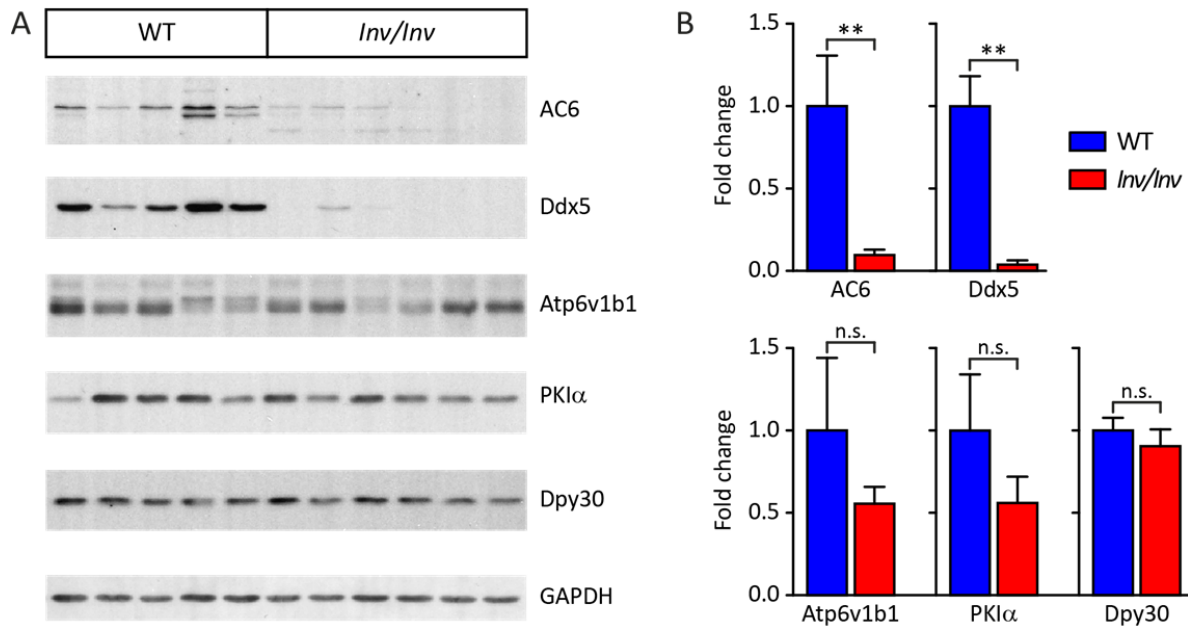
Figure 19. Expression of Bicc1 targets in inv/inv mutant kidneys. *(A) Western blot analysis of AC6, Ddx5, the ATPase subunit B1 (Atp6v1b1), PKIα, and Dpy30 in P0 old kidneys of the indicated genotypes. (B) Protein levels in (A) were normalized to GAPDH and calculated as fold change compared to WT expression. Both AC6 and Ddx5 show decreased expression in inv/inv mutant mice. **P< 0.01 (student t-test).*

mice and WT littermates. AC6 and the DEAD box RNA helicase (Ddx5) are markedly reduced *inv/inv* mutants (Fig. 19). The expression of Atp6v1b1, the B1 subunit of the vacuolar ATPase (V-ATPase) and PKIα are not significantly down-regulated and displayed variable levels among *inv/inv* and WT animals. However, a trend of reduction in *inv/inv* kidney could be observed. No difference in protein levels was detected for Dpy30 a component of the Set-1 like histone methyltransferase complex.

These results suggest that unopposed Bicc1 activity in *inv/inv* KO mice leads to a decrease of target gene expression as observed for AC6 and Ddx5. The consistent expression of Dpy30 may reflect regulatory differences between animal models and that Bicc1 is not involved in repressing Dpy30 in mice.

4.2.7 Reduced cAMP signaling in *inv/inv* mutant kidney

Increased renal accumulation of cAMP is a common feature in most if not all models of ADPKD and ARPKD and attributes to renal cyst expansion (Torres and Harris 2014). It has been suggested that a reduction in intracellular Ca^{2+}, as a consequence of mutation in PC1 or PC2, activates the calcium-inhibitable AC6 and decreases the activity of calcium-dependent PDE1. A combination of the two may

lead to elevated levels of cAMP. Cyclic AMP regulates target gene expression in part through PKA-mediated phosphorylation of the transcription factor cAMP response element–binding protein (CREB). Recently, Bicc1 has been implicated to act directly in the cAMP/PKA signaling pathway in part by regulating AC6 and PKIα translation (Piazzon et al. 2012). It was shown that Bicc1 is required to curb cAMP synthesis and increased cAMP levels and expression of its synthetic enzyme AC6 were observed in *Bicc1*^{-/-} kidneys. We evaluated whether the reduction of AC6 protein observed in *inv/inv* mutant kidneys affects cAMP activity *in vivo*. Immunohistochemical analysis of phosphorylated CREB (pCREB) levels in kidney sections of postnatal mice showed decreased nuclear expression in *inv/inv* animals compared to WT littermates (Fig. 20A). In contrast, *Bicc1*^{-/-} kidneys exhibited increased nuclear staining of pCREB in cyst lining cells. Interestingly, co-labeling with specific lectins demonstrated that cAMP activation was confined to collecting ducts and was almost completely absent in cysts arising from proximal tubules, regardless of the genotype or cyst burden. To validate those observations, high resolution images of the entire kidney were acquired by confocal imaging with a motorized stage and stitched together as described above. A careful examination of the images showed that pCREB is exclusively found in the nucleus, irrespective of the genotype. A DAPI staining mask was generated and used to define the nuclear regions of interests to measure the mean signal intensities of pCREB in each nucleus. It was found that PKA activity was generally reduced in *inv/inv* mutant kidneys. The majority of cells did not express pCREB and only a small fraction displayed low nuclear levels (Fig. 20B). Nuclei with medium or high pCREB signals were almost completely absent in those kidneys. In a *Bicc1*^{-/-} cystic kidney, a substantial amount of cells exhibited medium and high levels of pCREB expression, and this fraction was considerably higher compared to WT animals, indicating that PKA signaling is indeed activated. Unfortunately, only one *Bicc1*^{-/-} animal was examined and to validate hyperactivated PKA signaling further kidneys have to be analyzed. However, we showed that *inv/inv* mutant kidneys display low nuclear pCREB levels, suggesting that decreased expression of AC6 inactivates PKA signaling in those animals. Increased cAMP levels are a hallmark of PKD, but they have rarely been studied in animal models of nephronophthisis. The exception is the *pcy* mouse, in which the cystic kidney phenotype is caused by missense mutation in NPHP3, and where renal cAMP levels are elevated. Ciliary localization of NPHP3 is also regulated by Invs (Gattone et al. 2003; Sang et al. 2011), indicating that Invs might control cAMP synthesis by several mechanisms, or that NPHP3 and Invs act together to inhibit Bicc1.
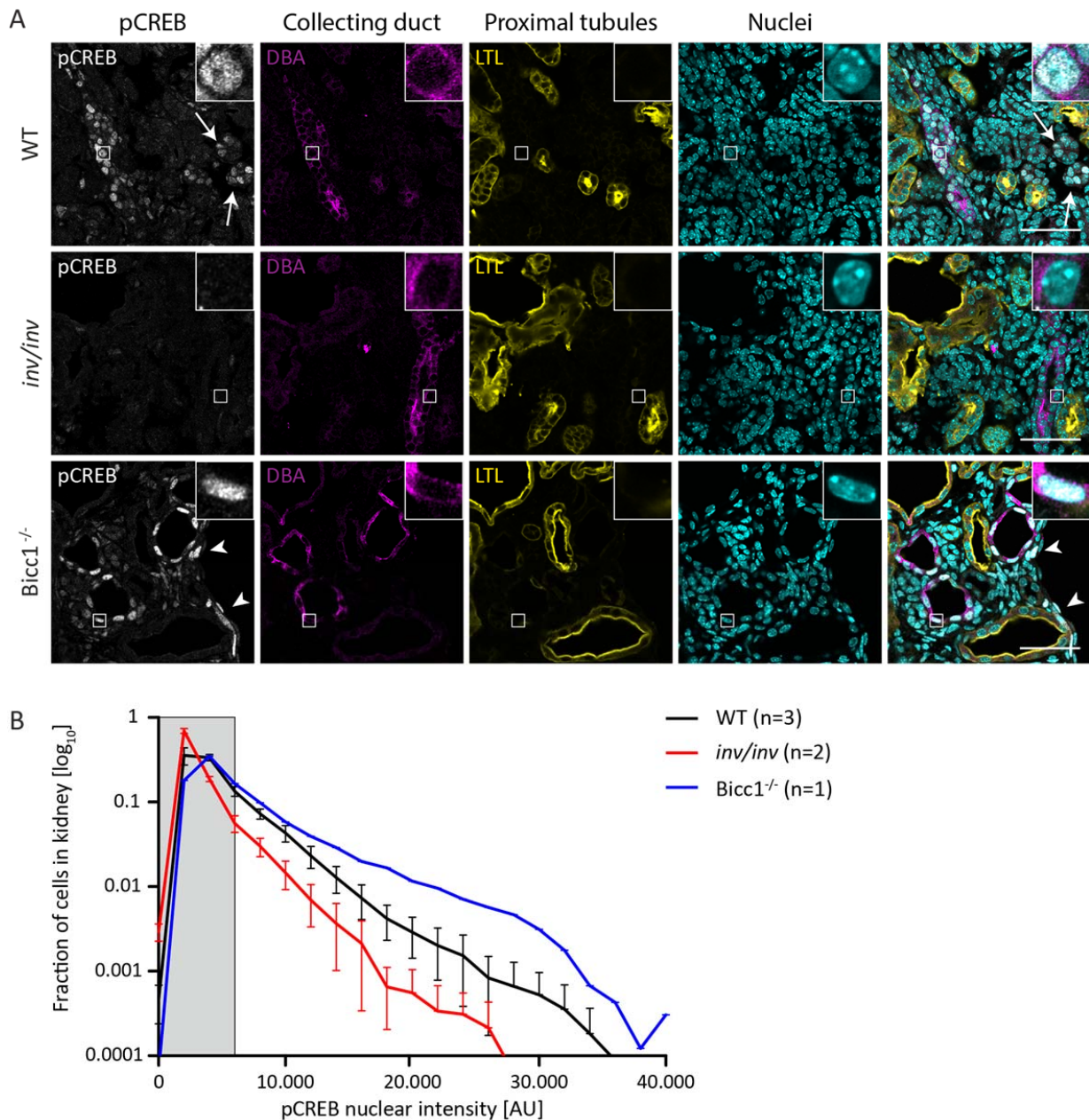
Figure 20. Bicc1 and Invs inversely regulate the PKA phosphorylation of CREB. (A) *Immunostaining of phosphorylated cAMP response element-binding protein (pCREB) at P0 of WT, inv/inv, and Bicc1 KO mice. Nuclei were counterstained with Dapi (cyan). Enlarged images show nuclear staining for pCREB (white). Immunofluorescent staining of pCREB in WT and Bicc1 KO mice revealed nuclear staining in the collecting ducts (DBA, magenta) that is possibly increased in Bicc1 KO animals. pCREB is absent in proximal tubules (LTL, yellow), irrespective of the genotype. By contrast, inv/inv cystic mice barely express nuclear pCREB. Nuclear pCREB staining was also observed in DBA-negative tubules in WT mice (arrow). In Bicc1 KO animals, cyst-lining epithelial cells which were not stained by any kidney tubule marker sporadically showed high nuclear pCREB (arrow heads). **(B)** Frequency distribution of pCREB nuclear expression analyzed by confocal microscopy for each genotype shown in A. Mean nuclear intensities for pCREB were quantified from whole kidney sections in at least 15'000 nuclei per kidney. Grey bar indicates background staining. The numbers of mice of each genotype analyzed are indicated in the histogram and error bars represent SEM. Scale bars: 50 µm (A).*

4.2.8 Combined inactivation of Bicc1 and Invs results in a cystic kidney phenotype resembling Bicc1$^{-/-}$ single mutant kidneys

The above findings argue that Bicc1 acts downstream of Invs in the newly discovered Invs-Bicc1 pathway. To further assess this hypothesis, we analyzed kidneys from mice with inactivation of *Bicc1* and *Invs* alone or in combination. Postnatal kidneys of *Bicc1$^{-/-}$*; *inv/inv* double mutant animals were symmetrically enlarged when compared to *inv/inv* and WT animals but remained reniform similar to *Bicc1$^{-/-}$* single mutants (Fig. 21A-D). Double mutant and *Bicc1$^{-/-}$* mice exhibited severe cystic disease at the same age, whereas inactivation of *Invs* alone resulted in an intermediate polycystic disease severity. Immunohistochemical analysis revealed numerous cysts arising predominantly from proximal tubules. Overall, since the *Bicc1$^{-/-}$*; *inv/inv* kidney phenotype resembles that of *Bicc1$^{-/-}$* mice, it seems possible that cyst progression is mainly driven by the depletion of Bicc1.

Due to the phenotypic overlap between *Bicc1$^{-/-}$*; *inv/inv* and *Bicc1$^{-/-}$* cystic kidneys we hypothesized that in double mutants Bicc1 target gene expression should be identical to *Bicc1$^{-/-}$* and not to *inv/inv* single mutant animals. To validate this conclusion, we monitored renal Ddx5 expression of the different genotypes. Ddx5 RNA helicase plays an important role in multiple aspects of RNA-metabolism, such as pre-mRNA splicing, alternative splicing, rRNA processing, and miRNA biogenesis (Fuller-Pace 2013). Alternatively, it has been found to act as transcriptional co-regulator independently of his helicase activity. Co-staining of kidney sections with anti-Ddx5 antibody and DAPI revealed an exclusive nuclear localization for Ddx5 which is in agreement with previous reports (Fuller-Pace 2013). Immunohistochemistry of WT animals demonstrated positive nuclear Ddx5 staining in proximal tubules (Fig. 21A'). WT mice also showed increased levels of Ddx5 in the nuclei of tubules that are negative for LTL. In *inv/inv* mutant mice, expression of Ddx5 is almost absent, which confirms the results observed by immunoblotting (Fig. 21C'). *Bicc1$^{-/-}$* single and *Bicc1$^{-/-}$*; *inv/inv* double mutant mice displayed increased nuclear Ddx5 expression in cyst-lining cells. Opposite to the pCREB staining, nuclear Ddx5 was upregulated in cysts emerging from proximal tubules as well as in cysts negative for LTL (Fig. 21 B',D'). The overall increase of Ddx5 in all epithelial cells lining the cysts suggests that Bicc1 activity is necessary in all nephron segments to attenuate Ddx5 expression. To validate these observations, high resolution images of the entire kidney were acquired, and the mean signal intensity of Ddx5 in each nuclei was measured as described for pCREB. The nuclear signal quantification confirmed that Ddx5 expression was greatly reduced in *inv/inv* mice: Few cells were weakly stained, and none of the nuclei showed medium or high Ddx5 expression (Fig. 21E). No significant difference was observed between WT, *Bicc1$^{-/-}$* single mutant, and *Bicc1$^{-/-}$*; *inv/inv* double mutant kidneys. In all three genotypes, approximately 50% of the
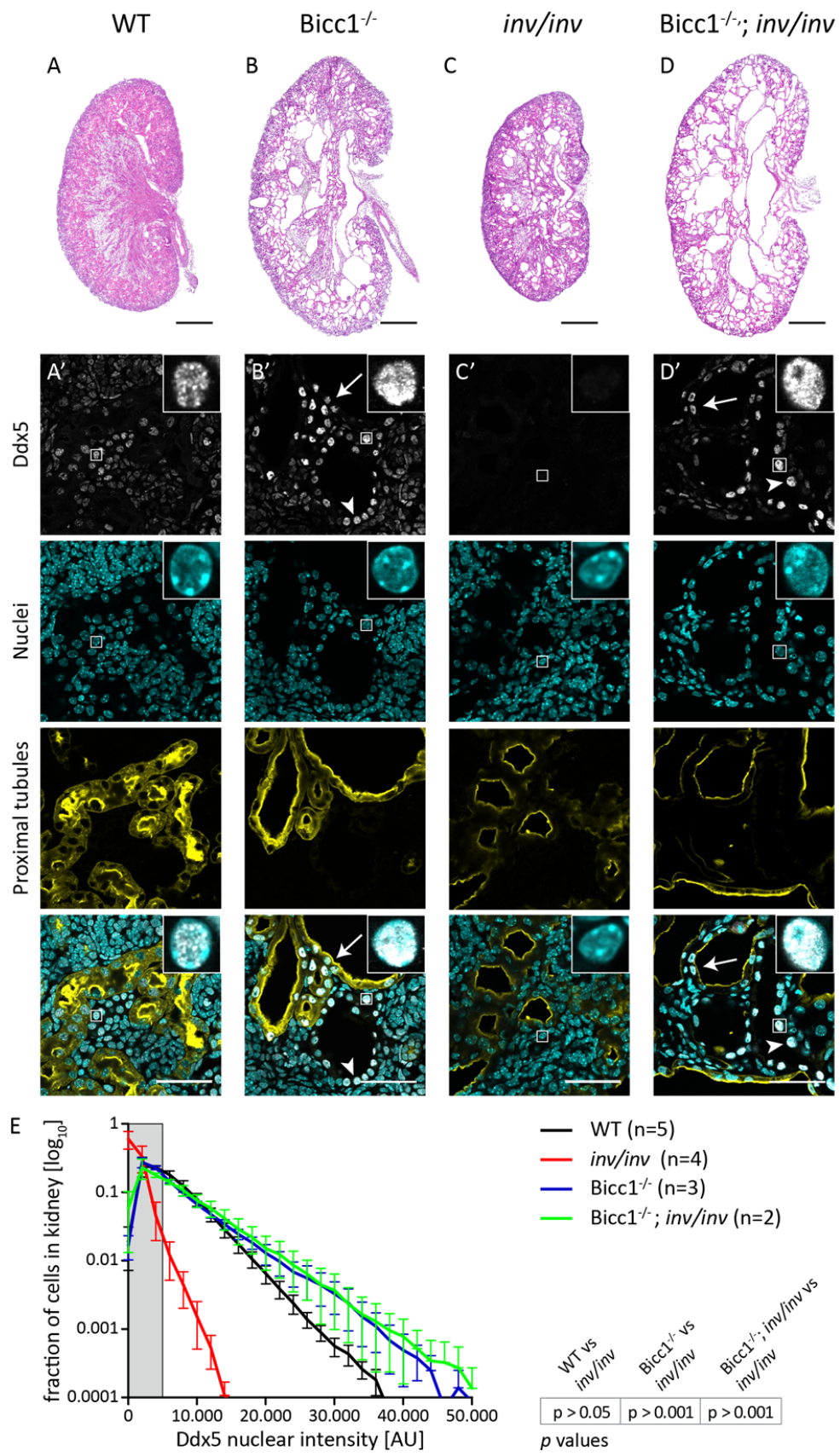
Figure 21. Combined inactivation of Bicc1 and Invs results in a cystic kidney phenotype resembling Bicc1*^{-/-}** ***single mutants. (A-D) *Haematoxylin-Eosin staining of frozen sections of P0 newborn kidneys. Representative images show kidneys from WT (A) and mice lacking Bicc1 (B) or Invs (C) alone, or in combination (D). The size and structure of Bicc1$^{-/-}$; inv/inv mutant kidneys are similar to Bicc1$^{-/-}$ single mutants. By contrast, inv/inv single mutants only develop small to medium size cysts and their overall kidney size is not increased compared to WT.* ***(A'-D')*** *Lectin labelling (LTL, yellow) of proximal tubules and immunostaining of Ddx5 (white) in P0 kidney of genotypes as indicated in A-D. Nuclei were stained with Dapi (cyan). Enlarged images show nuclear staining of Ddx5. Ddx5 is absent in inv/inv mutant kidneys, whereas Bicc1$^{-/-}$ single mutant and Bicc1$^{-/-}$; inv/inv double mutant animals show high Ddx5 expression in epithelial cells lining the cysts (B',D'). While arrows show nuclear Ddx5 staining in cyst-lining cells originating from proximal tubules, arrowheads mark Ddx5 in segments other than proximal tubules.* ***(E)*** *Frequency distribution of Ddx5 nuclear expression analyzed by confocal microscopy for each genotype shown in A-D. Mean nuclear intensities for Ddx5 were quantified from whole kidney sections in at least 15'000 nuclei per kidney. Grey bar indicates background staining. The numbers of mice of each genotype analyzed are indicated in the histogram. Multiple-group comparisons were performed using one-way ANOVA and error bars represent SEM. Significant p values are outlined in the table on the right side. Scale bars: 500 µm (A-D), 50 µm (A'-D').*

cells lacked nuclear Ddx5. However, a non-significant increase of medium and high expressing nuclei is observed both in *Bicc1*^{-/} and in *Bicc1*^{-/-}; *inv/inv* mice compared to WT mice. This quantification method probably underestimates an increase of Ddx5 expression in Bicc1 depleted animals, and comparing the signal intensities in the different nephron segments between each genotype might solve this issue. These data indicate that Invs acts upstream of Bicc1 *in vivo* and is necessary to regulate Bicc1 induced silencing activity.

4.2.9 Calcium regulates Bicc1/Invs interaction

Invs function may be directly regulated by Ca^{2+}. In the absence of Ca^{2+}, Invs can interact with calmodulin (CaM) via its IQ domains, and experiments in *Xenopus* showed that the IQ2 motif is critical for the ability of Invs to randomize left-right asymmetry when injected into the right blastomere (Yasuhiko et al. 2001). Therefore, we speculated that a change in calcium levels may resolve intraciliary Bicc1/Invs complexes to release and activate Bicc1. To test this, we incubated cellular extracts of HA-Bicc1 and Flag-Invs transfected HEK 293T cells with different concentrations of Ca^{2+} and performed co-immunoprecipitation experiments. Immunoblotting showed that HA-Bicc1 precipitates Flag-Invs in the absence of Ca^{2+} as demonstrated before (Fig. 22A). However, increasing amounts of calcium (2, 4 mM) inhibited the interaction in a dose-dependent manner (Fig. 22B). The calcium concentrations applied in this experiment do most probably not occur under physiological conditions. It has been suggested that the resting ciliary calcium concentration is approximately 1 µM (Delling et al. 2013). However, Ca^{2+} transients in the cilium have not been measured under flow conditions and given the size of the organelle even a small influx of Ca^{2+} might change the local concentration dramatically.
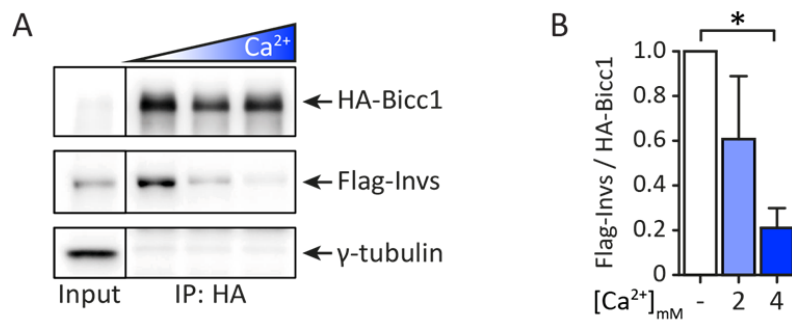
Figure 22. **Elevated calcium concentrations inhibit Bicc1/Invs co-immunoprecipitation ex vivo. (A)** *Representative Western blot of HA-Bicc1 immunoprecipitation experiments in the presence of different Ca^{2+} concentrations. Exogenous Ca^{2+} was added to cell extracts prior to the immunoprecipitation. Different Ca^{2+} concentrations are indicated and γ-tubulin served as negative control.* **(B)** *Densitometric analysis showed that elevated Ca^{2+} concentrations (2 or 4 mM) inhibit the co-immunoprecipitation of Flag-Invs with HA-Bicc1 in HEK 293T cell extracts. Three independent experiments were performed, and the percentage of Flag-Invs pull down was normalized to total HA-Bicc1 levels. $*P< 0.05$ (one-way ANOVA)*

4.2.10 Bicc1 binds calmodulin in the presence of Ca²⁺

To test whether Ca^{2+} directly targets Bicc1, we used an online CaM target database to analyze the sequence of Bicc1 (http://calcium.uhnres.utoronto.ca/ctdb/ctdb/home.html). Two putative CaM binding sites in Bicc1 were identified. The first one in amino acids 395-419 is situated at the beginning of the second KH-like domain (Fig. 23A). The second (amino acids 914-945) scores for a high putative binding site and is found in the C-terminal SAM domain. The CaM binding ability of Bicc1 was probed by pull down experiments with cellular extracts using CaM sepharose beads. Immunoblotting showed that CaM precipitated HA-Bicc1 that was ectopically expressed in HEK 293T cells (Fig. 23B). The interaction was confirmed with endogenous Bicc1 from mIMCD3 cellular extracts using the same CaM beads in pull-down assays. Unlike Invs, the CaM-Bicc1 interaction was abolished in the presence of the Ca^{2+} chelator EGTA (ethylene glycol tetraacetic acid). These results suggest that Ca^{2+} mediates the Bicc1/Invs binding via CaM and increased Ca^{2+} concentrations are necessary for Bicc1 activity.
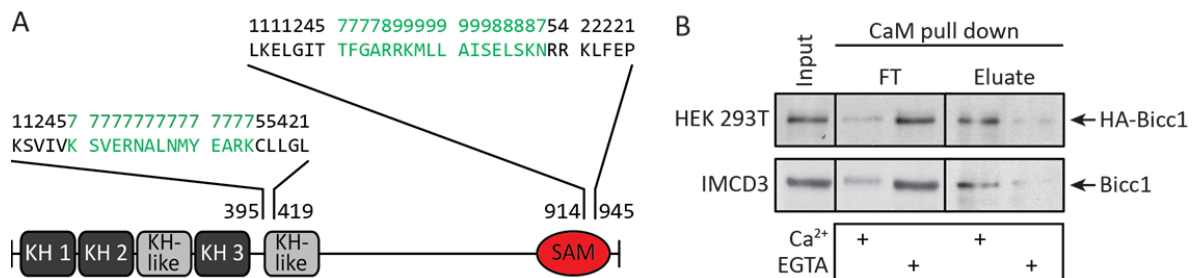
Figure 23. Bicc1 also binds CaM in a Ca²⁺ dependent manner. (A) *Two putative CaM binding motifs on Bicc1 were identified using the CaM target database (http://calcium.uhnres.utoronto.ca/ctdb/ctdb/home.html). Normalized scores are shown above the amino acid sequence. A consecutive string of high values indicates the location of a potential binding site.* ***(B)*** *Calcium-dependent interactions between calmodulin (CaM) and ectopic HA-Bicc1 or endogenous Bicc1 were probed by CaM-Sepharose pull-down assays from HEK 293T (upper panel) or mIMCD3 cell extracts, respectively (lower panel). Bicc1 only binds to CaM in the presence of 2 mM Ca²⁺, but not in its absence. 2 mM EGTA was used to chelate trace amounts of Ca²⁺. FT: flowthrough*

4.3 CaMK2 is a critical activator for Bicc1 in mRNA silencing

To further identify potential Bicc1 regulatory mechanisms relevant to the intracellular Ca^{2+} signaling, we studied to role of calmodulin kinase 2 (CaMK2). Altered calcium signaling is one of the pathways that has been implicated in ADPKD, and the polycystins play a critical role in controlling the influx of Ca^{2+} in response to mechanical stimuli. However the identification of downstream targets remains elusive. A recent study in zebrafish suggests that CaMK2 activation is dependent on PC2 and Ca^{2+}, and that CaMK2 is necessary to inhibit dilation of the pronephros (Rothschild et al. 2011). CaMK2 is evolutionary conserved across all metazoan species and is expressed in all adult mammalian tissue (Tobimatsu and Fujisawa 1989; Tombes et al. 2003). Most often it is linked to central nervous system function where it can constitute up to 1% of total protein (Hudmon and Schulman 2002). CaMK2 is unique compared to other CaM dependent kinase. It is able to multimerize, and prolonged Ca^{2+} stimulation leads to autophosphoryation and converts CaMK2 into a Ca^{2+}-independent state (Glazewski et al. 2000). Interestingly, preliminary data by Nathalie Piazzon in our laboratory showed that transfection of mIMCD3 cells with the specific inhibitory protein CaMK2-N blocked silencing of Bicc1 targets. To assess whether Bicc1 activity is directly mediated by Ca^{2+}/CaMK2 phosphorylation, we tried to identify target residues.

4.3.1 Bicc1 IVS is phosphorylated by CaMK2

To investigate if Bicc1 is phosphorylated, HEK 293T cells were transiently transfected with HA-Bicc1. The cells were labelled with ^{32}P-orthophosphate ($^{32}PO_4$) prior to lysis and immunoprecipitation. Metabolic labeling confirmed Bicc1 phosphorylation and phosphorylation was diminished in HEK 293T cells treated with the CaMK2 inhibitor KN-93 (Fig. 24A). Mining of phosphoproteome database revealed 11 phosphosites in mouse Bicc1 of which seven were also found to be phosphorylated in human (Huttlin et al. 2010; Olsen et al. 2010). One site was unique to human Bicc1 and not identified to be phosphorylated in the mouse homolog (Fig. 24B). Two specific regions emerged to be highly phosphorylated, the first one just in front of the KH domains and the second one in the IVS. The KH domains and the SAM domain itself were not found to harbor phosphorylated residues. Whether CaMK2 directly phosphorylates Bicc1 was tested in cell-free phosphorylation assays. Bicc1 KH domains, the SAM domain, the IVS or a serine- and glycine-rich region (S/G) within the IVS were fused to GST and incubated with recombinant CaMK2α (Fig. 24C). In the presence of γ-^{32}P-ATP, CaMK2α activated by CaM specifically phosphorylated the IVS

and S/G fusion proteins, but not the KH or SAM domains (Figs. 24D & 25B). Specificity of kinase activity was validated with inactive CaMK2α, which is incapable to phosphorylate the S/G-GST fusion protein.
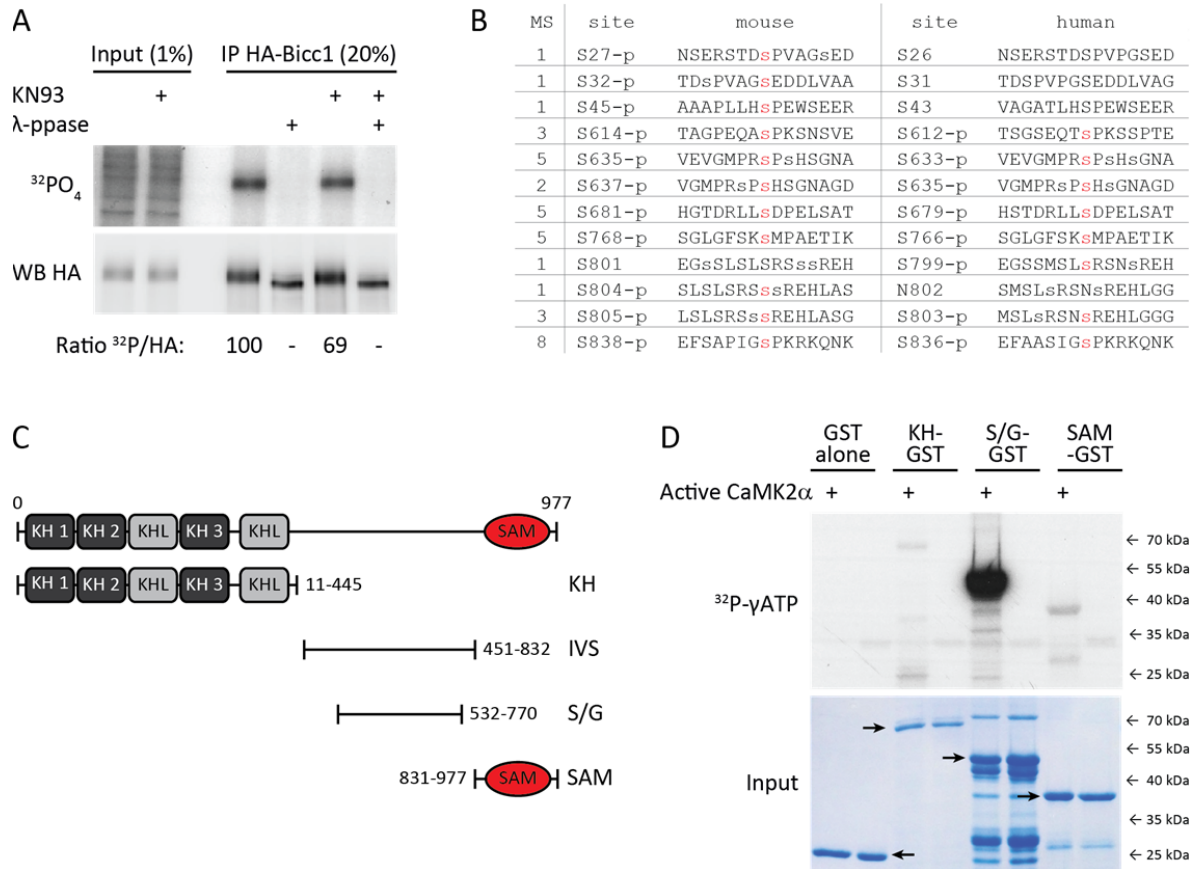
Figure 24. CaMK2 phosphorylates the Bicc1 IVS sequence. *(A) Metabolic labelling (top) and Western blot analysis (bottom) of HA-tagged Bicc1 in HEK 293T cells treated with the CaMK2 inhibitor KN-93 (10 µM). Percentages of radiolabelled signals normalized to total HA-Bicc1 as determined by densitometric analysis are shown below.* **(B)** *Table indicates putative phosphorylation sites of human and mouse Bicc1 listed by phosphosite.org (Hornbeck et al. 2004). Phosphorylation sites, identified using proteomic discovery mode mass spectrometry (MS), are indicated by red letters. The first row represents the number of independent studies in which this modification was identified.* **(C)** *Representation of GST fusion constructs comprising 3 K-homology (KH) domains and 2 KH-like (KHL) domains (KH), the C-terminal sterile alpha motif (SAM), the intervening sequence (IVS) or its serine/glycine-rich (S/G) region. The positions of the first and last amino acids of these fragments are indicated.* **(D)** In vitro *phosphorylation of GST fusion proteins of the Bicc1 KH1-5, S/G or SAM domains by recombinant CaMK2α in the presence of γ-^{32}P-ATP. GST alone served as negative control, and unspecific binding to γ-^{32}P-ATP was excluded by the addition of inactive CaMK2α. Proteins were separated by SDS-PAGE for autoradiography (top). Coomassie staining shows the input (bottom), and arrows indicate GST-fusion proteins.*

4.3.2 CaMK2 phosphorylates Bicc1 on T724 and S805

A group-based prediction system (GPS 2.1 software) identified potential CaMK2 target sites and assigned the highest scores to S805, S721, and S637 sites (Fig. 25A). Two additional low scoring residues in the IVS were ascertained S681, and T724 with T724 not harboring the classical CaMK2 recognition motif arginine-X-X-Serine/Threonine (White et al. 1998). Four of the phosphosites have bene annotated by phosphoproteome analysis and the locations of the predicted residues on the IVS are highlighted in Fig. 25A. Interestingly, *in vitro* CaMK2α phosphorylation of the IVS-GST fusion protein with γ-^{32}P-ATP labelled a breakdown product, albeit to a lesser extent (Fig. 25B). No breakdown product was observed with the S/G-GST protein, suggesting that at least one phosphosite is either in the N- or C-terminus of GST-IVS (Fig. 24D). To map the CaMK2 phosphosites, we performed an alanine mutation screen on candidate serines and threonines and purified mutated GST-IVS fusion proteins. Substitution of candidate residues by alanine prevents phosphorylation and phenotypes associated with the phosphorylation event. Phosphorylation of full length GST-IVS, but not of its truncated breakdown product was reduced by the mutation S805A (Fig. 25B). Replacing the high scoring S637 and S721 to alanine alone had no effect and combined mutation with S805A resembled the single S805A GST-IVS fusion construct (Fig. 25C). However, by extending the search to lower scoring candidate CaMK2 sites, the alanine substitution of T724 abolished the phosphorylation of the truncated IVS fragment and diminished full length phosphorylation. Combined mutation with S805A prevented the phosphorylation of GST-IVS completely (Fig. 25B). T724A and S805A mutations each reduced the CaMK2α phosphorylation of intact IVS by approximately 50%, indicating that those two sites account for *in vitro* CaMK2 phosphorylation.
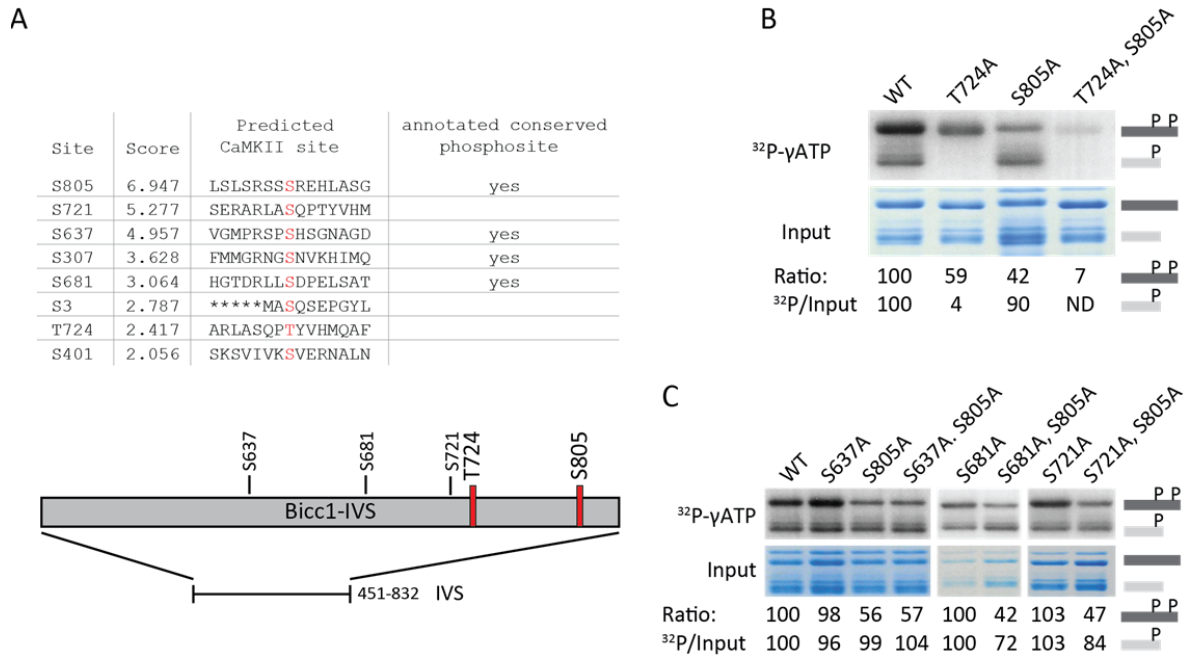
Figure 25. CaMK2 phosphorylates mouse Bicc1 threonine 724 and serine 805. (A) *Scores of potential CaMK2 motifs and their positions (red) in mouse Bicc1 predicted by the GPS server (http://gps.biocuckoo.org/ online.php). Phosphorylated sites found by phosphoproteomic analysis are indicated at the right. Bottom graph shows predicted CaMK2 target sites in the IVS, residues T724 and S805 are highlighted.* **(B, C)** *Cell-free CaMK2 phosphorylation of purified WT and mutant GST-IVS fusion proteins. Proteins were separated by SDS-PAGE for autoradiography, and coomassie staining shows the input. Note that partial degradation of IVS gives rise to a C-terminally truncated derivative lacking residue S805. Percentages of radiolabel normalized to total HA-Bicc1 as determined by densitometric analysis are shown below. Mutation of threonine (T) 724 and serine (S) 805 to alanine (A) results in the complete absence of phosphorylation (B), whereas alanine mutations on residues S637, S681, and S721 did not have any effect (C).*

4.3.3 Alanine mutation of T724 and S805 suppress Bicc1 activity

Phosphorylation plays an integral role in cell signaling and has a part in almost all cellular and developmental process. It tunes protein activity to the specific needs of each cell type or tissue. In order to validate the importance of T724 and S805 phosphorylation in Bicc1 activity, the two specific sites were substituted by alanine in full length HA-Bicc1 construct. HEK 293T cells were transiently transfected with WT or mutant HA-Bicc1 and subsequently metabolically labelled with $^{32}PO_4$. T724A, S805A mutated Bicc1 exhibits a 50% reduction in total protein phosphorylation compared to WT Bicc1 (Fig. 26A). The phosphorylation of Bicc1 was equally diminished in cells treated with the CaMK2 inhibitor KN-93. The combination of Bicc1 T724A, S805A mutation and KN-93 treatment did not further decrease total phosphorylation, indicating that T724 and S805 are the only targets of CaMK2 in full-length Bicc1. To

assess whether Bicc1 activity is dependent on T724 and S805, we monitored their influence on 3'UTR luciferase reporters of AC6 and PKIα mRNAs in HEK 293T cells. Co-expression of WT Bicc1 silenced luciferase reporter activity up to 50%. Conversely, the alanine mutations diminished the potential of Bicc1 to silence AC6 and PKIα 3' UTR reporters (Fig. 26B).

Previous analysis in cultured kidney cell lines proposed that Bicc1 poises AC6 and PKIα mRNA 3'UTR for silencing by recruiting the precursors of cognate miRNAs, and by guiding their assembly into miRISC with AGO2 (Piazzon et al. 2012). To validate if T724 and S805 are required for Bicc1-mediated miRISC assembly, the loading of target mRNAs unto AGO2 in HEK 293T cells was examined. While RT–PCR analysis detected AC6 and PKIα transcripts in immunoprecipitates of AGO2 from control cells, this interaction was blocked in cells transfected with T724A, S805A mutant Bicc1 (Fig. 26C). By contrast, binding of AGO2 to Bicc1 mRNA itself, which does not require Bicc1 silencing activity, was unaffected by the mutations and served as a positive control (Piazzon et al. 2012). Alanine mutations alone or in combination did not alter the expression of full-length Bicc1, excluding the possibility that changes in protein levels or stability accounted for decreased silencing activity and miRISC loading (Fig. 26D). Alignment of Bicc1 orthologues from different animals revealed extensive sequence conservation in the KH domains and SAM domain (Gamberi and Lasko 2012). The IVS is less conserved, though serine 805 as well as CaMK2 recognition motif arginine-X-X-serine/threonine exhibit strong conservation in vertebrae with the exception of zebrafish. Sequence comparison of threonine 724 showed no conservation, however in mammals the threonine was mainly substituted with a serine, indicating that this residue also accounts for a possible CaMK2 target site in other species. These results suggest that CaMK2 stimulates Bicc1 activity by phosphorylating T724 and the conserved S805.
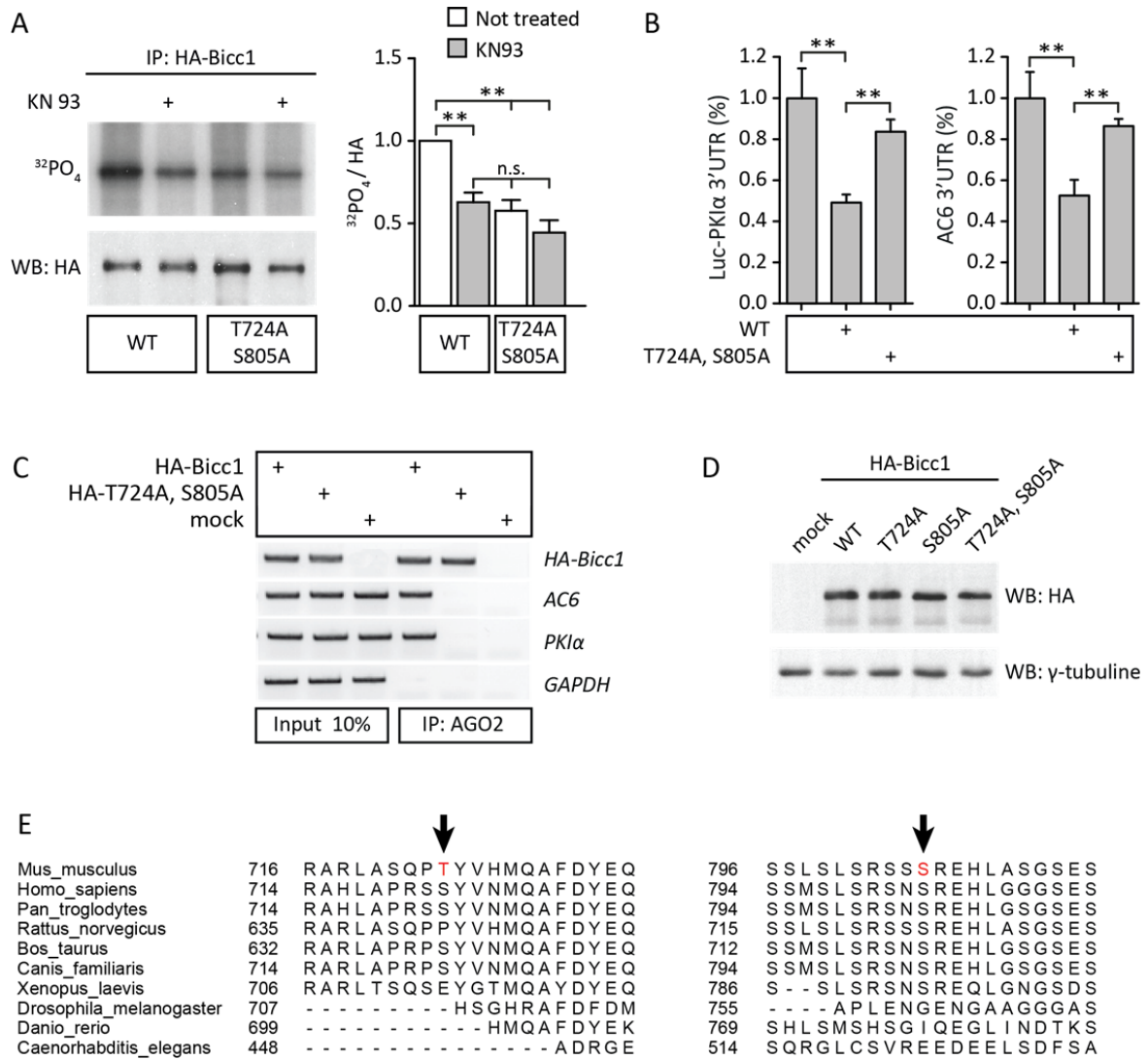
Figure 26. CaMK2 phosphorylation facilitates Bicc1-mediated miRISC assembly. (A) *Metabolic labelling (top), and Western blot analysis (bottom) of WT and T724A, S805A mutant Bicc1 in HEK 293T cells treated with the CaMK2 inhibitor KN-93 (10 µM). Histogram shows radiolabelled signal normalized to total HA-Bicc1 as determined by densitometric analysis in three independent experiments. **P< 0.01 (one-way ANOVA). **(B)** Expression of 3'UTR luciferase reporters in HEK 293T cells co-transfected with WT or T724A, S805A double mutant full length Bicc1 protein. **P< 0.01 (one-way ANOVA). **(C)** RT-PCR analysis of AGO2 immunoprecipitates in HEK 293T cells transfected as indicated to monitor miRISC loading. Expression of T724A, S805A mutant Bicc1 hinders AGO2 to bind Bicc1 target mRNA AC6 and PKIα. GAPDH mRNA served as negative control. **(D)** Expression of WT HA-Bicc1 and of its indicated mutant derivatives in HEK 293T cells analyzed by Western Blot experiments. **(E)** Clustal W was used to align Bicc1 ortholog sequences. The two potential CaMK2 phosphorylation sites T724 and S805 on mouse Bicc1 are indicated. Panels C is courtesy of Nathalie Piazzon.*

4.3.4 Bicc1 promotes flow-induced migration of mIMCD3 cells

A recent study showed that glutamate and its receptor N-methyl-D-aspartate receptor (NMDAR) are implicated in tumor cell invasion (Li and Hanahan 2013). Flow conditions mimicking interstitial fluid activated NMDAR and phosphorylated its downstream effectors MEK-MAPK and CaMK2/4. MEK-MAPK and CaMK2/4 signal transducers in turn phosphorylated and activated the transcription factor CREB that regulates a transcriptional program mediating invasion. Prompted by those observations we examined a possible role for Bicc1 in a flow-based migration assay. IMCD3 cells treated with siRNA against Bicc1 were seeded as a 3D culture consisting of a matrigel/collagen mixture unto a membrane (Fig. 27A). Hydrostatic pressure was applied by adding cell culture medium to the 3D culture to create a mimetic of interstitial fluid pressure and consequent fluid flow. Subsequently, migration was assayed by quantifying the number of cells translocating through the porous membrane (Fig. 27B). Transfection of cells with siBicc1 resulted in impaired migratory activity compared to WT or siScramble treated IMCD3 cells (Fig. 27C). Knock-down efficiency of siBicc1 was confirmed in Western blot experiments (Fig. 27D). The flow-based invasion assay characterizes a possible novel read-out for Bicc1 activity.
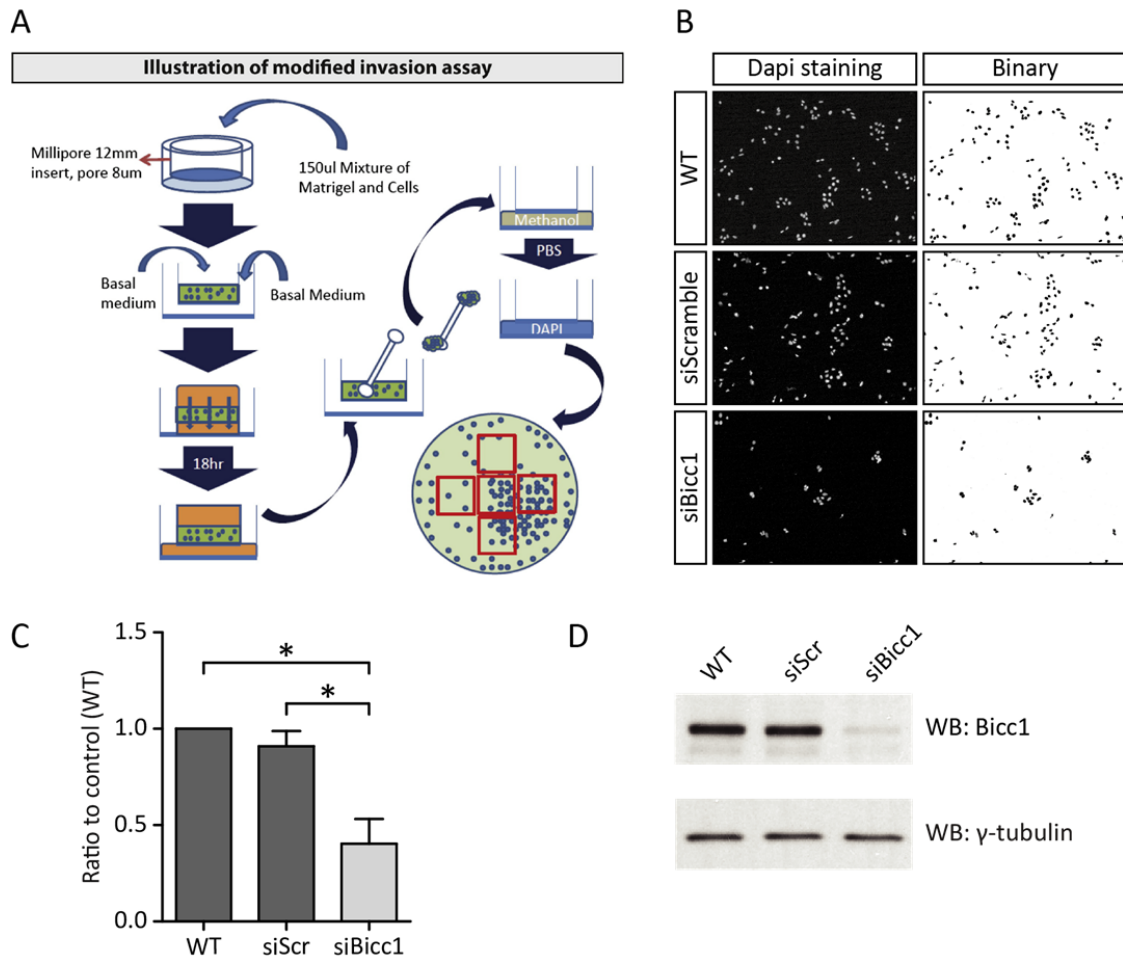
Figure 27. Bicc1 promotes migration of mIMCD3 cells. **(A)** *Illustration of migration assay mimicking pressure-driven flow conditions. Cells are seeded onto a porous disc as a 3D culture in a matrigel-collagen gel mixture. Culture medium is added on to the gel creating a hydrostatic pressure that generates fluid flow through the gel mixture and the membrane into the lower chamber. The assay allows to study the migration of cells under more physiological conditions.* **(B)** *Representative image from siBicc1 transfected mIMCD3 cells exhibits markedly decreased numbers of migrating cells compared to WT and siScramble transfected cells. Pictures were originally acquired in the DAPI channel (left) with a monochromic camera and subsequently quantified by creating a binary image (right).* **(C)** *Migration of mIMCD3 cells was impaired in cells treated with siRNA against Bicc1 analyzed in 3 independent experiments. Data were normalized to the control WT cells and a two –tailed student's t test was performed. *P< 0.05.* **(D)** *Efficiency of siRNA-mediated knock down of Bicc1 was assessed in Western blot experiments.*

5. Discussion

In this study we have investigated several mechanisms that are able to regulate the RNA binding capacity of Bicc1 in cell cultures and mice, and we showed that the unifying theory that defines cystic kidney diseases as 'ciliopathies' also holds true for Bicc1. Heterozygous *BICC1* mutations in humans associate with cystic renal dysplasia, and homozygous mutant mice form kidney cysts and pancreatic and liver bile duct dilations reminiscent of PKD. I have shown that Bicc1 localizes to a proximal ciliary subdomain called the Inversin compartment, and that Invs is required for proper accumulation of Bicc1 in this region. The Bicc1/Invs interaction is mediated by the RNA binding KH domains of Bicc1 and results in the inhibition of Bicc1 silencing activity. Importantly, expression of Bicc1 target genes was drastically diminished in *inv/inv* mice, indicating Bicc1 hyperactivation. Interestingly, *inv/inv* kidneys also showed dramatically reduced activation of pCREB by cAMP/PKA, contrasting previous reports that kidney cystogenesis is generally driven by elevated cAMP levels (Wallace 2011). Conversely, *Bicc1*$^{-/-}$; *inv/inv* kidneys showed ectopic pCREB staining similar to Bicc1 single mutants, indicating that Invs likely functions as a negative regulator of Bicc1. Furthermore, our results show phosphorylation of Bicc1 on threonine724 and serine805 by CaMK2, and that these residues are necessary to stimulate binding of Bicc1 to target RNAs.

5.1 Bicc1 is expressed in all nephron segments

Bicc1 is an important developmental regulator that is conserved in a variety of animal models including *Drosophila, C. elegans, Xenopus*, and mouse (Mahone et al. 1995; Wessely and De Robertis 2000; Wang et al. 2002; Cogswell et al. 2003). Distinct heterozygous mutations in HsBICC1 were also identified in two infants with renal cystic dysplasia (Kraus et al. 2012). Even though targeted deletion of Bicc1 in mice eventually induces renal cysts along the entire nephron, the first cysts initially form at the proximal end including Bowman's capsules and proximal tubules (Tran et al. 2010; Piazzon et al. 2012), suggesting that more distal segments are less sensitive to changes in the levels of Bicc1 targets, or that their Bicc1 is already laregely inhibited even in the wild-type. Here, lectin profiling of newborn *Bicc1*$^{-/-}$ mutant mouse kidneys by immunohistochemical analysis confirmed that cysts predominantly developed from proximal tubules and to a lesser extent from ascending limb of Henle and collecting ducts. We observed that nearly all proximal tubules underwent cystogenesis, whereas the other nephron segments were still

intact or displayed only relatively small cysts. The largest cysts at the center of the kidneys showed a patched LTL staining in epithelial cells, indicating that cells may lose their tubular fate or segment identity during cyst progression, or that cysts from different segments can amalgamate. The former possibility seems more likely since injured renal tubular cells can also adopt mesenchymal fates through epithelial-mesenchymal transitions (EMT) and thereby are thought to contribute to the development of fibrosis in chronic renal failure (Kriz et al. 2011). Expression profiles of kidneys from patients with ADPKD demonstrated that the disease associates with increased EMT markers (Schieren et al. 2006). In good agreement, a recent study using an orthologous PCK rat model of ADPKD showed that several epithelial cells lining large cysts acquired mesenchymal features, including loss of E-cadherin and *de novo* expression of vimentin and fibronectin (Togawa et al. 2011). However the data supporting the idea of EMT in cystic epithelial cells is controversial, and some studies suggest that kidney fibrosis instead mainly results from the proliferation of resident fibroblasts and their differentiation into myofibroblasts (reviewed in Kriz et al. 2011). In three renal fibrosis models that include unilateral ureteral obstruction, folic acid nephropathy, and severe ischemic-reperfusion injury, fibroblasts are the main source of scar-producing myofibroblasts (reviewed in Mack and Yanagita 2015).

The occurrence of cystogenesis in all nephron segments suggests that Bicc1 expression is necessary in all renal tubular cells to maintain proper kidney function. Indeed, Bicc1 mRNA is transcribed in all renal epithelial structures (Tran et al. 2010; Piazzon et al. 2012). Our novel antibody against the SAM domain not only confirmed the presence of Bicc1 protein in proximal tubules, but in addition also revealed expression in the loop of Henle and in collecting ducts. By contrast, an alternative antibody against a peptide in the S/G region previously detected Bicc1 primarily in proximal tubules (Piazzon et al. 2012). Whether access to the S/G peptide epitope in the distal segments of the nephron is masked by specific regulatory factors remains to be determined. In adult kidneys, Bicc1 expression has been described in the cortical and juxta-medullary regions at the age of 3 months, whereas it extended into the medullary regions at 1 year (Lian et al. 2014). We did not observe any restriction to the juxta-medullary region in 3 month old kidneys, and localization at both time points was confined to the medulla and cortex. However, we confirmed expression of Bicc1 in adult kidneys in proximal tubules and ascending limb of Henle.

ADPKD is a systemic disease with frequent extra-renal manifestations in the liver, pancreas, heart, and vasculature (Gabow 1990). The prevalence of hepatic cysts in patients has been estimated to be as high as 80%, and cysts have been shown to originate from bile ducts (Luciano and Dahl 2014). Pancreatic cysts were found in 10% of patients but tend to remain asymptomatic, with only rare instances of recurrent pancreatitis (Malka et al. 1998). Hepatic biliary cysts and dilated pancreatic ducts also develop in Bicc1

mutant mice (Flaherty et al. 1995; Tran et al. 2010). However, expression of Bicc1 is not well characterized in any of those organs. We show that in the liver, Bicc1 is exclusively localized in bile ducts, confirming and extending recent results of an independent report that employed a distinct commercial Bicc1 antibody (Lemaire et al. 2015). The same study also detected Bicc1 protein expression in the developing pancreas and showed that it is needed there for normal differentiation of endocrine progenitors (Lemaire et al. 2015). A role in the pancreas is especially interesting since novel heterozygous mutations in HsBICC1 distinct from those reported by (Kraus et al. 2012) in some instances associate renal cysts with diabetes. Among these, I found that the R800Q substitution blocks CaMK2 phosphorylation at the nearby residue Ser803 (collaboration with Grapin lab, unpublished observation). This is the first known human BICC1 mutation that has been associated with a specific molecular function. Overall, our finding that Bicc1 protein is expressed in all kidney and liver sites that form cysts in ADPKD indicates that it is essential to maintain the structure of those organs.

5.2 Bicc1 localizes to the primary cilium

Previous analysis in COS1 cells with ectopically expressed Bicc1 suggested that a C-terminal fragment encompassing the SAM domain localizes Bicc1 in cytoplasmic puncta outside and at the periphery of P-bodies. Interestingly, these foci overlap with cytoplasmic Dvl2 and reduce its activity in the canonical Wnt/β-catenin signaling pathway (Maisonneuve et al. 2009). Here, immunostaining of polarized IMCD3 cells as well as kidney and liver cryosections revealed that endogenous Bicc1 forms similar clusters both *in vivo* and in cultured renal tubule cells. In addition to these cytoplasmic puncta, Bicc1 to our surprise entered the primary cilium. The primary cilium of renal epithelial cells has been implicated in mechanosensation, and disruption of ciliary function in kidneys invariably leads to renal diseases. Although cystic kidney disorders are clinically discrete entities, multiple protein products of the mutated disease-associated genes localize to the primary cilium-basal body complex (Hildebrandt et al. 2011; Sang et al. 2011; Szymanska and Johnson 2012). It is now becoming apparent that most, if not all disorders of the primary cilium such as PKD, NPHP, Bardet-Biedl syndrome, Joubert syndrome, and Meckel syndrome have a cystogenic component, which defines kidney cyst formation as a hallmark of ciliopathies (Gascue et al. 2011). Given the striking phenotypic overlap between multiple ciliopathies, one should not be surprised that many of the associated proteins interact and function in common pathways. However, the mechanisms underlying most of the disease phenotypes associated with ciliary

dysfunction remain to be elucidated. Our finding that Bicc1 localizes to cilia the for the first time adds an RNA binding protein to the growing list of ciliopathy genes.

5.3 Bicc1 ciliary localization is regulated by Invs

In renal tubular epithelial cells, Bicc1 did not localize to the entire ciliary axoneme but rather to a distinct subregion at the base of the cilium reminiscent of the Invs compartment (Shiba et al. 2009). Using the Invs-GFP transgene mouse model, we were able to show that the Invs compartment and Bicc1 localization in renal epithelial cells completely overlapped. In addition, GFP-Invs was also observed in basal bodies as reported previously in cultured cells, but in this location there was no overlap with Bicc1 staining (Sang et al. 2011; Oud et al. 2014). Targeting of Invs to the cilium is considered essential since a homozygous nonsense mutation in the IQ1 domain that truncates Invs and prevents its ciliary localization has been identified in a fetus with infantile nephronophthisis (Oud et al. 2014). We therefore studied whether Invs expression is required for the intra-ciliary localization of Bicc1. The specific localization of Bicc1 to the Invs compartment was lost in *inv/inv* mutant mice, and depletion of Invs by RNAi in IMCD3 cells confirmed that Bicc1 ciliary localization depends on Invs. However, low levels of Bicc1 were still detected even in cilia of *inv/inv* cystic kidneys. Thus, while Bicc1 may enter primary cilia without Invs, the presence of Invs is needed for stabilization or to prevent rapid translocation back to the cytoplasm. Such a model is consistent with previous reports that identified Invs as an intra-ciliary molecular anchor for Nphp3, Nek8 (Nphp9), and ankyrin repeat and SAM domain-containing protein 6 (Anks6) (Shiba et al. 2010; Hoff et al. 2013; Czarnecki et al. 2015). It has been demonstrated that the ciliary architecture and function is dependent on the interaction of specific protein complexes that regulate cilium-specific biochemical processes, and those modules are often interconnected in larger protein networks (Garcia-Gonzalo et al. 2011; Sang et al. 2011; Williams et al. 2011). Modules such as the NPHP1-4-8 and MKS complex as well as IFT particles and the BBSome function in apical organization, cilia integrity, cell signaling, gatekeeping and protein transport. However, the biological role of the Inversin compartment nonetheless is unclear (Fig. 28), and how specific protein complexes are assembled and how their composition is regulated is unclear. Although the Inversin compartment proteins Invs, Nphp3, Nek8, and Anks6 are not required for ciliogenesis, mutations or genetic knockouts cause embryonic or perinatal lethality, left-right asymmetry defects, and renal-hepatic-pancreatic dysplasia similar to those observed in *Bicc1*^{-/-} knockout mice (Mochizuki et al. 1998; Liu et al. 2002; Bergmann et al. 2008; Manning et al. 2013; Czarnecki et al. 2015). There are contradictory results how Anks6 and Nek8 ciliary targeting is

regulated, but both of them clearly depend on Invs ciliary localization. Anks6, the first known component of the Invs compartment, has been reported to connect Nek8 to Invs and Nphp3 (Hoff et al. 2013). Although, discordant with those findings, Czernecki et al. showed that Anks6 is downstream of Nek8 and that its ciliary localization depends on Nek8 (Czarnecki et al. 2015). Nek8 stands out as the only known ciliary axonemal kinase, and its kinase activity is necessary for its biologic function in ciliary signaling and development. The same study by Czernecki et al. also demonstrated that an Anks6/Nek8 interaction stimulates NEK8 kinase activity and that Anks6 in turn serves as a phosphorylation substrate. Interestingly, Anks6 can also bind Bicc1 (Stagner et al. 2009). This observation raises the question whether Anks6 is the only physiological substrate of Nek8, or whether additional targets include Bicc1. Our finding that CaMK2 only accounts for half of phosphorylated Bicc1, a role for an additional kinase is possible. Nek8 also interacts with PC2, and Sohara et al. presented indirect evidence for Nek8-dependent phosphorylation of PC2 (Sohara et al. 2008). The *jck* (juvenile cystic kidneys) mouse which carries a missense mutation in the regulator of chromatin condensation domain of NEK8 showed increased phosphorylation of PC2. The mutation found in the *jck* mouse does not alter kinase activity, but mutated Nek8 was found ectopically along the entire length of the cilia instead of being restricted to the Invs compartment (Sohara et al. 2008; Zalli et al. 2012). Strict Invs compartment localization of Nek8 may be required for proper Nek8 function, and aberrant targeting possibly leads to increased PC2 phosphorylation. Our studies suggest that Bicc1 is a member of the Invs compartment and is able to interact with Invs itself and Anks6 (Fig. 28). Invs seems to act as an anchor in the Invs compartment and is necessary to target Invs compartment components to the proximal ciliary axoneme. Interestingly, the *C. elegans* ortholog of Invs localizes to the *C. elegans* ciliary middle segment and plays a role in transition zone placement (Warburton-Pitt et al. 2012). In the same study they also find that the genetic interaction between *C. elegans nphp-2* and the NPHP and MKS network reflects the physical interaction of the same modules in mammalian systems. It can be speculated that Invs ciliary localization is evolutionary conserved and acts as an essential modifier of the NPHP and MKS pathway (Sang et al. 2011).

Our findings add to increasing evidence that ciliary genes demonstrate pleiotropic effects with phenotypic overlap between related disorders and seemingly unrelated clinical entities. Nevertheless, it is still not clear how mutations in the same gene cause quite different pathological phenotypes (Hildebrandt et al. 2011). It is tempting to speculate that modifiers and epistatic effects of genetic interactions among components of the Invs compartment are causative for some of the observed phenotypic variability. Further experiments will be needed to validate if Bicc1 also interacts with Nphp3 or Nek8 and whether Bicc1 serves as a kinase substrate of Nek8.
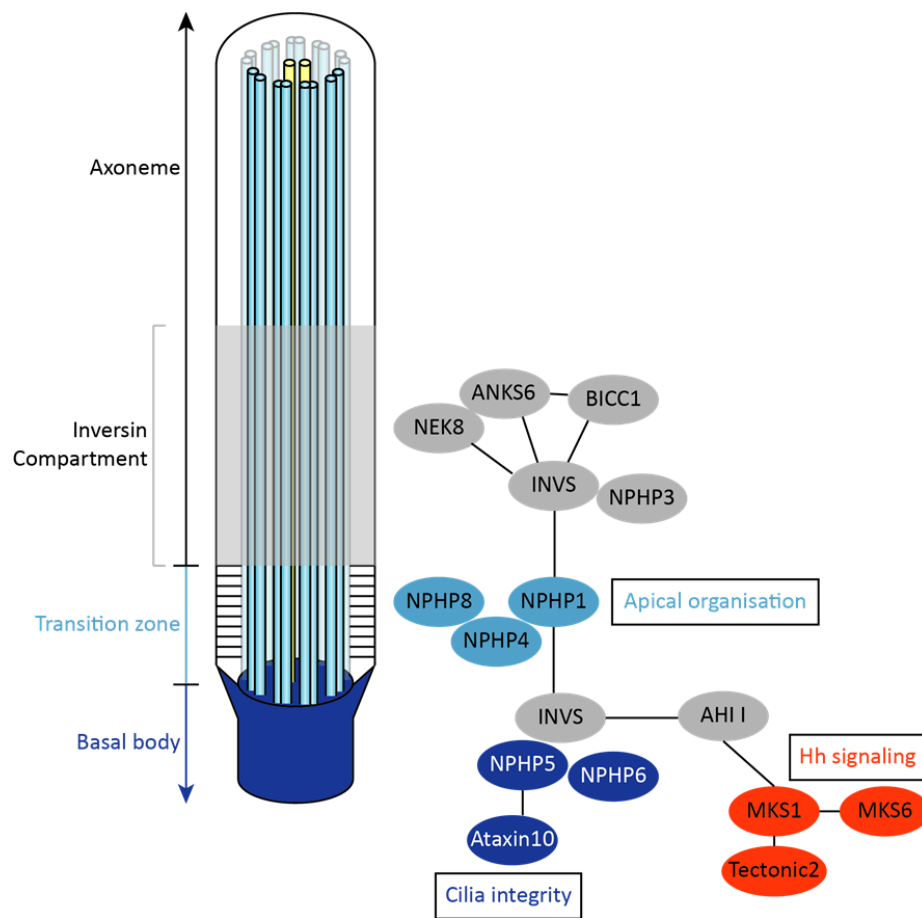
Figure 28. Bicc1 is a novel component of the Invs compartment. *Sang and colleagues identified four connected ciliary protein modules: the "NPHP3, Invs, Nek8 module" located in the Invs compartment, the "NPHP1-4-8 module " at the apical surface, "Nphp5-6" at centrosomes, and MKS (Meckel Gruber Syndrome) linked to sonic Hedgehog signaling (Sang et al. 2011). Several proteins seem to bridge the modules, notably Invs and Ahi. Recently Anks6 has been identified as a new member of the Invs compartment (Hoff et al. 2013; Czarnecki et al. 2015). Our data suggest that Bicc1 is recruited to this by the interaction with Invs, and that binding to Anks6 alone (Stagner et al. 2009) is not sufficient. Image was adapted from (Sang et al. 2011).*

5.4 Invs inhibits Bicc1 mediated mRNA silencing activity

As described above, *inv/inv* and *Bicc1*$^{-/-}$ mutant mice display major phenotypic overlap, including cystic kidney disease, renal and hepatic cysts, cardiac malformations and perinatal death. Unlike PKD, where an increasing number of large kidney cysts from all segments of the nephron lead to severely enlarged kidneys, nephronophthisis is characterized by cysts in the cortico-medullary border. Cystogenesis is

thought to occur in collecting ducts and distal tubules, and unique histological features of nephronophthisis are tubular basement membrane thickening and peritubular, inflammatory infiltration. Nephronophthisis kidneys are either diminished or normal in size. However, patients with nephronophthisis type II caused by mutations in *INVS* have often enlarged kidneys, mimicking rather ARPKD or ADPKD (Hildebrandt and Otto 2000; Otto et al. 2003; Simons and Walz 2006). The phenotypic similarities become even more evident by the fact that both mice develop situs defects due do to misorientation of motile cilia in the ventral node (Okada et al. 2005; Maisonneuve et al. 2009). The gene products Invs and Bicc1 have also been shown to inhibit canonical Wnt at the level of Dvl (Simons et al. 2005; Maisonneuve et al. 2009). Whereas Invs is thought to act as a molecular switch between canonical Wnt signaling and PCP signaling by targeting cytoplasmic Dvl for degradation, Bicc1 so far has only been implicated in Wnt/β-catenin signaling. This, together with the observation that Bicc1 ciliary targeting depends on Invs, prompted us to investigate whether Invs and Bicc1 directly interact. Overexpression of tagged Invs and Bicc1 in IMCD3 and MDCK cells demonstrated colocalization, and a direct binding between the two proteins was confirmed in HEK 293T cells by co-immunoprecipitation experiments and in yeast-two hybrid assays. Interestingly, the interaction was mediated by the RNA binding KH domains of Bicc1. This prompted us to test whether the RNA binding capabilities of Bicc1 are impeded by the interaction with Invs. Indeed, we demonstrated that Invs binding impaired Bicc1-mediated repression of PKIα 3'UTRs luciferase reporters in cultured HEK 293T cells. Previous analysis in cultured kidney cell lines showed that Bicc1 binds AC6 and PKIα mRNAs and cognate miRNAs to stimulate RISC loading (Piazzon et al. 2012). In line with this notion, co-expression with Invs selectively inhibited binding of Bicc1 to mRNAs and miRNAs. These results suggest a new role for Invs upstream of Bicc1 in the post-transcriptional regulation of gene expression.

To more directly evaluate a possible epistatic relationship between Invs and Bicc1, we analyzed the expression of Bicc1 target genes in *inv/inv* mutant kidneys. In *Bicc1*^{-/-} newborn kidneys, AC6 and PKIα are posttranscriptionally upregulated, and several other direct target mRNAs have been identified by protein/RNA coIP and functionally validated by overexpression in *Xenopus* animal cap luciferase experiments (Piazzon et al. 2012; Zhang et al. 2013). Here, we could demonstrate that AC6 and Ddx5 are almost absent in *inv/inv* cystic kidneys, whereas Dpy30 expression was not affected at all. For PKIα and Atp6v1b1 no significant reduction was observed, which is indicative of an additional layer of complexity in the regulation of Bicc1 targets. The unaltered Dpy30 protein levels might be explained by differences between animal models. These results suggest that posttranscriptional mRNA silencing activity of Bicc1 is also regulated by Invs *in vivo*. To date it was impossible to detect an endogenous interaction between

Invs and Bicc1, due to the lack of a suitable anti-Invs antibody. We tried to raise an anti-Invs monoclonal antibody against the N-terminal region of Invs; however ascites fluids from 13 mice injected with one out of five different peptides failed to react with either WT or Flag-tagged Invs. This problem might be circumvented by using cellular extracts of GFP-Invs transgenic mouse kidneys, but preliminary studies indicated that GFP-Invs is barely detected by anti-GFP antibody in immunoblotting experiments and could not be enriched by immunoprecipitation assays.

We speculate that the inhibitory effect of Invs on Bicc1 is fueled by its ciliary localization, and that translocation to the cytoplasm activates Bicc1. To our knowledge, there are no reports showing the localization of mRNA, miRNA or any members of the microRNA machinery to the cilium. To better understand the mechanistic details of Bicc1 activity it will therefore be necessary to identify its ciliary localization sequence. The ciliary targeting sequences of ciliary proteins have been extensively studied and the Vxp and Ax(S/A)xQ motifs have been identified as critical targeting sequence for PC2 and several ciliary G protein coupled receptors (Geng et al. 2006; Berbari et al. 2008). Also sequences important for nuclear localization may function as a ciliary targeting signal. However, only in a small subset of ciliary proteins such sequences have been identified (Dishinger et al. 2010). Ciliary localization of Bicc1 is most probably independent of Invs as shown by weak expression of Bicc1 in *inv/inv* kidneys, but Invs is necessary to retain Bicc1 in the axoneme. These results are similar to NPHP3 for which it was demonstrated that its ciliary localization is independent of Invs (Nakata et al. 2012). Mutation in the ciliary localization sequence might lead to a constitutively active form of Bicc1. It would be interesting to test in future studies whether any mutations found in human patients specifically affect the ciliary localization of Bicc1 (Kraus et al. 2012). In addition, we speculate that a transgenic mouse expressing a mutated Bicc1 protein lacking the nuclear localization signal could mimic the kidney phenotypes observed in *inv/inv* mutant mice. Mounting evidence that ciliary localization is necessary for protein function also comes from Nek8. Mutations which were identified in patients with nephronophthisis led to defects in ciliary localization, and loss of ciliary localization of Nek8 was also reported in primary kidney epithelial cells derived from *jck* mice (Smith et al. 2006; Otto et al. 2008).

In this study, we have identified a novel mechanism of the Invs compartment which is necessary to maintain kidney morphology and function. We were able to show that Bicc1 ciliary targeting is mediated by Invs and that this interaction inhibits Bicc1 mediated mRNA silencing.

5.5 Inhibition of cAMP/PKA signaling in *inv/inv* kidneys

Excess cAMP accumulates in various animal models of PKD, and it stimulates epithelial cell proliferation and secretion of fluid into cysts of ADPKD patients (reviewed in Wallace 2011). One of the major strategies to treat ADPKD is to reduce cellular cAMP levels by oral administration of a synthetic vasopressin V2 receptor antagonist. Development and progression of PKD in orthologous models of ARPKD, ADPKD, or nephronophthisis was successfully inhibited by treatment with the antagonist, and treated animals displayed lower levels of cAMP (Gattone et al. 2003; Torres et al. 2004; Wang et al. 2008). However, insights into the mechanisms leading to increased cAMP levels are limited. Elevated levels of cAMP have also been described in $Bicc1^{-/-}$ mutant animals, and Bicc1 has been shown to act directly in the cAMP/PKA pathway by regulating the expression of AC6 (Piazzon et al. 2012). To directly assess PKA signaling, we stained kidneys with an antibody against the phosphorylated form of CREB (pCREB). Binding of cAMP to PKA liberates catalytic subunits and results in the activation of the transcriptional factor CREB by Ser133 autophosphorylation. In $Bicc1^{-/-}$ mutant kidneys, the increase in cAMP levels was sufficient to activate PKA signaling in cyst-lining cells derived from distal tubules, but not in proximal tubules. The same phenotype was observed in kidneys of $Kif3a^{-/-}$;$Pkd1^{-/-}$ double and $Pkd1^{-/-}$ single mutant mice, whereas $Kif3a^{-/-}$ mutant animals showed activated signaling in cysts derived from both proximal tubules and collecting duct (Choi et al. 2011; Ma et al. 2013). This indicates that cAMP effectors are unlikely the major force promoting cyst growth in $Bicc1^{-/-}$ mice, because their activation is largely confined to distal nephron segments that exhibit late cystogenesis. However, it cannot be excluded that PKA signaling might be upregulated in proximal tubules at earlier time points. Alternatively, ectopic PKA signaling in distal nephron segments may cell non-autonomously promote cystic growth in proximal segments; possibly even at an early stage before distal tubules themselves have formed many cysts. PKA is not the only effector of cAMP, though. In particular, a cAMP response can also be mediated by Protein Kinase A-related X (PRKX), and constitutively active mutant PRKX can suppress cystic growth of human *Pkd1* depleted cells (Li et al. 2008). No change in expression of the catalytic subunit of PRKX was detected in cystic $Bicc1^{-/-}$ kidneys (Piazzon et al. 2012), but increased accumulation of cAMP is likely to activate both PKA and PRKX. A third cAMP signaling effector includes guanine nucleotide exchange factor (EPAC) which in turn may activate MAPK/ERK via B-Raf-Rap1 (Schmidt et al. 2013). Alternatively, EPAC can strongly activate JNK signaling (Hochbaum et al. 2003). JNK activation has been shown to mediate PCP signaling in the *Drosophila* eye and during convergent extension in *Xenopus* (Weber et al. 2000; Yamanaka et al. 2002). Studies in the PCK rat also suggest that EPACs are involved in the hepatic cystogenesis in PCK rats, a model for ARPKD (Banales et al. 2009). Thus,

increased levels of cAMP in *Bicc1*^{-/-} animals leading to upregulation of EPAC signaling might result in PCP defects.

To our knowledge, the nearly complete absence of pCREB staining observed in *inv/inv* mutant kidneys describes for the first time reduced PKA activity in any animal model with cystic kidney disease. Until now, increased cAMP signaling was suggested to be a general hallmark of cystic kidneys (Torres and Harris 2014). However, in animal models developing nephronophthisis cAMP levels were less extensively studied than in PKD models, but also the *pcy* mouse (mutation in Nphp3) and mice depleted for Nphp6 show clearly elevated cAMP levels (Gattone et al. 2003; Sayer et al. 2006). In addition, stable knockdown of *Nphp3*, *Nphp6*, and *Nphp8* resulted in increased cAMP levels and in reduced cilia numbers in mIMCD3 cells (Ghosh et al. 2012). Though, elevated cAMP does not always correlate with increased pCREB levels. One study reported increased cAMP concentrations that were accompanied by upregulation of PKA regulatory subunits in polycystic kidneys of PCK rats and *Pkd2*[−/WS25] mice, but no difference in the protein levels of pCREB were detected between WT and cystic rats or mice (Wang et al. 2010). In those kidneys the expression of CRE modulator proteins (CREMs), another cAMP responsive promoter element (CREs) that is downstream of PKA, was significantly upregulated. That study did not address the localization of pCREB in cystic kidneys. It is therefore possible that a local increase in protein levels specifically in cyst-lining cells was too small to be detected by immunoblotting of whole kidney extracts. Alternatively, PKA signaling might be mediated via CREMs instead of CREB. However, alternative CREMs signaling cannot explain the total absence of pCREB in *inv/inv* mutant kidneys.

Downregulation of pCREB in postnatal *inv/inv* kidneys coincided with a marked reduction in AC6 expression which is predicted to impair cAMP synthesis. By contrast, PKA inhibitor PKIα was only downregulated in *inv/inv* mutants at a later time point. These results point to an additional layer of complexity in the regulation of Bicc1 targets, and they suggest that pCREB levels are likely diminished due to a net decrease in cAMP/PKA signaling. A delay in the expression of PKIα fits with a potential role as a feedback inhibitor of excessive cAMP/PKA signaling. Sustained expression of PKIα in *inv/inv* kidneys might contribute to the inhibition of PKA signaling. We propose that cyclic AMP signaling should be assessed in patients with nephronophthisis type II. If reduced PKA activity can be recapitulated in those cystic kidneys, the therapy should avoid cAMP pathway antagonists.

5.6 The RNA helicase Ddx5 is a potential new target of Bicc1

Ddx5 mRNA was recently identified to be posttranscriptionally regulated by Bicc1 in *Xenopus* (Zhang et al. 2013). We found that in *inv/inv* mutant kidneys Ddx5 expression was significantly reduced, confirming our hypothesis that Invs acts upstream of Bicc1. To further test the epistatic relationship between Invs and Bicc1, we generated double mutant mice. Histological analysis of *Bicc1$^{-/-}$*; *inv/inv* double mutant kidney sections indicates that cyst progression and expansion are comparable to *Bicc1$^{-/-}$* mice, with most of the cysts arising from proximal tubules. Analysis of LR asymmetry defects showed that combined inactivation of Bicc1 and Invs resulted in situs randomization as it does in *Bicc1$^{-/-}$* single mutants, whereas *inv/inv* mutant mice display *situs inversus* (personal communication with Keiichi Katsumoto). To assess Ddx5 expression *in vivo*, we stained kidney sections of WT or mutant mice devoid of Bicc1 or Invs alone or in combination. Similar to pCREB, Ddx5 expression was reduced in *inv/inv* cystic kidneys. Interestingly, Ddx5 levels were upregulated in all cyst-lining cells in *Bicc1$^{-/-}$* mice, a phenotype that was also recapitulated in the double mutant kidneys. The role of the RNA helicase Ddx5 has not been studied in the context of cystic kidney disease. Gene disruption of Ddx5 in mice results in early lethality at embryonic day 11.5, which is before the onset of kidney organogenesis (Fukuda et al. 2007). Activated Ddx5 appears to have a pro-proliferation, pro-invasion, anti-apoptotic and hence oncogenic role in cells. Indeed, overexpression of Ddx5 has been reported in colorectal, breast, and prostate cancer (Janknecht 2010). Ddx5 is a highly conserved protein involved in a myriad of processes that functions in most steps of the gene expression process, however its *in vivo* targets and activities are not fully understood (reviewed in Fuller-Pace 2013; Dardenne et al. 2014). Ddx5 has been identified as a subunit of the Drosha complex which processes primary miRNA transcripts into pre-miRNA in the nucleus (Gregory et al. 2004). In the Drosha complex, Ddx5 is able to bind Smad proteins and the tumor suppressor p53 to stimulate the maturation of selected miRNAs (Davis et al. 2008; Suzuki et al. 2009). There is increasing evidence that Ddx5 is also implicated in the initiation of gene transcription. It has been shown to interact with the β-catenin and estrogen receptor α to stimulate transcription and it also acts as coactivator of CREB-binding protein, p53, MyoD and Runx2.

Altogether, our observations in *Bicc1$^{-/-}$*; *inv/inv* double mutant animals are consistent with a model for an epistatic relationship between Bicc1 and Invs and that Bicc1 silencing activity is regulated by Invs. In addition, our results suggest that Ddx5 is an *in vivo* target of Bicc1 and a possible novel suppressor of cyst formation in PKD. However, to exclude an indirect effect of Ddx5 upregulation in cystic epithelial cells, a direct interaction between Bicc1 and Ddx5 mRNA remains to be validated e.g. by RNA-

coimmunoprecipitation. In PKD, Ddx5 might promote proliferation and epithelial to mesenchymal transition in cyst-lining cells and thereby driving cyst expansion and/or fibrosis. Whether Ddx5 expression is upregulated in other animal models of PKD and whether Ddx5 is active in cystic epithelial cells remains to be determined. Contrary to this idea, recent expression profiling of *Pkd1cKO* kidneys revealed only subtle changes in global transcription profiles, and miRNA biogenesis also remained largely unaffected at least during early stages of cystic growth (Menezes et al. 2012). However, it is possible that changes in transcription occur at later timepoints of cyst progression.

5.7 Regulation of Bicc1/Invs interaction by Ca^{2+}

Bicc1 mediated regulation of PC2 suggests a role of Bicc1 in Ca^{2+} homeostasis, by controlling the Ca^{2+} influx of the cell (Tran et al. 2010). Conversely, Bicc1 activity may also respond to changes in Ca^{2+} levels. Here we showed that high Ca^{2+} concentrations result in the dissociation of the Bicc1/Invs complex. Invs binds CaM only in the absence of Ca^{2+} via its IQ domains, and injection of mouse WT but not IQ-mutated Invs into blastomeres reverses cardiac orientation in *Xenopus* (Yasuhiko et al. 2001; Morgan et al. 2002). The IQ domains are not essential for the ciliary targeting of Invs (Shiba et al. 2010). Therefore, and since CaM is also present in primary cilia, binding to CaM likely regulates Invs function within the cilium. Interaction of Invs with CaM may lead to a conformational change which enables the complex to bind Bicc1 and thereby possibly modulates Bicc1 activity. A single amino acid substitution of isoleucine by glutamic acid in either of the IQ domains eliminates CaM-Invs protein interaction (Yasuhiko et al. 2006). Such an Invs mutant that is unable to bind CaM would provide insights if Bicc1 silencing activity is inhibited by the Invs-CaM interaction and whether this interaction affects Bicc1 ciliary targeting. We hypothesize that Bicc1 is retained in the cilium by an Invs-CaM complex at low Ca^{2+} concentration, but that capacitative Ca^{2+} entry or influx via PC2 leads to the dissociation of the complex and liberates Bicc1 which in turn is able to translocate to the cytoplasm and silence target gene expression (Fig. 29). One possible though difficult experiment to test this hypothesis would be to directly visualize live calcium indicators within cilia (Delling et al. 2013; Jin et al. 2014) and to observe on a differential side-view platform the dynamics of Bicc1 localization in cultured cells in response to Ca^{2+} flux induced by shear stress or calcium ionophores (Jin et al. 2014).

5.8 Bicc1 interacts with CaM

We were able to show that Bicc1 itself is also prone to bind CaM. In contrast to Invs-CaM complexes, the Bicc1-CaM interaction is stabilized by Ca^{2+}. A high scoring putative CaM binding motif FGARRKMLLAISEL is predicted at the C-terminus of the Bicc1 SAM domain. This sequence corresponds to the consensus motif (FILVW)xxxxxx(FAILVW)xxxxx(FILVW) of a type 1-8-14 calmodulin binding site. This motif is likely relevant because its incorporation in Bicc1 is regulated by alternative splicing, and because its glutamic acid residue 932 is mutated to alanine in a heterozygous human patient with cystic kidneys (Cogswell et al. 2003; Kraus et al. 2012). It will be important to validate whether the E932A mutation affects Bicc1-CaM interaction and to test its impact on Bicc1 activity and/or ciliary targeting.

5.9 CaMK2 phosphorylates Bicc1 on Threonine 724 and Serine 805

Bicc1 modulates specific miRNA activities rather than their expression levels (Piazzon et al. 2012). Analysis of four other mouse models of PKD, including a kidney-specific knockout of *Pkd2* revealed that in the course of disease progression, kidneys with advanced cysts upregulate expression of the miR-17~92 cluster (Patel et al. 2013). Conditional ablation of miR-17~92 in *Kif3a*-deficient cystic kidneys attenuates disease, whereas overexpression of this cluster can induce tubular cysts, at least in part by targeting the 3'UTRs of *Pkd1*, *Pkd2* or *Hnf1b* mRNAs (Patel et al. 2013). Since Hnf1β transcriptionally activates several inhibitors of cystic disease, including the phosphodiesterase *PDE4C*, *Pkd2*, *Pkhd1* and *Bicc1*, the regulation of this network by the miR-17~92 cluster likely represents an important determinant of disease progression (Gresh et al. 2004; Verdeguer et al. 2010; Choi et al. 2011).

Silencing of *Pkd2* mRNA by miR-17 is antagonized by Bicc1 (Tran et al. 2010). Bicc1 thus may stimulate or inhibit gene silencing, depending on the context. Although, whether Bicc1 directly binds *Pkd2* mRNA or miR-17 remains to be determined. The same study showed that xBic-C in *Xenopus* cannot rescue pronephric ducts depleted of PC2 (Tran et al. 2010). By contrast, injection of *Pkd2* mRNA into xBic-C depleted embryos rescued the expression of a distal tubule marker in 50% of cases, arguing that Ca^{2+} influx via PC2 acts upstream of Bicc1 (Tran et al. 2010). Bicc1-independent functions of exogenous polycystin-2 may involve a physical interaction of its C-terminus with a ciliary pool of AC5 (Choi et al., 2011) or increased capacitative Ca^{2+} entry at the plasma membrane leading to direct inhibition of

adenylate cyclases by Ca^{2+} binding (Fagan et al. 2000; Choi et al. 2011). However, endogenous PC2 signaling in addition requires CaMK2, and a Ca^{2+}-independent constitutively active mutant CaMK2 is sufficient to rescue PC2 morphant zebrafish (Francescatto et al. 2010; Rothschild et al. 2011).

These observations point to CaMK2, rather than adenylate cyclases as the primary direct target of Ca^{2+}. We therefore asked whether CaMK2 directly acts on Bicc1. We found that CaMK2 phosphorylates Bicc1 on T724 and S805 in cell-free assays. Combined mutation of these residues by alanine substitutions in the full length protein inhibits Bicc1-mediated silencing and miRISC loading. To our knowledge, no other CaMK2 substrate with a role in PKD has been identified so far. Mechanistically the regulation of Bicc1 may rely on a similar mechanism as observed for the miRNA binding protein FMRP. Phosphorylation of FMRP promotes the formation of a miRNA-AGO2 complex that inhibits translation of target mRNAs. Dephosphorylation of FMRP results in the release of AGO2 from the mRNA and translation is activated (Muddashetty et al. 2011).

CaMK2 phosphorylation accounts for approximately 50% of total Bicc1 phosphorylation, indicating that different kinases may have Bicc1 regulatory functions. Proteomic discovery-mode mass spectrometry identified eleven phosphorylation sites on Bicc1, including serine residues 635, 637, 681, and 768 which are predicted to be phosphorylated by mTOR, PKA, MAPK-activated protein kinase-1 (S6K), and/or mTOR respectively. These kinases are implicated in playing a role in PKD and have been shown to be upregulated in the disease. Assessing their role in Bicc1 activity would provide further insights of polycystic disease-relevant mechanisms. Interestingly, aberrant mTOR activation also occurs in Bicc1$^{bpk/bpk}$ mice, and inhibition of mTOR by rapamicin is highly effective in reducing renal cystogenesis (Shillingford et al. 2006; Shillingford et al. 2010). In mice, gain-of-function of Wnt10b results in the activation of mTOR (Inoki et al. 2006). It is possible that *Bicc1$^{-/-}$* neonates similarly upregulate mTOR signaling through ectopic activation of Wnt signaling (Maisonneuve et al. 2009).

5.10 Invs and Bicc1 separately regulate Wnt signaling

In transgenic mice, hyperactivation as well as loss of Wnt stimulation can trigger cystic growth in the kidney (Pinson et al. 2000; Saadi-Kheddouci et al. 2001). There is increasing evidence that the cilium has the ability to modulate Wnt signaling. Several mouse models of cystic kidney disease after knockdown of ciliary proteins (e.g. Kif3A, IFT88, OFD2) exhibit abnormal Wnt signaling and upregulation of β-catenin (reviewed in Goggolidou 2014). Similar to Invs, Bicc1 is able to downregulate canonical Wnt signaling at

the level of Dvl, although without targeting Dvl for degradation (Simons et al. 2005; Maisonneuve et al. 2009). Studies in HEK cells confirmed that Bicc1 like Invs can inhibit the canonical Wnt signaling pathway. Interestingly, both of them together inhibit Wnt/β-catenin signaling in an additive manner, rather than acting synergistically. This observation suggests that both proteins function in parallel, converging on the same downstream targets when modulating canonical Wnt signaling. How Bicc1 inhibits Wnt/β-catenin remains unclear, one possible scenario suggests that Bicc1 mediates translational silencing of a GSK3β inhibitor. The findings that β-catenin can be released from Gsk3β by the novel identified Bicc1 target RNA helicase activity of Ddx5 and that mrhl RNA, a long noncoding RNA, negatively regulates Wnt signaling through its interaction with Ddx5 are consistent with such a model (Yang et al. 2006; Arun et al. 2012). Another study also showed that Ddx5 phosphorylation at Y593 mediates PDGF stimulated epithelial-mesenchymal transition by promoting β-catenin nuclear translocation via a Wnt-independent pathway (Yang et al. 2006).

The first evidence that cystic kidney disease proteins are involved in PCP and convergent extensions came from Invs-depleted *Xenopus* and in Zebrafish pronephros. In these studies, Invs promoted Dvl signaling in the Wnt/PCP pathway in a complex with Frizzled at the plasma membrane, apparently by binding to and depleting the cytoplasmic pool of Dvl1 that mediates canonical Wnt/β-catenin signaling (Simons et al. 2005; Lienkamp et al. 2010; Veland et al. 2013). Both PCP and Wnt/β-catenin signaling pathways rely on distinct subcellular pools of Dvl. In canonical Wnt signaling, Dvl shuttles between different subcellular compartments including cilia, cytoplasm, and plasma membrane, whereas in the PCP pathway, Dvl is tightly associated with the plasma membrane (Gao and Chen 2010). Although the activities of these distinct pools antagonize each other, the mechanisms regulating pathway selection are poorly understood. Knockdown of *Xenopus* xInvs prevents recruitment of Dvl to the plasma membrane in response to Frizzled-8, identifying Invs as one of the few known molecules that link Dvl to Frizzled receptors (Lienkamp et al. 2010). The core PCP protein Diversin, which is structurally related to Invs, ameliorates renal cysts in *Xenopus* caused by the depletion of Invs (Simons et al. 2005). These observations led to the notion that Invs may function as a molecular switch between canonical Wnt and PCP signaling. In multi-ciliated mucosal epithelial cells, membrane bound Dvl and Inturned mediate the activation of Rho GTPase specifically at basal bodies and together enable docking of basal bodies at the apical plasma membrane (Park et al. 2008). Once docked, basal bodies again require Dvl and Rho for the planar polarization that underlies directional beating of cilia (Park et al. 2008). Whether Invs controls the planar orientation of cilia in the node by regulating the basal docking via PCP has to be determined. Apart from Invs, also several core PCP proteins are required to establish LR asymmetry, including

Dvl1,2,3, Vangl1,2 (Antic et al. 2010; Borovina et al. 2010; Hashimoto et al. 2010; Song et al. 2010). It is possible that also Bicc1 links cilia orientation in the node to PCP signals by counteracting Dvl-induced activation of β-catenin, although Bicc1 is not a core PCP protein as demonstrated by normal eyelid closure, hair follicle and stereo cilia orientation in *Bicc1*^{-/-} mice (Maisonneuve et al. 2009).

A recent study investigated the role of Invs in coordinated cell migration of mouse embryonic fibroblasts (MEF) which highly depends on polarity processes at the single cell level (Veland et al. 2013). MEFs from *inv/inv* embryos exhibited defects in cell migration, in conjunction with defective orientation of primary cilia towards the leading edge. It is suggested that ciliary orientation and positioning are critically linked to the polarity of migrating cells and that the correct orientation is required for directional cell migration in fibroblasts (Christensen et al. 2008; Schneider et al. 2010). In addition Rho and Rac GTPases acting downstream of Dvl/PCP signaling strongly influence cytoskeletal organization, and correct targeting of Rac1 and RhoA at the leading edge is essential for proper directional migration of MEFs (Jaffe and Hall 2005). The same study showed that Invs-depleted MEFs displayed altered cytoplasmic localization of RhoA and Rac which led to actin rearrangements (Veland et al. 2013). In addition, the PKA anchoring protein Ezrin which is reciprocally regulated by RhoA was significantly downregulated in the mutant MEFs. Ezrin serves as intermediate between the plasma membrane and the actin cytoskeleton and has been implicated in kidney tubulogenesis (Orellana et al. 2003). In our flow induced 3D migration assay, we observed a similar defect in migration of IMCD3 cells depleted of Bicc1. Similar to Invs, Bicc1 is also needed to maintain filamentous actin in the kidney (Phillips et al. 2004; Piazzon et al. 2012). It is therefore possible, that Bicc1 modulates cytoskeletal organization by regulating PCP signaling. However, actin dynamics are regulated by multiple signaling pathways, including PKA, and actin organization is influenced by cAMP levels in human ADPKD cells (Howe 2004). In light of these findings we cannot rule out that Bicc1 indirectly affects PCP signaling by regulating PKA.

5.11 Model for Bicc1 regulation

Bicc1^{-/-} mutant animals develop kidney cysts in all segments in the nephron, whereas the initiation of cystogenesis starts in proximal tubules. We could show that Bicc1 is present throughout the kidney tubules, with maximal expression being observed in the ascending loop of Henle, suggesting a functional role for Bicc1 in all renal epithelial cells. Taken all the results together, we propose a model of how we think Bicc1 is spatially regulated by Invs and, probably at a later timepoint, by the phosphorylation of

Ca^{2+}/CaMK2 (Fig. 29). It should be noted that the model is speculative to some extent, especially the relative order of events of Invs binding and CaMK2 phosphorylation of Bicc1.

Invs regulation of Bicc1: Invs, the protein mutated in nephronophthisis type II, regulates Bicc1 specific activities by binding to the RNA binding KH domains and by sequestering it in the proximal part of the cilium in the so-called Invs compartment. The interaction inhibits the association of Bicc1 with target RNAs, thereby promoting de-repression of Bicc1 target genes. We suggest that urinary flow mediates an influx of Ca^{2+} via PC2 and eventually abrogates the interaction between Bicc1 and Invs, especially in proximal tubules. Indeed, Invs normally seems to inhibit Bicc1 more potently in distal segments of the nephron than in proximal tubules since the latter only express Ddx5 in $Bicc1^{-/-}$ but not in WT kidneys, and the basal expression of Ddx5 that is normally observed in more distal segments in the WT was almost completely lost in *inv/inv* mutants but restored in $Bicc1^{-/-}$; *inv/inv* double mutants. Such gradation of Bicc1 activity along the nephron axis may also account for the graded expression of Bicc1 itself due to autoinhibition (Chicoine et al. 2007; Maisonneuve et al. 2009), because Bicc1 staining by anti-SAM antibodies was clearly reduced in proximal tubules compared to the ascending loop of Henle. Conversely, an antibody raised against the S/G region has previously been shown to detect Bicc1 primarily in the cytoplasm of proximal tubules but not in cilia, indicating that this epitope is likely masked in cells where Bicc1 is associated with Invs or other interacting factors. Both Bicc1 and Invs are prone to bind CaM in the presence or absence of Ca^{2+}, respectively. An increase of Ca^{2+} concentrations leads to the dissociation of the Invs-CaM complex, whereas Bicc1 is able to bind to CaM. These altered interactions with CaM may induce conformational changes that allow Bicc1 to uncouple from Invs and to translocate to the cytoplasm. In the absence of Invs, Bicc1 is not retained in the cilium and constitutively represses target gene translation independently of PC2/Ca^{2+} signaling. Cysts also arise upon loss of Invs. Our results thus predict that both loss and gain of Bicc1 function trigger cystic growth, and that gene silencing activity of Bicc1 therefore must be tightly regulated, possibly by dynamic fluctuations in calcium levels. In addition, graded repression of Bicc1 activity by Invs may also be the critical determinant downstream of calcium signaling to mediate visceral left-right patterning.

Bicc1 is regulated by CaMK2 phosphorylation: In response to Ca^{2+} influx, CaMK2 is activated by autophosphorylation at the base of the cilium. Activated Ca^{2+}/CaMK2 subsequently phosphorylates Bicc1 on T724 and S805 and enables miRISC assembly by stimulating Bicc1 binding to target mRNAs and miRNAs. A T724A and S805A Bicc1 mutant construct immune to Ca^{2+}/CaMK2 phosphorylation is unable

to induce silencing activity. An interesting experiment would involve phosphomimicking Bicc1 mutants and whether they are able to restore Bicc1 mediated silencing function in the absence of CaMK2.

Our study proposes a dual role for Ca^{2+} in activating Bicc1 by dissociating the Bicc1/Invs complex and by activating CaMK2. These findings are very important because Bicc1 suppresses cystic growth in mice and humans, and no other targets of Ca^{2+}/CaMK2 have been identified downstream of polycystins. A far-reaching implication is that ADPKD therapies should restore the regulation of Bicc1 function. However, whether Bicc1 activity is directly regulated by Ca^{2+} flux via PC2 has to be further examined.
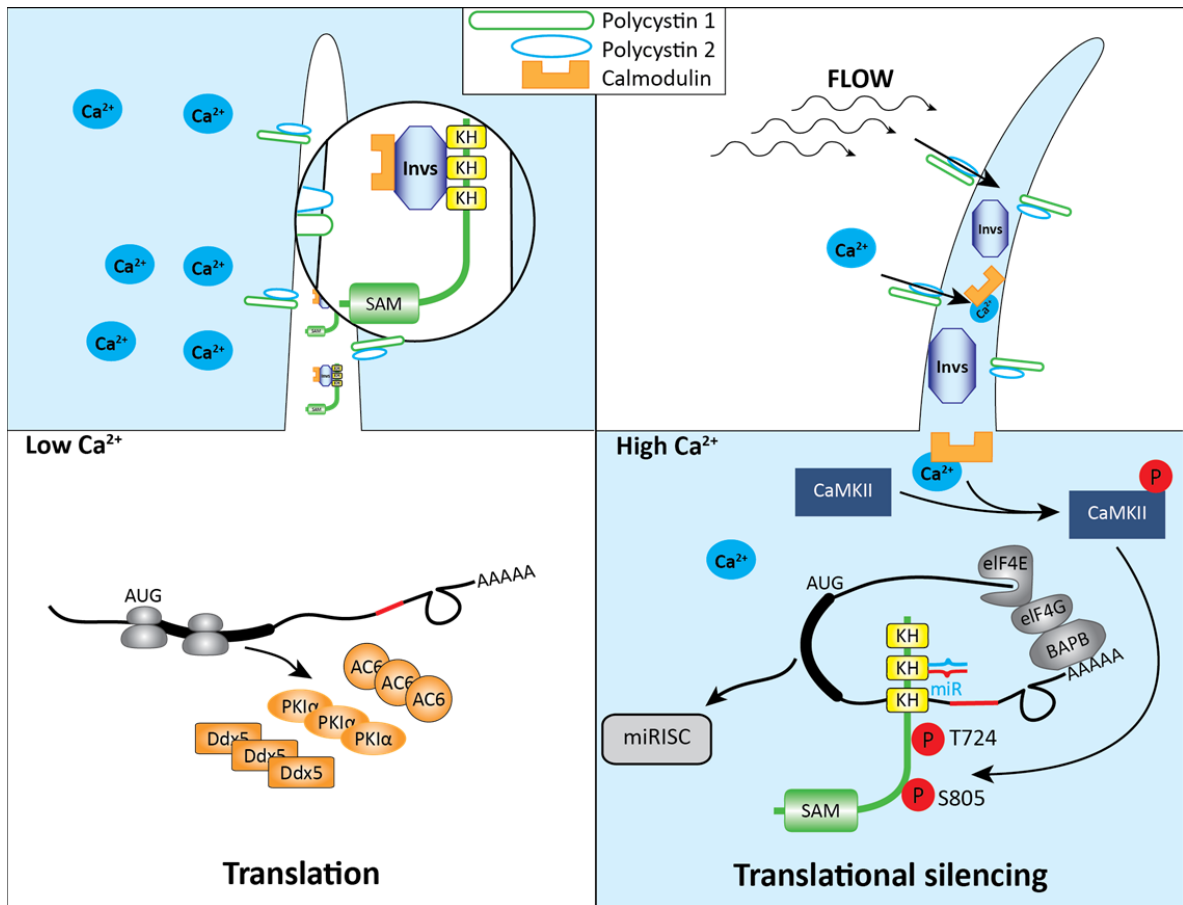
Figure 29. Working model for the regulation of Bicc1 localization by Invs. *Calcium influx in cilia and renal epithelial cells is controlled by mechanosenory complexes of PC1 and PC2. In the absence of urinary flow, Bicc1 and Invs-CaM form a complex in the Invs compartment and Bicc1 target genes such as PKIα, AC6 and Ddx5 are translated (left). Urinary flow allows the entry of extracellular Ca^{2+} via PC2, which leads to the dissociation of Bicc1-Invs as well as Invs-CaM (right). Bicc1 translocates to the cytoplasm and is phosphorylated at T724 and S805 by Ca^{2+}/CaMKII. In this activated state Bicc1 binds target mRNAs and miRNAs and enables miRISC assembly. Translocation of Bicc1 to the cytoplasm and release from Invs may be induced by calcium to enable RNA binding and translational repression.*

6. Materials and Methods

6.1 Mouse models

All experiments with mice were approved by the Veterinary Service of the Swiss canton of Vaud. Mice heterozygous for a targeted allele of *Bicc1* (Maisonneuve et al. 2009) were maintained on a C57BL/6 genetic background in individually ventilated cages at the EPFL animal facility. Inversin (Yokoyama et al. 1993) and Inversin-GFP (Watanabe et al. 2003) mice were a gift from Hiroshi Hamada and they were maintained in a C57Bl/6 J genetic background. The *BOS-Invs-GFP* is under the control of the elongation factor 1α to ensure that the fusion gene is expressed ubiquitously and robustly. Crossing of *invs/+*; *Invs-GFP* mice with *invs/+* mice yielded *inv/inv*; *Invs-GFP* animals. The transgene is able to rescue the situs defects and PKD phenotype of *inv/inv* mice. After crossing and genotyping, mutant mice and control littermates were sacrificed on postnatal day P0 or P2.

6.1.1 Genotyping

Tails of mice were collected during dissection and lysed for 10 min at 110°C in 600 μl 50 mM NaOH. After the samples cooled down to room temperature, the pH was equilibrated with 50 μl 1M Tris.HCL pH 8. Samples were centrifuged full speed for 6 min in a table top centrifuge at room temperature. 1 ul of lysate was used for the genotyping the protocol is described below.

Detection of Bicc1 mutation

Bgt5-U	CCCAACACGGCATCTTTAGTC
Bgt5-N	CAGGGTCGCTCGGTGTTC
Bgt5-L2	GCACGGAAGCAGGGTTATGTC

	Final Concentration	ul
10× Sigma PCR Buffer	1×	2.1
dNTP (10mM stock)	200 μM (each)	0.42
Primer (10uM stock)	300 nM (each)	0.63 each
Template	1 μL	1
Taq polymerase	0.2μL	0.2
ddH$_2$0		15.39
Final Volume		21 μL

PCR touch-down program for Bicc1:

10 cycles:
94 °C   10 min
94 °C   30 sec
63 °C   45 sec, -0.5°C/cycle (during 9 cycles)
72 °C   1 min 20 sec
and 22 cycles:
94 °C   30 sec
58 °C   30 sec
72 °C   1 min 20 sec
and
72 °C   10 min

Mutant *Bicc1* allele: Bgt5-U with Bgt5-N: 622bp

WT *Bicc1* allele: Bgt5-U with Bgt5-L2: 368bp

Detection of Invs-GFP transgene and *inv* mutation

A: *Invs* wild type allele (genomic DNA exon 8-intron 8)
        inv ex8/9-S1   : 5'- cac tgt tcc gag cct gtg aga -3'
        inv ex8/9-A9   : 5'-gtt tgg aga ggt tgg gac tc-3'
        This primer pair yields a 292 bp product

B: *GFP-Invs* transgene allele (inv cDNA exon 8-11)
        inv ex8/9-S1   : 5'-cac tgt tcc gag cct gtg aga-3'
        inv ex11-A   : 5'-ttg gct gca gcg tct ttc ctc a-3'
        This primer pair yields a 607 bp product

C: *Invs* mutant allele *inv* (insertion of exon 2-3 of the tyrosinase gene)
        tyrosinase-S   : 5'-tca gaa gag tat aat agc cat c-3'
        tyrosinase-A   : 5'-tgt cca caa aag cat ggt gaa gaa g-3'
        This primer pair yields a 348 bp product

	Final Concentration	ul
10× Sigma PCR Buffer	1×	2.1
dNTP (10mM stock)	200 μM (each)	0.42
Primer (10uM stock)	300 nM (each)	0.63 each
Template	1 μL	1
Taq polymerase	0.2μL	0.2μL
ddH$_2$0		Add up to 21 μl
Final Volume	21 μL	21

PCR program for:
Wild type allele and Invs-GFP
Primer pair A + B (inv ex8/9-S1 / inv ex8/9-A9 _and_ inv ex8/9-S1 / inv ex11-A)

98°C - 3 seconds
60°C - 20 seconds   ×30
72°C - 30 seconds

Primer pair C (tyrosinase-S/ tyrosinase-A)

98°C - 3 seconds
57°C - 20 seconds   ×32
72°C - 30 seconds

6.1.2 Mouse tissue embedding for cryostat sectioning

Postnatal mouse kidneys and livers as well as adult kidneys were fixed in 4% paraformaldehyde in PBS for 2 hrs to over-night at 4°C, rinsed with PBS, and soaked in 15% sucrose at least over-night at 4°C, after which the tissues should sink to the bottom of the tube. Tissues were embedded in Optimum Cutting Temperature (OCT) compound on dry ice. Blocks were stored at -20°C and sectioned at -20°C.

6.2 Plasmids and cloning

The GST fusion plasmid GEX-1λT::KH, pGEX-1λT::G/S, pGEX-1λT::IVS, pGEX-1λT::SAM and the luciferase reporter plasmids pCS+::AC6-3'UTRprox, pCS+::PKIα-3'UTRprox, as well as the Tcf/Lef-sensitive reporter TOPflash have been described previously (Korinek et al. 1997; Piazzon et al. 2012). A full length Invs cDNA (gift of Tom Strachan) was cured of base changes by overlap extension PCR to restore the reference sequence NM_010569.3 and fused to an N-terminal FLAG epitope. To construct Bicc1-HA and GST-IVS alanine mutant plasmids, round-the-horn PCR was performed using the pCMV-SPORT::HA-Bicc1 vector (Maisonneuve et al. 2009) or pGEX-1λT::IVS, respectively, as a template. Adjacent but non-overlapping primers were designed harbouring serine/threonine to alanine mutations and, where possible, a silent diagnostic restriction site (http://watcut.uwaterloo.ca/template.php?act=silent_new). PCR was executed using PfuUltra II fusion polymerase (Agilent) and the mother plasmid was digested with DpnI restriction enzyme. Prior to ligation, the PCR fragments were phosphorylated at their 5' end

using T4 polynucleotide kinase. The sequences of all mutated expression vectors were verified by Sanger sequencing.

HA-Bicc1 and GST-IVS mutant plasmids diagnostic site and primer sequences:

S637 to A637	FspI	fwd: TGCGCATTCTGGAAACGCTGGCGACT;	rev: GGACTTCGAGGCATGCCCACTTCAA
S721 to A721	FspI	fwd: TGCGCAGCCAACATATGTCCACATGC;	rev: GCCAGGCGGGCCCTCTCC
S681 to A681	XbaI	fwd: GCTAGCAGACCCTGAACTGAGCGCCAC;	rev: AGTCTGTCAGTCCCGTGGAGGTGC
T724 to A724	ApaI	fwd: CADCATATGTCCACATGCAGGCATTTG;	rev: GCTGCGAGGCCAGGCGTG
S805 to A805	AfeI	fwd: GCTCGTGAGCACCTGGCAAGTGGAA;	rev: CCGATTGGTGCTGAGAATTCACTGTGACCCAT

6.3 Cell culture and transfection

HEK 293T, MDCK, and IMCD3 cells were maintained in DMEM (Sigma) supplemented with 10 % fetal bovine serum (FBS, Sigma), glutamine 1 % (Invitrogen) and gentamycin 1 % (Invitrogen). Polarized IMCD3 cells were obtained after culturing them for a minimum of 4 days in fully supplemented medium and then transferring them to medium without FBS for 2 days. Plasmids were transfected using jetPEI or INTERFERin (Polyplus Transfection) according to the manufacturer instructions. To inhibit proteasomal degradation of Flag-Invs, HEK 293T cells were incubated with 10 µM MG-132 for 12 or 24 hours.

The following siRNA duplexes (Microsynth) were used: A scrambled negative control siRNA (Ambion) and siBicc1 (5'- CCA ACC ACG UAU CCU AUA A dTdT -3'), as well as two siRNA probes against Invs (siInvs1: 5'- GGA ACG AUC CCU UCG GAC A dTdT-3' and siInvs2 5'-UGU CCG AAG GGA UCG UUC C dTdT-3' (Sang et al. 2011). Cells were transfected with 40 nM siRNA or 2*20 nM siInvs1&2, respectively, using INTERFERIN^{TM} (Polyplus transfection). Knockdown was confirmed by immunoblotting or by qRT-PCR 72 hrs after transfection.

6.4. Western blots and Immunoprecipitations

Kidney samples were immediately frozen in liquid nitrogen after dissection. On the day of use, the tissue was disrupted with a pestle directly in an Eppendorf tube. Grinded tissue and cells were lysed and subsequently sonicated and centrifuged. Protein concentrations were quantified using Bradford assay (Bio-rad) according to the manufacturer's protocol to ensure equal loading on SDS-PAGE.

For immunoprecipitation and CaM pull-down experiments, anti-HA or anti-Flag-M2 (both from Sigma) agarose beads and CaM sepharose-beads 4b (GE Healthcare) were incubated with cellular extract of IMCD3 cells or HEK 293T cells O/N at 4°C. 10 % of the extract was usually kept for the input. 2 mM EGTA

or different concentrations (2 mM and 4 mM) of Ca^{2+} were added to the immunoprecipitation buffer to validate CaM-Bicc1 as well as Invs-Bicc1 binding. The following day, samples were washed, resuspended in reducing sample buffer and boiled for 3 min at 95°C to elute the proteins. Primary antibodies used in this study: anti-HA 1:2000 (rabbit, Sigma), anti-Flag M2 1:2000 (mouse, Sigma), anti-Bicc1 SAM 1:300 (rabbit, Proteogenix), anti-γ-tubulin 1:2000 (mouse, Sigma), anti-GAPDH 1:4000 (rabbit, Abcam), anti-PKIα 1:200 (goat, Santa Cruz), anti-ATP6V1B1 1:2000 (mouse, Origene), anti-Ddx5 1:2000 (rabbit, Bethyl), anti-AC6 1:1000 (rabbit, ProteinTech). Immunoblot signals were quantified using Fiji image analysis software and loadings were normalized to γ-tubulin in cells and GAPDH in kidney samples.

6.5. Luciferase reporter assays

The luciferase reporter plasmids pCS+::AC6-3'UTRprox and pCS+::PKIα-3'UTRprox as well as the Tcf/Lef-sensitive reporter TOPflash were used (Maisonneuve et al. 2009; Piazzon et al. 2012). HEK 293T cells were plated in 24-well plates. After 12 hrs, triplicates were transfected with the indicated plasmids (1x dose: 0.1 μg/well) and with a *lacZ* expression vector (0.05 μg/well) using jetPEI (Polyplus Transfection). 36 or 48 hrs after transfection, cell extracts were prepared in 25 mM Tris-phosphate buffer, pH 7.8, containing 2 mM DTT, 2 mM CDTA, 10 % glycerol, and 0.5 % Triton X-100. The measurements of luciferase expression levels were carried out using 20-fold diluted extracts, and luminescent counts were normalized to β-galactosidase activity.

6.6 Yeast two-hybrid assay (Y2H)

Y2H allows assessing the interaction between two proteins in the yeast *Saccharomyces cerevisiae*. It relies on the expression of two fusion proteins. The first one, encoded by the pGBKT7 plasmid, is composed of the DNA binding domain of the GAL4 transcription factor (GAL4-BD) fused with the bait protein at its C-terminal extremity. The second, encoded by the pACTII plasmid, is composed of the activation domain of the GAL4 transcription factor (GAL4-AD) fused with the prey protein at its C-terminal extremity. The interaction between the two partners allows the reconstitution of an active transcription factor inducing the expression of a reporter gene under control of the *GAL1* activator sequence. The reporter gene used in this study is the *HIS3* gene required for histidine biosynthesis.

For Y2H, appropriate pACTII (*LEU2*) and pGBKT7 (*TRP1*) plasmids were used to transform (lithium acetate method) haploid cells from strain CG1945 (mat a; *ura3*-52, *his3*-200, *ade2*-101, *lys2*-801, *trp1*-901, *leu2*-3, 112, *gal4*-542, *gal80*-538, cyhr2, *LYS2*::GAL1UAS-GAL1TATA-*HIS3*, *URA3*::GAL417-mers(x3)-CYC1TATA-*LacZ*) and strain Y187 (mat α; *gal4*␣ *gal80*␣ *ade2*-101 *his3*-200 *leu2-3,*112 *lys2*-801 *trp1*-901 *ura3*-52, *URA3*::Gal1UAS GAL1TATA-*LacZ*), respectively. After crossing on YPD medium, diploid cells were selected on media suitable for double selection (Leu⁻, Trp⁻) and then plated on media suitable for triple selection (Leu⁻, Trp⁻, His⁻). 3-Amino-1, 2, 4-triazol (3-AT), a competitive inhibitor of histidine synthesis, was used to evaluate the strength of the interactions. Growth was assessed after three days of incubation at 30°C.

6.7 Indirect immunofluorescent labelling

6.7.1 IF on cells

For immunostaining, MDCK or IMCD3 cells were grown in 6-well plates and transfected with expression vectors for HA-Bicc1 and Flag-Invs with JetPEI (Polyplus transfection). After 24 hrs, cells were passaged into 24-well plates on sterile coverslips. Forty-eight hours after transfection, cells were fixed and permeabilized for 10 minutes at -20°C in methanol, and subsequently washed with PBS. For the ciliary staining, IMCD3 cells were split 12 hrs after transfection to reach 100% confluency. Cells were grown for 4 days and the last two days, the IMCD3 cells were cultured in the absence of 10% fetal bovine serum to ensure that the cells do not proliferate.

Coverslips were incubated for 1 hr at RT for blocking in PBS containing 1% BSA, and then for 2 hrs at RT in blocking buffer containing the primary antibodies anti-HA 1:1000 (rabbit, Sigma), anti-Flag 1:800 (mouse, Sigma), anti-Arl13b 1:1000 (mouse, Abcam), and/or anti-acetylated tubulin (mouse, Sigma). After washes in PBS, coverslips were incubated with the secondary antibodies anti-mouse or anti rabbit Alexa 488, Alexa 568, or Alexa 647 (Invitrogen), in blocking buffer for 1 hr at RT in presence of DAPI (1:10000). Stained coverslips were mounted with DABCO, and images were acquired with a 60x objective on a Leica LSM700 upright confocal microscope with an Axiocam MRm (B/W) camera. Cilia on IMCD3 cells were reconstructed from z-stacks using Fiji image analysis software.

6.7.2 IF on tissue sections

Cryosections (8 μM) were permeabilized for 10 min with 0.2% Triton X-100 in PBS, blocked with PBS containing 1 % BSA. Kidneys were additionally blocked with streptavidin-biotin blocking kit (Vector labs, #SP-2002). Biotinylated DBA (Vector labs, B-1035), or LTL (Vector labs, B-1325) 1:200, and primary antibodies were preabsorbed with embryo powder and incubated overnight at 4°C in buffer containing PBS, 0.1% Triton X-100. Dilutions for primary antibody were: anti-THP 1:20 (R&D Systems, AF5175), anti-SAM Bicc1 1:1000 (Proteogenix), anti-DDX5 1:2000 (Bethyl, A300-523A), anti-CK19 1:50 (Santa Cruz Biotechnology), anti-Arl13b 1:1000 (Abcam, ab136648), anti-pCREB 1:1000 (Cell Signaling). Sections were washed 3 times with PBS containing 0.2 % Triton-X 100 for 10 min. Alexa Fluor secondary antibodies (all from Invitrogen) were used for multicolor detection and anti-sheep 568 (Invitrogen) were incubated for 2 hrs at room temperature at dilutions of 1:800, and 1:200 , respectively, in PBS containing 0.1 % Triton X-100. Kidney sections stained with biotinylated DBA or LTL were incubated with streptavidin conjugated green, red, or far red antibodies (Lifetechnologies) for 2 hrs at room temperature at 1:400 dilution in PBS containing 0.1 % Triton X-100. Sections were washed 4 times with PBS containing 0.2 % Triton-X 100 for 20 min at RT and mounted in DABCO. Dapi (50 ng/μl, Sigma) staining was done during the second last wash. Images were acquired with a 20x, 40x or 60x objective on a Leica LSM700 upright confocal microscope with an Axiocam MRm (B/W) camera. Whole kidney pictures were acquired with an automated stage and stitched together with the Fiji image analysis software and the plugin stitching (Preibisch et al. 2009). For the cilia analysis, z-stacks were acquired to capture the whole cilium. Pictures were deconvoluted with Huygens Remote manger (http://huygens-rm.org/home/) and z-projections were done by Fiji software. Imaris was used to calculate the length of cilia, Bicc1 and Invs-GFP compartment as well as to measure the mean intensity of Bicc1 and Invs in the ciliary axoneme.

6.7.3 Hematoxylin and eosin staining

The Hematoxylin and eosin staining uses two separate dyes; Hematein interacts with DNA and stains the nuclei blue, and Erythrosyne stains basic cells structures like plasma proteins in pink. Frozen sections were dewaxed, rehydrated in water and the slides were stained with hematoxylin for 5 min. Sections were washed extensively under tap water and differentiated in 1% acid-alcohol for a few seconds. The cytoplasm was stained by placing the sections in 0.25% erythrosine for 1min. Slides were washed briefly and sections were dehydrated, cleared, and subsequently mounted (Eukitt).

6.7.4 Quantification and statistical analysis of nuclear staining

Co-immunofluorescent staining with DAPI and anti-pCREB or anti-DDX5 was performed on either half or the whole kidney. 16 bit pictures were acquired with an automated stage on a 40x objective on a Leica LSM700 upright confocal microscope and individual images were stitched together with the Fiji plugin stitching (Preibisch et al. 2009). All quantification steps were executed on Fiji software (Schindelin et al. 2012). Briefly, a nuclear mask was generated using the DAPI-channel, sections which were too big or had an abnormal shape were excluded. The mask was overlaid with the channel of interest and mean fluorescent intensities in each nuclei was measured (16 bit range: 0 - 65535). Nuclear intensities measured on images not stained with primary anti-pCREB or anti-DDX5 served as baseline for the absence of nuclear staining. All intensities above this threshold were considered as true signal. For each kidney, intensities in a minimum of 15'000 nuclei were measured. Frequency distribution analysis with a bin center of 2000 was used to quantify intensity distribution between the different genotypes. One-way ANOVA test was used to compare groups of unpaired values. Tukey's multiple comparison post-test served to identify the significance (*p* values) of differences in the sum of ranks between each pair of groups.

6.8 Custom rabbit polyclonal Bicc1 antibody

A custom rabbit polyclonal Bicaudal-C antibody (Bicc1) was raised by Proteogenix (Oberhausbergen, France) against the mouse Bicc1 SAM domain (residues 870-977) fused to an N-terminal His-tag. The antibody was affinity-purified and tested against the antigen by ELISA.

Bicaudal C locus: AF319464_1 (The SAM domain is highlighted in red)

```
  1 masqsepgyl aaaqsdpgsn serstdspva gseddlvaaa pllhspewse erfrvdrkkl
 61 eamlqaaaeg kgrsgedffq kimeetntqi awpsklkiga kskkdphikv sgkkedvkea
121 kemimsvldt ksnrvtlkmd vshtehshvi gkggnnikkv medtgchihf pdsnrnnqae
181 ksnqvsiagq pagvesarar irellplvlm felpiagilq pvpdpntpsi qhisqtysvs
241 vsfkqrsrmy gatvtvrgsq nntnavkegt amllehlags lasaipvstq ldiaaqhhlf
301 mmgrngsnvk himqrtgaqi hfpdpsnpqk kstvylqgti esvclarqyl mgclplvlmf
361 dmkedievdp qviaqlmeql dvfisikpkp kqpsksvivk svernalnmy earkcllgle
421 ssgvsiatsl spascpagla cpsldilasa glgltglgll gpttlslnts atpnsllnal
481 ntsvsplqss ssgtpsptlw appiantasa tgfstiphlm lpstaqatlt nillsgvpty
541 ghtapspppg ltpvdvhins mqtegknisa singhvqpan mkygplstss lgekvlssnh
601 gdpsmqtagp eqaspksnsv egcndafvev gmprspshsg nagdlkqmlg askvscakrq
661 tvellqgtkn shlhgtdrll sdpelsates pladkkapgs eraaeraaaa qqkserarla
721 sqptyvhmqa fdyeqkklla tkamlkkpvv tevrtptntw sglgfsksmp aetikelrra
781 nhvsykptmt tayegsslsl srsssrehla sgsesdnwrd rngigpmghs efsapigspk
841 rkqnksrehy lsssnymdci ssltgsngcn lnscfkgsdl pelfsklglg kytdvfqqqe
901 idlqtfltlt dqdlkelgit tfgarrkmll aiselsknrr klfeppnasc tsfleggasg
961 rlprqyhsdi asvsgrw
```

6.9 qRT-PCR

IMCD3 cells transfected with specific siRNA were grown for 3 days in 6 well plates. 1 ml of TRIzol (Life technologies) was added per well and RNA was extracted according to the manufactures protocol. Total RNA was digested with RNase free DNase (Turbo DNase Kit, Invitrogen) and concentration and RNA quality was evaluated with NanoDrop Spectrometer ND-100. Reverse transcription of cDNA was carried out using random hexamer primers (Promega) and SuperScriptIII reverse transcriptase (Invitrogen). The qPCR was performed with Step one plus real time PCR systems from Applied Biosystems using Power Sybr Green mix (Applied Biosystems). Samples were analyzed as triplicates and expression levels were calculated with the manufacturer's software using the DDCt method. A standard curve was created for each primer pair.

Primers pairs used in this study (5'-3'):

Invs1:	fwd: ACCTTGCAGCTCAAAAGGGA;	rev: TGCAGAGCTGTTTGCTTGTT	size: 205bp
Invs2:	fwd: TGGGCAGCCTTACTAGGTCA;	rev: GCATAGTGCAAGGGTGTTGC	size: 107bp
Actin:	fwd: GGCTGTATTCCCCTCCATCG;	rev: CCAGTTGGTAACAATGCCATGT	size: 154bp

6.10 RT-PCR analysis of protein-RNA co-immunoprecipitates.

To monitor protein-RNA and protein-miRNA interactions, AGO2 and ectopic HA-Bicc1 was immunoprecipitated from HEK-293T cell extracts as described in (Piazzon et al. 2012). Briefly, HEK-293T cells were transfected in 10 cm dishes using jetPEI (Polyplus Transfection). 36 hrs after transfection, cells were washed with PBS, resuspended in extraction buffer (10 mM Tris-HCl, pH 7.4, 2.5 mM MgCl$_2$, 100 mM NaCl) supplemented with 0.02% NP-40 and protease inhibitors (Roche). After sonication and centrifugation at 10'000 rpm for 15 min, extracts were incubated for 2 h at 4°C with anti-HA (Sigma) and anti-AGO2 (Millipore) conjugated IgG beads. Immunoprecipitates were washed 5 times in extraction buffer supplemented with 0.01% NP-40 and extracted with buffer-saturated phenol. Samples were treated with DNAse I (10 U; Ambion) for 15 min at 37 °C, followed by phenol-chloroform extraction and ethanol precipitation. Equal amounts of samples were reverse transcribed using qScript cDNA synthesis kit (Quanta Biosciences) or QuantiMir RT kit (System Biosciences). The PCR program was 95 °C for 5 min; 30 cycles of 95 °C for 1 min; 60 °C for 1 min; and 72 °C for 1 min. Detection of miRNAs by QuantiMir^{TM} was performed at 95°C for 10 min; 30 cycles of 95 °C; 15 sec; 60 °C for 1 min. From each 25 µl PCR reaction, 10 µl were resolved on 1% or 3.5% agarose gels.

6.11 Recombinant GST fusion proteins

Recombinant GST-Bicc1 KH, GST-Bicc1 IVS, GST-Bicc1 S/G, GST-Bicc1 SAM and GST alone were expressed in *Escherichia coli* BL21 (DE3) pLysS cells (Promega). GST-fusion proteins were purified by affinity chromatography on glutathione-sepharose beads 4B (GE Healthcare) as recommended by the manufacturer. Purification was carried out in buffer containing 50 mM Tris·HCl pH 8 and 200 mM NaCl. For in vitro kinase assays, GST-fusion proteins were not eluted from glutathion beads until after the reaction.

6.12 In vitro kinase assay and metabolic labeling

For *in vitro* kinase assays, 2 µg of GST-tagged proteins bound to glutathione-sepharose beads were incubated with purified and activated CaMKII (BioConcept) in kinase buffer (70 mM Tris·HCl, 10 mM MgCl$_2$, 5 mM DTT) supplemented with calmodulin (1.2 µM), CaCl$_2$ (2 mM), ATP (100 µM) and gamma-labeled ATP (10 µCi) (Hartmann analytics) for 4h at 30°C. The reaction was terminated by addition of SDS sample buffer supplied with 5% β-mercaptoethanol. Beads were boiled for 3 min at 95°C, and 25% of supernatants were separated by SDS-PAGE followed by autoradiography. Metabolic labelling in HEK 293T cells was conducted 36 hrs after transfection by replacing culture medium with phosphate-free DMEM containing 10% dialyzed FBS, 1% glutamax (Life Technologies) and 0.5 mCi/ml Phosphorus-32 (H$_3$^{32}PO$_4$). After 4 hrs, cells were lysed, and HA-Bicc1 was immunoprecipated and treated for 2 hrs at room temperature with or without 400 U of lambda phosphatase (Santa Cruz) prior to analysis.

6.13 Modified invasion assay

The modified Boyden chamber assay was performed as described in (Shields et al. 2007; Li and Hanahan 2013). IMCD3 cells were split into 6 well plates and transfected with scramble siRNA or siRNA against Bicc1. 2 days after transfection cells were seeded into a mixture of 1.2 mg/ml rat tail collagen type I (BD Biosciences) and growth factor reduced matrigel (BD Bioscience), pipetted onto transwell inserts with 2 mm PCF and 8.0 µm pore size (Millipore) and subsequently incubated for 1 hrs at 37 °C to solidify the matrix. To generate flow conditions, 650 µl basal medium was added onto the transwell inserts (~1cm water head) and 150 µl into the bottom of the well. After incubation overnight, the gels were discarded and the upper side of the membrane was cleaned with a cotton tip to remove all cells that did not cross

the transwell. Cells on the bottom side were fixed in methanol and stained with DAPI (50 ng/µl, Sigma). To count the number of migrated cells, five images/well were acquired with a 10x objective, which covered most of the membrane area. Results were quantified using Fiji image analysis software. All experiments were in triplicates and performed three times.

6.14 Sequence alignment

Clustal W software was used for multiple-sequence alignment (Larkin et al. 2007). The Gene Bank ID numbers for Bicaudal-C protein sequences were:

gi|13994223   *Mus musculus*

gi|122937472   *Homo sapiens*

gi|332834316   *Pan troglodytes*

gi|157818393   *Rattus norvegicus*

gi|297491437   *Bos taurus*

gi|345798974   *Canis familiaris*

gi|82115500   *Xenupos laevis*

gi|17136720   *Drosophila melanogaster*

gi|292623098   *Danio rerio*

gi|212646112   *Caenorhabditis elegans*

6.15 Statistical analysis

Error bars show standard error of the mean (SEM). A two tailed students-t test was used to test differences in means between two groups or conditions to calculate *p* values. One-way ANOVA test was used to compare groups of unpaired values. Tukey's multiple comparison post-test served to identify the significance (*p* values) of differences in the sum of ranks between each pair of groups. Linear regression analysis was used to validate correlation between cilia length and the different ciliary compartments, the *p* value was calculated to test linear relationship between the two (F-test).

7. References

Abdul-Majeed S, Nauli SM. 2011. Calcium-mediated mechanisms of cystic expansion. *Biochim Biophys Acta* **1812**: 1281-1290.

Aberle H, Bauer A, Stappert J, Kispert A, Kemler R. 1997. beta-catenin is a target for the ubiquitin-proteasome pathway. *EMBO J* **16**: 3797-3804.

Antic D, Stubbs JL, Suyama K, Kintner C, Scott MP, Axelrod JD. 2010. Planar cell polarity enables posterior localization of nodal cilia and left-right axis determination during mouse and Xenopus embryogenesis. *PLoS One* **5**: e8999.

Arun G, Akhade VS, Donakonda S, Rao MR. 2012. mrhl RNA, a long noncoding RNA, negatively regulates Wnt signaling through its protein partner Ddx5/p68 in mouse spermatogonial cells. *Mol Cell Biol* **32**: 3140-3152.

Attanasio M, Uhlenhaut NH, Sousa VH, O'Toole JF, Otto E, Anlag K, Klugmann C, Treier AC, Helou J, Sayer JA et al. 2007. Loss of GLIS2 causes nephronophthisis in humans and mice by increased apoptosis and fibrosis. *Nat Genet* **39**: 1018-1024.

Audrezet MP, Cornec-Le Gall E, Chen JM, Redon S, Quere I, Creff J, Benech C, Maestri S, Le Meur Y, Ferec C. 2012. Autosomal dominant polycystic kidney disease: comprehensive mutation analysis of PKD1 and PKD2 in 700 unrelated patients. *Human mutation* **33**: 1239-1250.

Babich V, Zeng WZ, Yeh BI, Ibraghimov-Beskrovnaya O, Cai Y, Somlo S, Huang CL. 2004. The N-terminal extracellular domain is required for polycystin-1-dependent channel activity. *J Biol Chem* **279**: 25582-25589.

Banales JM, Masyuk TV, Gradilone SA, Masyuk AI, Medina JF, LaRusso NF. 2009. The cAMP effectors Epac and protein kinase a (PKA) are involved in the hepatic cystogenesis of an animal model of autosomal recessive polycystic kidney disease (ARPKD). *Hepatology* **49**: 160-174.

Barford D. 2011. Structure, function and mechanism of the anaphase promoting complex (APC/C). *Q Rev Biophys* **44**: 153-190.

Barnes BG. 1961. Ciliated secretory cells in the pars distalis of the mouse hypophysis. *Journal of ultrastructure research* **5**: 453-467.

Belibi FA, Reif G, Wallace DP, Yamaguchi T, Olsen L, Li H, Helmkamp GM, Jr., Grantham JJ. 2004. Cyclic AMP promotes growth and secretion in human polycystic kidney epithelial cells. *Kidney Int* **66**: 964-973.

Berbari NF, Johnson AD, Lewis JS, Askwith CC, Mykytyn K. 2008. Identification of ciliary localization sequences within the third intracellular loop of G protein-coupled receptors. *Molecular biology of the cell* **19**: 1540-1547.

Berbari NF, O'Connor AK, Haycraft CJ, Yoder BK. 2009. The primary cilium as a complex signaling center. *Curr Biol* **19**: R526-535.

Bergmann C, Fliegauf M, Bruchle NO, Frank V, Olbrich H, Kirschner J, Schermer B, Schmedding I, Kispert A, Kranzlin B et al. 2008. Loss of nephrocystin-3 function can cause embryonic lethality, Meckel-Gruber-like syndrome, situs inversus, and renal-hepatic-pancreatic dysplasia. *American journal of human genetics* **82**: 959-970.

Bernhard W, De Harven E. 1956. [Electron microscopic study of the ultrastructure of centrioles in vertebra]. *Zeitschrift fur Zellforschung und mikroskopische Anatomie* **45**: 378-398.

Bertram JF, Douglas-Denton RN, Diouf B, Hughson MD, Hoy WE. 2011. Human nephron number: implications for health and disease. *Pediatr Nephrol* **26**: 1529-1533.

Borovina A, Superina S, Voskas D, Ciruna B. 2010. Vangl2 directs the posterior tilting and asymmetric localization of motile primary cilia. *Nat Cell Biol* **12**: 407-412.

Bouvrette DJ, Price SJ, Bryda EC. 2008. K homology domains of the mouse polycystic kidney disease-related protein, Bicaudal-C (Bicc1), mediate RNA binding in vitro. *Nephron Exp Nephrol* **108**: e27-34.

Bouvrette DJ, Sittaramane V, Heidel JR, Chandrasekhar A, Bryda EC. 2010. Knockdown of bicaudal C in zebrafish (Danio rerio) causes cystic kidneys: a nonmammalian model of polycystic kidney disease. *Comparative medicine* **60**: 96-106.

Brown NE, Murcia NS. 2003. Delayed cystogenesis and increased ciliogenesis associated with the re-expression of polaris in Tg737 mutant mice. *Kidney Int* **63**: 1220-1229.

Burckle C, Gaude HM, Vesque C, Silbermann F, Salomon R, Jeanpierre C, Antignac C, Saunier S, Schneider-Maunoury S. 2011. Control of the Wnt pathways by nephrocystin-4 is required for morphogenesis of the zebrafish pronephros. *Hum Mol Genet* **20**: 2611-2627.

Cai Y, Maeda Y, Cedzich A, Torres VE, Wu G, Hayashi T, Mochizuki T, Park JH, Witzgall R, Somlo S. 1999. Identification and characterization of polycystin-2, the PKD2 gene product. *J Biol Chem* **274**: 28557-28565.

Canaud G, Knebelmann B, Harris PC, Vrtovsnik F, Correas JM, Pallet N, Heyer CM, Letavernier E, Bienaime F, Thervet E et al. 2010. Therapeutic mTOR inhibition in autosomal dominant polycystic kidney disease: What is the appropriate serum level? *American journal of transplantation : official journal of the American Society of Transplantation and the American Society of Transplant Surgeons* **10**: 1701-1706.

Carroll TJ, Das A. 2013. Defining the signals that constitute the nephron progenitor niche. *J Am Soc Nephrol* **24**: 873-876.

Carroll TJ, Park JS, Hayashi S, Majumdar A, McMahon AP. 2005. Wnt9b plays a central role in the regulation of mesenchymal to epithelial transitions underlying organogenesis of the mammalian urogenital system. *Dev Cell* **9**: 283-292.

Chapin HC, Caplan MJ. 2010. The cell biology of polycystic kidney disease. *J Cell Biol* **191**: 701-710.

Chauvet V, Qian F, Boute N, Cai Y, Phakdeekitacharoen B, Onuchic LF, Attie-Bitach T, Guicharnaud L, Devuyst O, Germino GG et al. 2002. Expression of PKD1 and PKD2 transcripts and proteins in human embryo and during normal kidney development. *Am J Pathol* **160**: 973-983.

Chen WS, Antic D, Matis M, Logan CY, Povelones M, Anderson GA, Nusse R, Axelrod JD. 2008. Asymmetric homotypic interactions of the atypical cadherin flamingo mediate intercellular polarity signaling. *Cell* **133**: 1093-1105.

Cheng HT, Kim M, Valerius MT, Surendran K, Schuster-Gossler K, Gossler A, McMahon AP, Kopan R. 2007. Notch2, but not Notch1, is required for proximal fate acquisition in the mammalian nephron. *Development* **134**: 801-811.

Chicoine J, Benoit P, Gamberi C, Paliouras M, Simonelig M, Lasko P. 2007. Bicaudal-C recruits CCR4-NOT deadenylase to target mRNAs and regulates oogenesis, cytoskeletal organization, and its own expression. *Dev Cell* **13**: 691-704.

Choi YH, Suzuki A, Hajarnis S, Ma Z, Chapin HC, Caplan MJ, Pontoglio M, Somlo S, Igarashi P. 2011. Polycystin-2 and phosphodiesterase 4C are components of a ciliary A-kinase anchoring protein complex that is disrupted in cystic kidney diseases. *Proc Natl Acad Sci U S A* **108**: 10679-10684.

Christensen ST, Pedersen SF, Satir P, Veland IR, Schneider L. 2008. The primary cilium coordinates signaling pathways in cell cycle control and migration during development and tissue repair. *Current topics in developmental biology* **85**: 261-301.

Clevers H, Nusse R. 2012. Wnt/beta-catenin signaling and disease. *Cell* **149**: 1192-1205.

Cogswell C, Price SJ, Hou X, Guay-Woodford LM, Flaherty L, Bryda EC. 2003. Positional cloning of jcpk/bpk locus of the mouse. *Mamm Genome* **14**: 242-249.

Corbit KC, Shyer AE, Dowdle WE, Gaulden J, Singla V, Chen MH, Chuang PT, Reiter JF. 2008. Kif3a constrains beta-catenin-dependent Wnt signalling through dual ciliary and non-ciliary mechanisms. *Nat Cell Biol* **10**: 70-76.

Czarnecki PG, Gabriel GC, Manning DK, Sergeev M, Lemke K, Klena NT, Liu X, Chen Y, Li Y, San Agustin JT et al. 2015. ANKS6 is the critical activator of NEK8 kinase in embryonic situs determination and organ patterning. *Nature communications* **6**: 6023.

Dardenne E, Polay Espinoza M, Fattet L, Germann S, Lambert MP, Neil H, Zonta E, Mortada H, Gratadou L, Deygas M et al. 2014. RNA helicases DDX5 and DDX17 dynamically orchestrate transcription, miRNA, and splicing programs in cell differentiation. *Cell reports* **7**: 1900-1913.

Davis BN, Hilyard AC, Lagna G, Hata A. 2008. SMAD proteins control DROSHA-mediated microRNA maturation. *Nature* **454**: 56-61.

Delling M, DeCaen PG, Doerner JF, Febvay S, Clapham DE. 2013. Primary cilia are specialized calcium signalling organelles. *Nature* **504**: 311-314.

Dishinger JF, Kee HL, Jenkins PM, Fan S, Hurd TW, Hammond JW, Truong YN, Margolis B, Martens JR, Verhey KJ. 2010. Ciliary entry of the kinesin-2 motor KIF17 is regulated by importin-beta2 and RanGTP. *Nat Cell Biol* **12**: 703-710.

Eccles MR, Stayner CA. 2014. Polycystic kidney disease - where gene dosage counts. *F1000prime reports* **6**: 24.

Eckmann CR, Kraemer B, Wickens M, Kimble J. 2002. GLD-3, a bicaudal-C homolog that inhibits FBF to control germline sex determination in C. elegans. *Dev Cell* **3**: 697-710.

Ekser B, Rigotti P. 2010. Images in clinical medicine. Autosomal dominant polycystic kidney disease. *N Engl J Med* **363**: 71.

Fagan KA, Smith KE, Cooper DM. 2000. Regulation of the Ca2+-inhibitable adenylyl cyclase type VI by capacitative Ca2+ entry requires localization in cholesterol-rich domains. *J Biol Chem* **275**: 26530-26537.

Feistel K, Blum M. 2006. Three types of cilia including a novel 9+4 axoneme on the notochordal plate of the rabbit embryo. *Developmental dynamics : an official publication of the American Association of Anatomists* **235**: 3348-3358.

Fisch C, Dupuis-Williams P. 2011. Ultrastructure of cilia and flagella - back to the future! *Biology of the cell / under the auspices of the European Cell Biology Organization* **103**: 249-270.

Flaherty L, Bryda EC, Collins D, Rudofsky U, Montogomery JC. 1995. New mouse model for polycystic kidney disease with both recessive and dominant gene effects. *Kidney Int* **47**: 552-558.

Francescatto L, Rothschild SC, Myers AL, Tombes RM. 2010. The activation of membrane targeted CaMK-II in the zebrafish Kupffer's vesicle is required for left-right asymmetry. *Development* **137**: 2753-2762.

Fukuda T, Yamagata K, Fujiyama S, Matsumoto T, Koshida I, Yoshimura K, Mihara M, Naitou M, Endoh H, Nakamura T et al. 2007. DEAD-box RNA helicase subunits of the Drosha complex are required for processing of rRNA and a subset of microRNAs. *Nat Cell Biol* **9**: 604-611.

Fuller-Pace FV. 2013. The DEAD box proteins DDX5 (p68) and DDX17 (p72): multi-tasking transcriptional regulators. *Biochim Biophys Acta* **1829**: 756-763.

Gabow PA. 1990. Autosomal dominant polycystic kidney disease--more than a renal disease. *American journal of kidney diseases : the official journal of the National Kidney Foundation* **16**: 403-413.

Gamberi C, Lasko P. 2012. The bic-C family of developmental translational regulators. *Comparative and functional genomics* **2012**: 141386.

Gao B. 2012. Wnt regulation of planar cell polarity (PCP). *Current topics in developmental biology* **101**: 263-295.

Gao C, Chen YG. 2010. Dishevelled: The hub of Wnt signaling. *Cell Signal* **22**: 717-727.

Garcia-Gonzalo FR, Corbit KC, Sirerol-Piquer MS, Ramaswami G, Otto EA, Noriega TR, Seol AD, Robinson JF, Bennett CL, Josifova DJ et al. 2011. A transition zone complex regulates mammalian ciliogenesis and ciliary membrane composition. *Nat Genet* **43**: 776-784.

Gascue C, Katsanis N, Badano JL. 2011. Cystic diseases of the kidney: ciliary dysfunction and cystogenic mechanisms. *Pediatr Nephrol* **26**: 1181-1195.

Gattone VH, 2nd, Wang X, Harris PC, Torres VE. 2003. Inhibition of renal cystic disease development and progression by a vasopressin V2 receptor antagonist. *Nat Med* **9**: 1323-1326.

Geng L, Okuhara D, Yu Z, Tian X, Cai Y, Shibazaki S, Somlo S. 2006. Polycystin-2 traffics to cilia independently of polycystin-1 by using an N-terminal RVxP motif. *J Cell Sci* **119**: 1383-1395.

Gerdes JM, Liu Y, Zaghloul NA, Leitch CC, Lawson SS, Kato M, Beachy PA, Beales PL, DeMartino GN, Fisher S et al. 2007. Disruption of the basal body compromises proteasomal function and perturbs intracellular Wnt response. *Nat Genet* **39**: 1350-1360.

Ghosh AK, Hurd T, Hildebrandt F. 2012. 3D spheroid defects in NPHP knockdown cells are rescued by the somatostatin receptor agonist octreotide. *Am J Physiol Renal Physiol* **303**: F1225-1229.

Glazewski S, Giese KP, Silva A, Fox K. 2000. The role of alpha-CaMKII autophosphorylation in neocortical experience-dependent plasticity. *Nature neuroscience* **3**: 911-918.

Goetz SC, Anderson KV. 2010. The primary cilium: a signalling centre during vertebrate development. *Nat Rev Genet* **11**: 331-344.

Goggolidou P. 2014. Wnt and planar cell polarity signaling in cystic renal disease. *Organogenesis* **10**: 86-95.

Gonzalez-Perrett S, Kim K, Ibarra C, Damiano AE, Zotta E, Batelli M, Harris PC, Reisin IL, Arnaout MA, Cantiello HF. 2001. Polycystin-2, the protein mutated in autosomal dominant polycystic kidney disease (ADPKD), is a Ca2+-permeable nonselective cation channel. *Proc Natl Acad Sci U S A* **98**: 1182-1187.

Grantham JJ, Cook LT, Torres VE, Bost JE, Chapman AB, Harris PC, Guay-Woodford LM, Bae KT. 2008. Determinants of renal volume in autosomal-dominant polycystic kidney disease. *Kidney Int* **73**: 108-116.

Grantham JJ, Cook LT, Wetzel LH, Cadnapaphornchai MA, Bae KT. 2010. Evidence of extraordinary growth in the progressive enlargement of renal cysts. *Clinical journal of the American Society of Nephrology : CJASN* **5**: 889-896.

Grantham JJ, Geiser JL, Evan AP. 1987. Cyst formation and growth in autosomal dominant polycystic kidney disease. *Kidney Int* **31**: 1145-1152.

Gregory RI, Yan KP, Amuthan G, Chendrimada T, Doratotaj B, Cooch N, Shiekhattar R. 2004. The Microprocessor complex mediates the genesis of microRNAs. *Nature* **432**: 235-240.

Gresh L, Fischer E, Reimann A, Tanguy M, Garbay S, Shao X, Hiesberger T, Fiette L, Igarashi P, Yaniv M et al. 2004. A transcriptional network in polycystic kidney disease. *The EMBO journal* **23**: 1657-1668.

Guay-Woodford LM, Bryda EC, Christine B, Lindsey JR, Collier WR, Avner ED, D'Eustachio P, Flaherty L. 1996. Evidence that two phenotypically distinct mouse PKD mutations, bpk and jcpk, are allelic. *Kidney Int* **50**: 1158-1165.

Hanaoka K, Qian F, Boletta A, Bhunia AK, Piontek K, Tsiokas L, Sukhatme VP, Guggino WB, Germino GG. 2000. Co-assembly of polycystin-1 and -2 produces unique cation-permeable currents. *Nature* **408**: 990-994.

Harris PC, Torres VE. 2014. Genetic mechanisms and signaling pathways in autosomal dominant polycystic kidney disease. *The Journal of clinical investigation* **124**: 2315-2324.

Hashimoto M, Shinohara K, Wang J, Ikeuchi S, Yoshiba S, Meno C, Nonaka S, Takada S, Hatta K, Wynshaw-Boris A et al. 2010. Planar polarization of node cells determines the rotational axis of node cilia. *Nat Cell Biol* **12**: 170-176.

Helou J, Otto EA, Attanasio M, Allen SJ, Parisi MA, Glass I, Utsch B, Hashmi S, Fazzi E, Omran H et al. 2007. Mutation analysis of NPHP6/CEP290 in patients with Joubert syndrome and Senior-Loken syndrome. *Journal of medical genetics* **44**: 657-663.

Hildebrandt F, Benzing T, Katsanis N. 2011. Ciliopathies. *N Engl J Med* **364**: 1533-1543.

Hildebrandt F, Otto E. 2000. Molecular genetics of nephronophthisis and medullary cystic kidney disease. *J Am Soc Nephrol* **11**: 1753-1761.

Hochbaum D, Tanos T, Ribeiro-Neto F, Altschuler D, Coso OA. 2003. Activation of JNK by Epac is independent of its activity as a Rap guanine nucleotide exchanger. *J Biol Chem* **278**: 33738-33746.

Hoey DA, Downs ME, Jacobs CR. 2012. The mechanics of the primary cilium: an intricate structure with complex function. *Journal of biomechanics* **45**: 17-26.

Hoff S, Halbritter J, Epting D, Frank V, Nguyen T-MT, van Reeuwijk J, Boehlke C, Schell C, Yasunaga T, Helmstadter M et al. 2013. ANKS6 is a central component of a nephronophthisis module linking NEK8 to INVS and NPHP3. *Nat Genet* **45**: 951-956.

Hogan MC, Masyuk TV, Page LJ, Kubly VJ, Bergstralh EJ, Li X, Kim B, King BF, Glockner J, Holmes DR, 3rd et al. 2010. Randomized clinical trial of long-acting somatostatin for autosomal dominant polycystic kidney and liver disease. *J Am Soc Nephrol* **21**: 1052-1061.

Hornbeck PV, Chabra I, Kornhauser JM, Skrzypek E, Zhang B. 2004. PhosphoSite: A bioinformatics resource dedicated to physiological protein phosphorylation. *Proteomics* **4**: 1551-1561.

Howe AK. 2004. Regulation of actin-based cell migration by cAMP/PKA. *Biochim Biophys Acta* **1692**: 159-174.

Huan Y, van Adelsberg J. 1999. Polycystin-1, the PKD1 gene product, is in a complex containing E-cadherin and the catenins. *The Journal of clinical investigation* **104**: 1459-1468.

Huang P, Schier AF. 2009. Dampened Hedgehog signaling but normal Wnt signaling in zebrafish without cilia. *Development* **136**: 3089-3098.

Huangfu D, Liu A, Rakeman AS, Murcia NS, Niswander L, Anderson KV. 2003. Hedgehog signalling in the mouse requires intraflagellar transport proteins. *Nature* **426**: 83-87.

Hudmon A, Schulman H. 2002. Neuronal CA2+/calmodulin-dependent protein kinase II: the role of structure and autoregulation in cellular function. *Annual review of biochemistry* **71**: 473-510.

Hughes J, Ward CJ, Peral B, Aspinwall R, Clark K, San Millan JL, Gamble V, Harris PC. 1995. The polycystic kidney disease 1 (PKD1) gene encodes a novel protein with multiple cell recognition domains. *Nature genetics* **10**: 151-160.

Huttlin EL, Jedrychowski MP, Elias JE, Goswami T, Rad R, Beausoleil SA, Villen J, Haas W, Sowa ME, Gygi SP. 2010. A tissue-specific atlas of mouse protein phosphorylation and expression. *Cell* **143**: 1174-1189.

Ibraghimov-Beskrovnaya O, Dackowski WR, Foggensteiner L, Coleman N, Thiru S, Petry LR, Burn TC, Connors TD, Van Raay T, Bradley J et al. 1997. Polycystin: in vitro synthesis, in vivo tissue expression, and subcellular localization identifies a large membrane-associated protein. *Proc Natl Acad Sci U S A* **94**: 6397-6402.

Ingham PW, Nakano Y, Seger C. 2011. Mechanisms and functions of Hedgehog signalling across the metazoa. *Nat Rev Genet* **12**: 393-406.

Inoki K, Ouyang H, Zhu T, Lindvall C, Wang Y, Zhang X, Yang Q, Bennett C, Harada Y, Stankunas K et al. 2006. TSC2 integrates Wnt and energy signals via a coordinated phosphorylation by AMPK and GSK3 to regulate cell growth. *Cell* **126**: 955-968.

Ishikawa H, Marshall WF. 2011. Ciliogenesis: building the cell's antenna. *Nat Rev Mol Cell Biol* **12**: 222-234.

Jaffe AB, Hall A. 2005. Rho GTPases: biochemistry and biology. *Annu Rev Cell Dev Biol* **21**: 247-269.

Janknecht R. 2010. Multi-talented DEAD-box proteins and potential tumor promoters: p68 RNA helicase (DDX5) and its paralog, p72 RNA helicase (DDX17). *American journal of translational research* **2**: 223-234.

Jin X, Mohieldin AM, Muntean BS, Green JA, Shah JV, Mykytyn K, Nauli SM. 2014. Cilioplasm is a cellular compartment for calcium signaling in response to mechanical and chemical stimuli. *Cellular and molecular life sciences : CMLS* **71**: 2165-2178.

Jonassen JA, San Agustin J, Follit JA, Pazour GJ. 2008. Deletion of IFT20 in the mouse kidney causes misorientation of the mitotic spindle and cystic kidney disease. *J Cell Biol* **183**: 377-384.

Jonassen JA, SanAgustin J, Baker SP, Pazour GJ. 2012. Disruption of IFT complex A causes cystic kidneys without mitotic spindle misorientation. *J Am Soc Nephrol* **23**: 641-651.

Jones C, Roper VC, Foucher I, Qian D, Banizs B, Petit C, Yoder BK, Chen P. 2008. Ciliary proteins link basal body polarization to planar cell polarity regulation. *Nat Genet* **40**: 69-77.

Karner CM, Das A, Ma Z, Self M, Chen C, Lum L, Oliver G, Carroll TJ. 2011. Canonical Wnt9b signaling balances progenitor cell expansion and differentiation during kidney development. *Development* **138**: 1247-1257.

Kikuchi A, Yamamoto H, Sato A. 2009. Selective activation mechanisms of Wnt signaling pathways. *Trends Cell Biol* **19**: 119-129.

Kim S, Dynlacht BD. 2013. Assembling a primary cilium. *Curr Opin Cell Biol* **25**: 506-511.

Kim SE, Huang H, Zhao M, Zhang X, Zhang A, Semonov MV, MacDonald BT, Zhang X, Garcia Abreu J, Peng L et al. 2013. Wnt stabilization of beta-catenin reveals principles for morphogen receptor-scaffold assemblies. *Science* **340**: 867-870.

Kispert A, Vainio S, McMahon AP. 1998. Wnt-4 is a mesenchymal signal for epithelial transformation of metanephric mesenchyme in the developing kidney. *Development* **125**: 4225-4234.

Ko JY, Park JH. 2013. Mouse models of polycystic kidney disease induced by defects of ciliary proteins. *BMB reports* **46**: 73-79.

Korinek V, Barker N, Morin PJ, van Wichen D, de Weger R, Kinzler KW, Vogelstein B, Clevers H. 1997. Constitutive transcriptional activation by a beta-catenin-Tcf complex in APC-/- colon carcinoma. *Science* **275**: 1784-1787.

Kozminski KG, Johnson KA, Forscher P, Rosenbaum JL. 1993. A motility in the eukaryotic flagellum unrelated to flagellar beating. *Proc Natl Acad Sci U S A* **90**: 5519-5523.

Kramer-Zucker AG, Olale F, Haycraft CJ, Yoder BK, Schier AF, Drummond IA. 2005. Cilia-driven fluid flow in the zebrafish pronephros, brain and Kupffer's vesicle is required for normal organogenesis. *Development* **132**: 1907-1921.

Kraus MR, Clauin S, Pfister Y, Di Maio M, Ulinski T, Constam D, Bellanne-Chantelot C, Grapin-Botton A. 2012. Two mutations in human BICC1 resulting in Wnt pathway hyperactivity associated with cystic renal dysplasia. *Human mutation* **33**: 86-90.

Kriz W, Kaissling B, Le Hir M. 2011. Epithelial-mesenchymal transition (EMT) in kidney fibrosis: fact or fantasy? *The Journal of clinical investigation* **121**: 468-474.

Kurkowiak M, Zietkiewicz E, Witt M. 2015. Recent advances in primary ciliary dyskinesia genetics. *Journal of medical genetics* **52**: 1-9.

Lammert E, Zeeb M. 2014. Metabolism of Human Diseases. *Organ Physiology and Pathophysiology*: 416 p.

Lancaster MA, Schroth J, Gleeson JG. 2011. Subcellular spatial regulation of canonical Wnt signalling at the primary cilium. *Nat Cell Biol* **13**: 700-707.

Larkin MA, Blackshields G, Brown NP, Chenna R, McGettigan PA, McWilliam H, Valentin F, Wallace IM, Wilm A, Lopez R et al. 2007. Clustal W and Clustal X version 2.0. *Bioinformatics* **23**: 2947-2948.

Lemaire LA, Goulley J, Kim YH, Carat S, Jacquemin P, Rougemont J, Constam DB, Grapin-Botton A. 2015. Bicaudal C1 promotes pancreatic NEUROG3+ endocrine progenitor differentiation and ductal morphogenesis. *Development* **142**: 858-870.

Li L, Hanahan D. 2013. Hijacking the neuronal NMDAR signaling circuit to promote tumor growth and invasion. *Cell* **153**: 86-100.

Li VS, Ng SS, Boersema PJ, Low TY, Karthaus WR, Gerlach JP, Mohammed S, Heck AJ, Maurice MM, Mahmoudi T et al. 2012. Wnt signaling through inhibition of beta-catenin degradation in an intact Axin1 complex. *Cell* **149**: 1245-1256.

Li X, Burrow CR, Polgar K, Hyink DP, Gusella GL, Wilson PD. 2008. Protein kinase X (PRKX) can rescue the effects of polycystic kidney disease-1 gene (PKD1) deficiency. *Biochim Biophys Acta* **1782**: 1-9.

Lian P, Li A, Li Y, Liu H, Liang D, Hu B, Lin D, Jiang T, Moeckel G, Qin D et al. 2014. Loss of polycystin-1 inhibits Bicc1 expression during mouse development. *PLoS One* **9**: e88816.

Lienkamp S, Ganner A, Boehlke C, Schmidt T, Arnold SJ, Schafer T, Romaker D, Schuler J, Hoff S, Powelske C et al. 2010. Inversin relays Frizzled-8 signals to promote proximal pronephros development. *Proc Natl Acad Sci U S A*.

Lienkamp SS, Liu K, Karner CM, Carroll TJ, Ronneberger O, Wallingford JB, Walz G. 2012. Vertebrate kidney tubules elongate using a planar cell polarity-dependent, rosette-based mechanism of convergent extension. *Nat Genet* **44**: 1382-1387.

Lin F, Hiesberger T, Cordes K, Sinclair AM, Goldstein LS, Somlo S, Igarashi P. 2003. Kidney-specific inactivation of the KIF3A subunit of kinesin-II inhibits renal ciliogenesis and produces polycystic kidney disease. *Proc Natl Acad Sci U S A* **100**: 5286-5291.

Liu S, Lu W, Obara T, Kuida S, Lehoczky J, Dewar K, Drummond IA, Beier DR. 2002. A defect in a novel Nek-family kinase causes cystic kidney disease in the mouse and in zebrafish. *Development* **129**: 5839-5846.

Liu W, Murcia NS, Duan Y, Weinbaum S, Yoder BK, Schwiebert E, Satlin LM. 2005. Mechanoregulation of intracellular Ca2+ concentration is attenuated in collecting duct of monocilium-impaired orpk mice. *Am J Physiol Renal Physiol* **289**: F978-988.

Luciano RL, Dahl NK. 2014. Extra-renal manifestations of autosomal dominant polycystic kidney disease (ADPKD): considerations for routine screening and management. *Nephrology, dialysis, transplantation : official publication of the European Dialysis and Transplant Association - European Renal Association* **29**: 247-254.

Luyten A, Su X, Gondela S, Chen Y, Rompani S, Takakura A, Zhou J. 2010. Aberrant regulation of planar cell polarity in polycystic kidney disease. *J Am Soc Nephrol* **21**: 1521-1532.

Ma M, Tian X, Igarashi P, Pazour GJ, Somlo S. 2013. Loss of cilia suppresses cyst growth in genetic models of autosomal dominant polycystic kidney disease. *Nat Genet* **45**: 1004-1012.

Mack M, Yanagita M. 2015. Origin of myofibroblasts and cellular events triggering fibrosis. *Kidney Int* **87**: 297-307.

Mahone M, Saffman EE, Lasko PF. 1995. Localized Bicaudal-C RNA encodes a protein containing a KH domain, the RNA binding motif of FMR1. *EMBO J* **14**: 2043-2055.

Maisonneuve C, Guilleret I, Vick P, Weber T, Andre P, Beyer T, Blum M, Constam DB. 2009. Bicaudal C, a novel regulator of Dvl signaling abutting RNA-processing bodies, controls cilia orientation and leftward flow. *Development* **136**: 3019-3030.

Malka D, Hammel P, Vilgrain V, Flejou JF, Belghiti J, Bernades P. 1998. Chronic obstructive pancreatitis due to a pancreatic cyst in a patient with autosomal dominant polycystic kidney disease. *Gut* **42**: 131-134.

Manning DK, Sergeev M, van Heesbeen RG, Wong MD, Oh JH, Liu Y, Henkelman RM, Drummond I, Shah JV, Beier DR. 2013. Loss of the ciliary kinase Nek8 causes left-right asymmetry defects. *J Am Soc Nephrol* **24**: 100-112.

Mekahli D, Parys JB, Bultynck G, Missiaen L, De Smedt H. 2013. Polycystins and cellular Ca2+ signaling. *Cellular and molecular life sciences : CMLS* **70**: 2697-2712.

Menezes LF, Zhou F, Patterson AD, Piontek KB, Krausz KW, Gonzalez FJ, Germino GG. 2012. Network analysis of a Pkd1-mouse model of autosomal dominant polycystic kidney disease identifies HNF4alpha as a disease modifier. *PLoS genetics* **8**: e1003053.

Mitchell B, Stubbs JL, Huisman F, Taborek P, Yu C, Kintner C. 2009. The PCP pathway instructs the planar orientation of ciliated cells in the Xenopus larval skin. *Curr Biol* **19**: 924-929.

Mochizuki T, Saijoh Y, Tsuchiya K, Shirayoshi Y, Takai S, Taya C, Yonekawa H, Yamada K, Nihei H, Nakatsuji N et al. 1998. Cloning of inv, a gene that controls left/right asymmetry and kidney development. *Nature* **395**: 177-181.

Mochizuki T, Tsuchiya K, Nitta K. 2013. Autosomal dominant polycystic kidney disease: recent advances in pathogenesis and potential therapies. *Clinical and experimental nephrology* **17**: 317-326.

Mochizuki T, Wu G, Hayashi T, Xenophontos SL, Veldhuisen B, Saris JJ, Reynolds DM, Cai Y, Gabow PA, Pierides A et al. 1996. PKD2, a gene for polycystic kidney disease that encodes an integral membrane protein. *Science* **272**: 1339-1342.

Mohler J, Wieschaus EF. 1986. Dominant maternal-effect mutations of Drosophila melanogaster causing the production of double-abdomen embryos. *Genetics* **112**: 803-822.

Morgan D, Goodship J, Essner JJ, Vogan KJ, Turnpenny L, Yost HJ, Tabin CJ, Strachan T. 2002. The left-right determinant inversin has highly conserved ankyrin repeat and IQ domains and interacts with calmodulin. *Human genetics* **110**: 377-384.

Morgan D, Turnpenny L, Goodship J, Dai W, Majumder K, Matthews L, Gardner A, Schuster G, Vien L, Harrison W et al. 1998. Inversin, a novel gene in the vertebrate left-right axis pathway, is partially deleted in the inv mouse. *Nat Genet* **20**: 149-156.

Muddashetty RS, Nalavadi VC, Gross C, Yao X, Xing L, Laur O, Warren ST, Bassell GJ. 2011. Reversible inhibition of PSD-95 mRNA translation by miR-125a, FMRP phosphorylation, and mGluR signaling. *Mol Cell* **42**: 673-688.

Mugford JW, Yu J, Kobayashi A, McMahon AP. 2009. High-resolution gene expression analysis of the developing mouse kidney defines novel cellular compartments within the nephron progenitor population. *Dev Biol* **333**: 312-323.

Mutig K, Paliege A, Kahl T, Jons T, Muller-Esterl W, Bachmann S. 2007. Vasopressin V2 receptor expression along rat, mouse, and human renal epithelia with focus on TAL. *Am J Physiol Renal Physiol* **293**: F1166-1177.

Nakata K, Shiba D, Kobayashi D, Yokoyama T. 2012. Targeting of Nphp3 to the primary cilia is controlled by an N-terminal myristoylation site and coiled-coil domains. *Cytoskeleton* **69**: 221-234.

Nauli SM, Alenghat FJ, Luo Y, Williams E, Vassilev P, Li X, Elia AE, Lu W, Brown EM, Quinn SJ et al. 2003. Polycystins 1 and 2 mediate mechanosensation in the primary cilium of kidney cells. *Nat Genet* **33**: 129-137.

Niehrs C. 2012. The complex world of WNT receptor signalling. *Nat Rev Mol Cell Biol* **13**: 767-779.

Nonaka S. 2009. Modification of mouse nodal flow by applying artificial flow. *Methods in cell biology* **91**: 287-297.

Nonaka S, Tanaka Y, Okada Y, Takeda S, Harada A, Kanai Y, Kido M, Hirokawa N. 1998. Randomization of left-right asymmetry due to loss of nodal cilia generating leftward flow of extraembryonic fluid in mice lacking KIF3B motor protein. *Cell* **95**: 829-837.

Nozawa YI, Lin C, Chuang PT. 2013. Hedgehog signaling from the primary cilium to the nucleus: an emerging picture of ciliary localization, trafficking and transduction. *Curr Opin Genet Dev* **23**: 429-437.

Nurnberger J, Bacallao RL, Phillips CL. 2002. Inversin forms a complex with catenins and N-cadherin in polarized epithelial cells. *Molecular biology of the cell* **13**: 3096-3106.

Nurnberger J, Kribben A, Opazo Saez A, Heusch G, Philipp T, Phillips CL. 2004. The Invs gene encodes a microtubule-associated protein. *J Am Soc Nephrol* **15**: 1700-1710.

O'Brien LL, McMahon AP. 2014. Induction and patterning of the metanephric nephron. *Seminars in cell & developmental biology* **36C**: 31-38.

Ocbina PJ, Tuson M, Anderson KV. 2009. Primary cilia are not required for normal canonical Wnt signaling in the mouse embryo. *PLoS One* **4**: e6839.

Oh EC, Katsanis N. 2013. Context-dependent regulation of Wnt signaling through the primary cilium. *J Am Soc Nephrol* **24**: 10-18.

Okada Y, Takeda S, Tanaka Y, Belmonte JC, Hirokawa N. 2005. Mechanism of nodal flow: a conserved symmetry breaking event in left-right axis determination. *Cell* **121**: 633-644.

Olsen JV, Vermeulen M, Santamaria A, Kumar C, Miller ML, Jensen LJ, Gnad F, Cox J, Jensen TS, Nigg EA et al. 2010. Quantitative phosphoproteomics reveals widespread full phosphorylation site occupancy during mitosis. *Sci Signal* **3**: ra3.

Orellana SA, Quinones AM, Mandapat ML. 2003. Ezrin distribution is abnormal in principal cells from a murine model of autosomal recessive polycystic kidney disease. *Pediatric research* **54**: 406-412.

Otto EA, Schermer B, Obara T, O'Toole JF, Hiller KS, Mueller AM, Ruf RG, Hoefele J, Beekmann F, Landau D et al. 2003. Mutations in INVS encoding inversin cause nephronophthisis type 2, linking renal cystic disease to the function of primary cilia and left-right axis determination. *Nat Genet* **34**: 413-420.

Otto EA, Trapp ML, Schultheiss UT, Helou J, Quarmby LM, Hildebrandt F. 2008. NEK8 mutations affect ciliary and centrosomal localization and may cause nephronophthisis. *J Am Soc Nephrol* **19**: 587-592.

Oud MM, van Bon BW, Bongers EM, Hoischen A, Marcelis CL, de Leeuw N, Mol SJ, Mortier G, Knoers NV, Brunner HG et al. 2014. Early presentation of cystic kidneys in a family with a homozygous INVS mutation. *American journal of medical genetics Part A* **164A**: 1627-1634.

Park JS, Valerius MT, McMahon AP. 2007. Wnt/beta-catenin signaling regulates nephron induction during mouse kidney development. *Development* **134**: 2533-2539.

Park TJ, Mitchell BJ, Abitua PB, Kintner C, Wallingford JB. 2008. Dishevelled controls apical docking and planar polarization of basal bodies in ciliated epithelial cells. *Nat Genet* **40**: 871-879.

Patel V, Li L, Cobo-Stark P, Shao X, Somlo S, Lin F, Igarashi P. 2008. Acute kidney injury and aberrant planar cell polarity induce cyst formation in mice lacking renal cilia. *Hum Mol Genet* **17**: 1578-1590.

Patel V, Williams D, Hajarnis S, Hunter R, Pontoglio M, Somlo S, Igarashi P. 2013. miR-17~92 miRNA cluster promotes kidney cyst growth in polycystic kidney disease. *Proceedings of the National Academy of Sciences of the United States of America* **110**: 10765-10770.

Paul BM, Vanden Heuvel GB. 2014. Kidney: polycystic kidney disease. *Wiley interdisciplinary reviews Developmental biology* **3**: 465-487.

Pazour GJ, Bloodgood RA. 2008. Targeting proteins to the ciliary membrane. *Current topics in developmental biology* **85**: 115-149.

Pazour GJ, Dickert BL, Vucica Y, Seeley ES, Rosenbaum JL, Witman GB, Cole DG. 2000. Chlamydomonas IFT88 and its mouse homologue, polycystic kidney disease gene tg737, are required for assembly of cilia and flagella. *J Cell Biol* **151**: 709-718.

Pazour GJ, San Agustin JT, Follit JA, Rosenbaum JL, Witman GB. 2002. Polycystin-2 localizes to kidney cilia and the ciliary level is elevated in orpk mice with polycystic kidney disease. *Curr Biol* **12**: R378-380.

Pedersen LB, Rosenbaum JL. 2008. Intraflagellar transport (IFT) role in ciliary assembly, resorption and signalling. *Current topics in developmental biology* **85**: 23-61.

Pei Y. 2001. A "two-hit" model of cystogenesis in autosomal dominant polycystic kidney disease? *Trends in molecular medicine* **7**: 151-156.

Perantoni AO, Timofeeva O, Naillat F, Richman C, Pajni-Underwood S, Wilson C, Vainio S, Dove LF, Lewandoski M. 2005. Inactivation of FGF8 in early mesoderm reveals an essential role in kidney development. *Development* **132**: 3859-3871.

Peters DJ, van de Wal A, Spruit L, Saris JJ, Breuning MH, Bruijn JA, de Heer E. 1999. Cellular localization and tissue distribution of polycystin-1. *The Journal of pathology* **188**: 439-446.

Phillips CL, Miller KJ, Filson AJ, Nurnberger J, Clendenon JL, Cook GW, Dunn KW, Overbeek PA, Gattone VH, 2nd, Bacallao RL. 2004. Renal cysts of inv/inv mice resemble early infantile nephronophthisis. *J Am Soc Nephrol* **15**: 1744-1755.

Piazzon N, Maisonneuve C, Guilleret I, Rotman S, Constam DB. 2012. Bicc1 links the regulation of cAMP signaling in polycystic kidneys to microRNA-induced gene silencing. *J Mol Cell Biol* **4**: 398-408.

Pinson KI, Brennan J, Monkley S, Avery BJ, Skarnes WC. 2000. An LDL-receptor-related protein mediates Wnt signalling in mice. *Nature* **407**: 535-538.

Piontek K, Menezes LF, Garcia-Gonzalez MA, Huso DL, Germino GG. 2007. A critical developmental switch defines the kinetics of kidney cyst formation after loss of Pkd1. *Nat Med* **13**: 1490-1495.

Polakis P. 2012. Wnt signaling in cancer. *Cold Spring Harbor perspectives in biology* **4**.

Popatia R, Haver K, Casey A. 2014. Primary Ciliary Dyskinesia: An Update on New Diagnostic Modalities and Review of the Literature. *Pediatric allergy, immunology, and pulmonology* **27**: 51-59.

Porter ME, Sale WS. 2000. The 9 + 2 axoneme anchors multiple inner arm dyneins and a network of kinases and phosphatases that control motility. *J Cell Biol* **151**: F37-42.

Praetorius HA, Spring KR. 2003. The renal cell primary cilium functions as a flow sensor. *Current opinion in nephrology and hypertension* **12**: 517-520.

Preibisch S, Saalfeld S, Tomancak P. 2009. Globally optimal stitching of tiled 3D microscopic image acquisitions. *Bioinformatics* **25**: 1463-1465.

Qian F, Watnick TJ, Onuchic LF, Germino GG. 1996. The molecular basis of focal cyst formation in human autosomal dominant polycystic kidney disease type I. *Cell* **87**: 979-987.

Qiao F, Bowie JU. 2005. The many faces of SAM. *Sci STKE* **2005**: re7.

Reginensi A, Scott RP, Gregorieff A, Bagherie-Lachidan M, Chung C, Lim DS, Pawson T, Wrana J, McNeill H. 2013. Yap- and Cdc42-dependent nephrogenesis and morphogenesis during mouse kidney development. *PLoS genetics* **9**: e1003380.

Rohatgi R, Snell WJ. 2010. The ciliary membrane. *Curr Opin Cell Biol* **22**: 541-546.

Ross AJ, May-Simera H, Eichers ER, Kai M, Hill J, Jagger DJ, Leitch CC, Chapple JP, Munro PM, Fisher S et al. 2005. Disruption of Bardet-Biedl syndrome ciliary proteins perturbs planar cell polarity in vertebrates. *Nat Genet* **37**: 1135-1140.

Rossetti S, Consugar MB, Chapman AB, Torres VE, Guay-Woodford LM, Grantham JJ, Bennett WM, Meyers CM, Walker DL, Bae K et al. 2007. Comprehensive molecular diagnostics in autosomal dominant polycystic kidney disease. *J Am Soc Nephrol* **18**: 2143-2160.

Rothschild SC, Francescatto L, Drummond IA, Tombes RM. 2011. CaMK-II is a PKD2 target that promotes pronephric kidney development and stabilizes cilia. *Development* **138**: 3387-3397.

Saadi-Kheddouci S, Berrebi D, Romagnolo B, Cluzeaud F, Peuchmaur M, Kahn A, Vandewalle A, Perret C. 2001. Early development of polycystic kidney disease in transgenic mice expressing an activated mutant of the beta-catenin gene. *Oncogene* **20**: 5972-5981.

Saffman EE, Styhler S, Rother K, Li W, Richard S, Lasko P. 1998. Premature translation of oskar in oocytes lacking the RNA-binding protein bicaudal-C. *Mol Cell Biol* **18**: 4855-4862.

Sands J, M, Verlander J, W. . 2004. Anatomy and Physiology of the Kidneys. in *Toxicology of the Kidney, 3rd Edition*, pp. 3-56. Informa Healthcare.

Sang L, Miller JJ, Corbit KC, Giles RH, Brauer MJ, Otto EA, Baye LM, Wen X, Scales SJ, Kwong M et al. 2011. Mapping the NPHP-JBTS-MKS protein network reveals ciliopathy disease genes and pathways. *Cell* **145**: 513-528.

Sayer JA, Otto EA, O'Toole JF, Nurnberg G, Kennedy MA, Becker C, Hennies HC, Helou J, Attanasio M, Fausett BV et al. 2006. The centrosomal protein nephrocystin-6 is mutated in Joubert syndrome and activates transcription factor ATF4. *Nat Genet* **38**: 674-681.

Schieren G, Rumberger B, Klein M, Kreutz C, Wilpert J, Geyer M, Faller D, Timmer J, Quack I, Rump LC et al. 2006. Gene profiling of polycystic kidneys. *Nephrology, dialysis, transplantation : official publication of the European Dialysis and Transplant Association - European Renal Association* **21**: 1816-1824.

Schindelin J, Arganda-Carreras I, Frise E, Kaynig V, Longair M, Pietzsch T, Preibisch S, Rueden C, Saalfeld S, Schmid B et al. 2012. Fiji: an open-source platform for biological-image analysis. *Nature methods* **9**: 676-682.

Schmidt M, Dekker FJ, Maarsingh H. 2013. Exchange protein directly activated by cAMP (epac): a multidomain cAMP mediator in the regulation of diverse biological functions. *Pharmacological reviews* **65**: 670-709.

Schneider L, Cammer M, Lehman J, Nielsen SK, Guerra CF, Veland IR, Stock C, Hoffmann EK, Yoder BK, Schwab A et al. 2010. Directional cell migration and chemotaxis in wound healing response to PDGF-AA are coordinated by the primary cilium in fibroblasts. *Cellular physiology and biochemistry : international journal of experimental cellular physiology, biochemistry, and pharmacology* **25**: 279-292.

Schnell U, Carroll TJ. 2014. Planar cell polarity of the kidney. *Experimental cell research*.

Schrick JJ, Onuchic LF, Reeders ST, Korenberg J, Chen XN, Moyer JH, Wilkinson JE, Woychik RP. 1995. Characterization of the human homologue of the mouse Tg737 candidate polycystic kidney disease gene. *Hum Mol Genet* **4**: 559-567.

Seifert JR, Mlodzik M. 2007. Frizzled/PCP signalling: a conserved mechanism regulating cell polarity and directed motility. *Nat Rev Genet* **8**: 126-138.

Shiba D, Manning DK, Koga H, Beier DR, Yokoyama T. 2010. Inv acts as a molecular anchor for Nphp3 and Nek8 in the proximal segment of primary cilia. *Cytoskeleton* **67**: 112-119.

Shiba D, Yamaoka Y, Hagiwara H, Takamatsu T, Hamada H, Yokoyama T. 2009. Localization of Inv in a distinctive intraciliary compartment requires the C-terminal ninein-homolog-containing region. *J Cell Sci* **122**: 44-54.

Shields JD, Fleury ME, Yong C, Tomei AA, Randolph GJ, Swartz MA. 2007. Autologous chemotaxis as a mechanism of tumor cell homing to lymphatics via interstitial flow and autocrine CCR7 signaling. *Cancer cell* **11**: 526-538.

Shillingford JM, Murcia NS, Larson CH, Low SH, Hedgepeth R, Brown N, Flask CA, Novick AC, Goldfarb DA, Kramer-Zucker A et al. 2006. The mTOR pathway is regulated by polycystin-1, and its inhibition reverses renal cystogenesis in polycystic kidney disease. *Proc Natl Acad Sci U S A* **103**: 5466-5471.

Shillingford JM, Piontek KB, Germino GG, Weimbs T. 2010. Rapamycin ameliorates PKD resulting from conditional inactivation of Pkd1. *J Am Soc Nephrol* **21**: 489-497.

Simons M, Gloy J, Ganner A, Bullerkotte A, Bashkurov M, Kronig C, Schermer B, Benzing T, Cabello OA, Jenny A et al. 2005. Inversin, the gene product mutated in nephronophthisis type II, functions as a molecular switch between Wnt signaling pathways. *Nat Genet* **37**: 537-543.

Simons M, Walz G. 2006. Polycystic kidney disease: cell division without a c(l)ue? *Kidney Int* **70**: 854-864.

Smith HW. 1951. The Kidney: Structure and Function in Health and Disease. *New York: Oxford Univ Press*: 1,049 pp.

Smith LA, Bukanov NO, Husson H, Russo RJ, Barry TC, Taylor AL, Beier DR, Ibraghimov-Beskrovnaya O. 2006. Development of polycystic kidney disease in juvenile cystic kidney mice: insights into pathogenesis, ciliary abnormalities, and common features with human disease. *J Am Soc Nephrol* **17**: 2821-2831.

Sohara E, Luo Y, Zhang J, Manning DK, Beier DR, Zhou J. 2008. Nek8 regulates the expression and localization of polycystin-1 and polycystin-2. *J Am Soc Nephrol* **19**: 469-476.

Song H, Hu J, Chen W, Elliott G, Andre P, Gao B, Yang Y. 2010. Planar cell polarity breaks bilateral symmetry by controlling ciliary positioning. *Nature* **466**: 378-382.

Stagner EE, Bouvrette DJ, Cheng J, Bryda EC. 2009. The polycystic kidney disease-related proteins Bicc1 and SamCystin interact. *Biochem Biophys Res Commun* **383**: 16-21.

Stark K, Vainio S, Vassileva G, McMahon AP. 1994. Epithelial transformation of metanephric mesenchyme in the developing kidney regulated by Wnt-4. *Nature* **372**: 679-683.

Strutt H, Warrington SJ, Strutt D. 2011. Dynamics of core planar polarity protein turnover and stable assembly into discrete membrane subdomains. *Dev Cell* **20**: 511-525.

Su S, Phua SC, DeRose R, Chiba S, Narita K, Kalugin PN, Katada T, Kontani K, Takeda S, Inoue T. 2013. Genetically encoded calcium indicator illuminates calcium dynamics in primary cilia. *Nature methods* **10**: 1105-1107.

Sugiyama N, Tsukiyama T, Yamaguchi TP, Yokoyama T. 2011. The canonical Wnt signaling pathway is not involved in renal cyst development in the kidneys of inv mutant mice. *Kidney Int* **79**: 957-965.

Sullivan LP, Wallace DP, Grantham JJ. 1998. Chloride and fluid secretion in polycystic kidney disease. *J Am Soc Nephrol* **9**: 903-916.

Suzuki HI, Yamagata K, Sugimoto K, Iwamoto T, Kato S, Miyazono K. 2009. Modulation of microRNA processing by p53. *Nature* **460**: 529-533.

Sweeney WE, Jr., Kusner L, Carlin CR, Chang S, Futey L, Cotton CU, Dell KM, Avner ED. 2001. Phenotypic analysis of conditionally immortalized cells isolated from the BPK model of ARPKD. *American journal of physiology Cell physiology* **281**: C1695-1705.

Szymanska K, Johnson CA. 2012. The transition zone: an essential functional compartment of cilia. *Cilia* **1**: 10.

Taelman VF, Dobrowolski R, Plouhinec JL, Fuentealba LC, Vorwald PP, Gumper I, Sabatini DD, De Robertis EM. 2010. Wnt signaling requires sequestration of glycogen synthase kinase 3 inside multivesicular endosomes. *Cell* **143**: 1136-1148.

Takakura A, Contrino L, Zhou X, Bonventre JV, Sun Y, Humphreys BD, Zhou J. 2009. Renal injury is a third hit promoting rapid development of adult polycystic kidney disease. *Hum Mol Genet* **18**: 2523-2531.

Takeda S, Narita K. 2012. Structure and function of vertebrate cilia, towards a new taxonomy. *Differentiation; research in biological diversity* **83**: S4-11.

Tanigawa S, Wang H, Yang Y, Sharma N, Tarasova N, Ajima R, Yamaguchi TP, Rodriguez LG, Perantoni AO. 2011. Wnt4 induces nephronic tubules in metanephric mesenchyme by a non-canonical mechanism. *Dev Biol* **352**: 58-69.

Thoma CR, Frew IJ, Hoerner CR, Montani M, Moch H, Krek W. 2007. pVHL and GSK3beta are components of a primary cilium-maintenance signalling network. *Nat Cell Biol* **9**: 588-595.

Thomas C, Strutt D. 2012. The roles of the cadherins Fat and Dachsous in planar polarity specification in Drosophila. *Developmental dynamics : an official publication of the American Association of Anatomists* **241**: 27-39.

Tobimatsu T, Fujisawa H. 1989. Tissue-specific expression of four types of rat calmodulin-dependent protein kinase II mRNAs. *J Biol Chem* **264**: 17907-17912.

Togawa H, Nakanishi K, Mukaiyama H, Hama T, Shima Y, Sako M, Miyajima M, Nozu K, Nishii K, Nagao S et al. 2011. Epithelial-to-mesenchymal transition in cyst lining epithelial cells in an orthologous PCK rat model of autosomal-recessive polycystic kidney disease. *Am J Physiol Renal Physiol* **300**: F511-520.

Tombes RM, Faison MO, Turbeville JM. 2003. Organization and evolution of multifunctional Ca(2+)/CaM-dependent protein kinase genes. *Gene* **322**: 17-31.

Tomita M, Asada M, Asada N, Nakamura J, Oguchi A, Higashi AY, Endo S, Robertson E, Kimura T, Kita T et al. 2013. Bmp7 maintains undifferentiated kidney progenitor population and determines nephron numbers at birth. *PloS one* **8**: e73554.

Torres VE, Chapman AB, Devuyst O, Gansevoort RT, Grantham JJ, Higashihara E, Perrone RD, Krasa HB, Ouyang J, Czerwiec FS. 2012. Tolvaptan in Patients with Autosomal Dominant Polycystic Kidney Disease. *New England Journal of Medicine* **367**: 2407-2418.

Torres VE, Harris PC. 2014. Strategies targeting cAMP signaling in the treatment of polycystic kidney disease. *J Am Soc Nephrol* **25**: 18-32.

Torres VE, Harris PC, Pirson Y. 2007. Autosomal dominant polycystic kidney disease. *Lancet* **369**: 1287-1301.

Torres VE, Wang X, Qian Q, Somlo S, Harris PC, Gattone VH, 2nd. 2004. Effective treatment of an orthologous model of autosomal dominant polycystic kidney disease. *Nat Med* **10**: 363-364.

Tory K, Rousset-Rouviere C, Gubler MC, Moriniere V, Pawtowski A, Becker C, Guyot C, Gie S, Frishberg Y, Nivet H et al. 2009. Mutations of NPHP2 and NPHP3 in infantile nephronophthisis. *Kidney Int* **75**: 839-847.

Tran PV, Sharma M, Li X, Calvet JP. 2014a. Developmental signaling: does it bridge the gap between cilia dysfunction and renal cystogenesis? *Birth defects research Part C, Embryo today : reviews* **102**: 159-173.

Tran PV, Talbott GC, Turbe-Doan A, Jacobs DT, Schonfeld MP, Silva LM, Chatterjee A, Prysak M, Allard BA, Beier DR. 2014b. Downregulating hedgehog signaling reduces renal cystogenic potential of mouse models. *J Am Soc Nephrol* **25**: 2201-2212.

Tran U, Pickney LM, Ozpolat BD, Wessely O. 2007. Xenopus Bicaudal-C is required for the differentiation of the amphibian pronephros. *Dev Biol* **307**: 152-164.

Tran U, Zakin L, Schweickert A, Agrawal R, Doger R, Blum M, De Robertis EM, Wessely O. 2010. The RNA-binding protein bicaudal C regulates polycystin 2 in the kidney by antagonizing miR-17 activity. *Development* **137**: 1107-1116.

Uhlenhaut NH, Treier M. 2008. Transcriptional regulators in kidney disease: gatekeepers of renal homeostasis. *Trends in genetics : TIG* **24**: 361-371.

Valverde R, Edwards L, Regan L. 2008. Structure and function of KH domains. *The FEBS journal* **275**: 2712-2726.

Veland IR, Montjean R, Eley L, Pedersen LB, Schwab A, Goodship J, Kristiansen K, Pedersen SF, Saunier S, Christensen ST. 2013. Inversin/Nephrocystin-2 is required for fibroblast polarity and directional cell migration. *PLoS One* **8**: e60193.

Verdeguer F, Le Corre S, Fischer E, Callens C, Garbay S, Doyen A, Igarashi P, Terzi F, Pontoglio M. 2010. A mitotic transcriptional switch in polycystic kidney disease. *Nat Med* **16**: 106-110.

Vinyoles M, Del Valle-Perez B, Curto J, Vinas-Castells R, Alba-Castellon L, Garcia de Herreros A, Dunach M. 2014. Multivesicular GSK3 sequestration upon Wnt signaling is controlled by p120-catenin/cadherin interaction with LRP5/6. *Mol Cell* **53**: 444-457.

Wallace DP. 2011. Cyclic AMP-mediated cyst expansion. *Biochim Biophys Acta* **1812**: 1291-1300.

Wallingford JB, Mitchell B. 2011. Strange as it may seem: the many links between Wnt signaling, planar cell polarity, and cilia. *Genes Dev* **25**: 201-213.

Wang L, Eckmann CR, Kadyk LC, Wickens M, Kimble J. 2002. A regulatory cytoplasmic poly(A) polymerase in Caenorhabditis elegans. *Nature* **419**: 312-316.

Wang X, Ward CJ, Harris PC, Torres VE. 2010. Cyclic nucleotide signaling in polycystic kidney disease. *Kidney International* **77**: 129-140.

Wang X, Wu Y, Ward CJ, Harris PC, Torres VE. 2008. Vasopressin directly regulates cyst growth in polycystic kidney disease. *J Am Soc Nephrol* **19**: 102-108.

Warburton-Pitt SR, Jauregui AR, Li C, Wang J, Leroux MR, Barr MM. 2012. Ciliogenesis in Caenorhabditis elegans requires genetic interactions between ciliary middle segment localized NPHP-2 (inversin) and transition zone-associated proteins. *J Cell Sci* **125**: 2592-2603.

Watanabe D, Saijoh Y, Nonaka S, Sasaki G, Ikawa Y, Yokoyama T, Hamada H. 2003. The left-right determinant Inversin is a component of node monocilia and other 9+0 cilia. *Development* **130**: 1725-1734.

Watnick T, He N, Wang K, Liang Y, Parfrey P, Hefferton D, St George-Hyslop P, Germino G, Pei Y. 2000. Mutations of PKD1 in ADPKD2 cysts suggest a pathogenic effect of trans-heterozygous mutations. *Nat Genet* **25**: 143-144.

Watnick TJ, Torres VE, Gandolph MA, Qian F, Onuchic LF, Klinger KW, Landes G, Germino GG. 1998. Somatic mutation in individual liver cysts supports a two-hit model of cystogenesis in autosomal dominant polycystic kidney disease. *Molecular cell* **2**: 247-251.

Weber U, Paricio N, Mlodzik M. 2000. Jun mediates Frizzled-induced R3/R4 cell fate distinction and planar polarity determination in the Drosophila eye. *Development* **127**: 3619-3629.

Wessely O, De Robertis EM. 2000. The Xenopus homologue of Bicaudal-C is a localized maternal mRNA that can induce endoderm formation. *Development* **127**: 2053-2062.

White RR, Kwon YG, Taing M, Lawrence DS, Edelman AM. 1998. Definition of optimal substrate recognition motifs of Ca2+-calmodulin-dependent protein kinases IV and II reveals shared and distinctive features. *J Biol Chem* **273**: 3166-3172.

Williams CL, Li C, Kida K, Inglis PN, Mohan S, Semenec L, Bialas NJ, Stupay RM, Chen N, Blacque OE et al. 2011. MKS and NPHP modules cooperate to establish basal body/transition zone membrane associations and ciliary gate function during ciliogenesis. *J Cell Biol* **192**: 1023-1041.

Wu G, D'Agati V, Cai Y, Markowitz G, Park JH, Reynolds DM, Maeda Y, Le TC, Hou H, Jr., Kucherlapati R et al. 1998. Somatic inactivation of Pkd2 results in polycystic kidney disease. *Cell* **93**: 177-188.

Xu C, Rossetti S, Jiang L, Harris PC, Brown-Glaberman U, Wandinger-Ness A, Bacallao R, Alper SL. 2007. Human ADPKD primary cyst epithelial cells with a novel, single codon deletion in the PKD1 gene exhibit defective ciliary polycystin localization and loss of flow-induced Ca2+ signaling. *Am J Physiol Renal Physiol* **292**: F930-945.

Yamaguchi T, Nagao S, Kasahara M, Takahashi H, Grantham JJ. 1997. Renal accumulation and excretion of cyclic adenosine monophosphate in a murine model of slowly progressive polycystic kidney disease. *American journal of kidney diseases : the official journal of the National Kidney Foundation* **30**: 703-709.

Yamanaka H, Moriguchi T, Masuyama N, Kusakabe M, Hanafusa H, Takada R, Takada S, Nishida E. 2002. JNK functions in the non-canonical Wnt pathway to regulate convergent extension movements in vertebrates. *EMBO reports* **3**: 69-75.

Yang L, Lin C, Liu ZR. 2006. P68 RNA helicase mediates PDGF-induced epithelial mesenchymal transition by displacing Axin from beta-catenin. *Cell* **127**: 139-155.

Yasuhiko Y, Imai F, Ookubo K, Takakuwa Y, Shiokawa K, Yokoyama T. 2001. Calmodulin binds to inv protein: implication for the regulation of inv function. *Dev Growth Differ* **43**: 671-681.

Yasuhiko Y, Shiokawa K, Mochizuki T, Asashima M, Yokoyama T. 2006. Isolation and characterization of Xenopus laevis homologs of the mouse inv gene and functional analysis of the conserved calmodulin binding sites. *Cell research* **16**: 337-346.

Yoder BK, Hou X, Guay-Woodford LM. 2002. The polycystic kidney disease proteins, polycystin-1, polycystin-2, polaris, and cystin, are co-localized in renal cilia. *J Am Soc Nephrol* **13**: 2508-2516.

Yokoyama T, Copeland NG, Jenkins NA, Montgomery CA, Elder FF, Overbeek PA. 1993. Reversal of left-right asymmetry: a situs inversus mutation. *Science* **260**: 679-682.

Yuan S, Sun Z. 2013. Expanding horizons: ciliary proteins reach beyond cilia. *Annual review of genetics* **47**: 353-376.

Zalli D, Bayliss R, Fry AM. 2012. The Nek8 protein kinase, mutated in the human cystic kidney disease nephronophthisis, is both activated and degraded during ciliogenesis. *Hum Mol Genet* **21**: 1155-1171.

Zhang Y, Cooke A, Park S, Dewey CN, Wickens M, Sheets MD. 2013. Bicaudal-C spatially controls translation of vertebrate maternal mRNAs. *RNA* **19**: 1575-1582.

Zhang Y, Park S, Blaser S, Sheets MD. 2014. Determinants of RNA binding and translational repression by the Bicaudal-C regulatory protein. *J Biol Chem* **289**: 7497-7504.

Zimmermann KW. 1898. Beiträge zur Kenntniss einiger Drüsen un Epithelien. *Archiv für Mikroskopische Anatomie* **52**: 552-706.

8. Articles

Urine Fetuin-A is a biomarker of Autosomal Dominant Polycystic Kidney Disease progression

Piazzon N, Bernet F, Guihard L, Wouter LN, Urfer S, Firsov D, Chehade H, Vogt B, Piergiovanni S, Peters DJ, Bonny O and Constam DB.

BioMed Central
The Open Access Publisher

Urine Fetuin-A is a biomarker of autosomal dominant polycystic kidney disease progression

Nathalie Piazzon (nathalie.piazzon@unil.ch)
Florian Bernet (florian.bernet@epfl.ch)
Linda Guihard (Linda.Guihard@chuv.ch)
Wouter N Leonhard (W.N.Leonhard@lumc.nl)
Séverine Urfer (severine.urfer@epfl.ch)
Dmitri Firsov (Dmitri.Firsov@unil.ch)
Hassib Chehade (Hassib.Chehade@chuv.ch)
Bruno Vogt (bruno.vogt@insel.ch)
Sophia Piergiovanni (sophia.piergiovanni@chuv.ch)
Dorien JM Peters (D.J.M.Peters@lumc.nl)
Olivier Bonny (Olivier.Bonny@chuv.ch)
Daniel B Constam (Daniel.Constam@epfl.ch)

For information about publishing your research in BioMed Central journals, go to
http://www.biomedcentral.com/info/authors/

Urine Fetuin-A is a biomarker of autosomal dominant polycystic kidney disease progression

Nathalie Piazzon[1,2]
Email: nathalie.piazzon@unil.ch

Florian Bernet[1]
Email: florian.bernet@epfl.ch

Linda Guihard[3]
Email: Linda.Guihard@chuv.ch

Wouter N Leonhard[4]
Email: W.N.Leonhard@lumc.nl

Séverine Urfer[1]
Email: severine.urfer@epfl.ch

Dmitri Firsov[2]
Email: Dmitri.Firsov@unil.ch

Hassib Chehade[5]
Email: Hassib.Chehade@chuv.ch

Bruno Vogt[6]
Email: bruno.vogt@insel.ch

Sophia Piergiovanni[2]
Email: sophia.piergiovanni@chuv.ch

Dorien JM Peters[4]
Email: D.J.M.Peters@lumc.nl

Olivier Bonny[2,3]*
* Corresponding author
Email: Olivier.Bonny@chuv.ch

Daniel B Constam[1]*
* Corresponding author
Email: Daniel.Constam@epfl.ch

[1] Ecole Polytechnique Fédérale de Lausanne (EPFL), Bâtiment SV ISREC, Station 19, Lausanne, Switzerland

[2] Department of Pharmacology and Toxicology, University of Lausanne (UNIL), Quartier UNIL-CHUV, Lausanne, Switzerland

[3] Service of Nephrology, Lausanne University Hospital (CHUV), Lausanne, Switzerland

4 Department of Human Genetics, Leiden Univ. Medical Center, Leiden, The Netherlands

5 Department of Pediatrics, Division of Pediatric Nephrology, Lausanne University Hospital (CHUV), Lausanne, Switzerland

6 Department of Nephrology and Hypertension, Inselspital, Bern, Switzerland

Abstract

Background

Autosomal dominant polycystic kidney disease (ADPKD) is a genetic disorder characterized by numerous fluid-filled cysts that frequently result in end-stage renal disease. While promising treatment options are in advanced clinical development, early diagnosis and follow-up remain a major challenge. We therefore evaluated the diagnostic value of Fetuin-A as a new biomarker of ADPKD in human urine.

Results

We found that renal Fetuin-A levels are upregulated in both *Pkd1* and *Bicc1* mouse models of ADPKD. Measurement by ELISA revealed that urinary Fetuin-A levels were significantly higher in 66 ADPKD patients (17.5 ± 12.5 μg/mmol creatinine) compared to 17 healthy volunteers (8.5 ± 3.8 μg/mmol creatinine) or 50 control patients with renal diseases of other causes (6.2 ± 2.9 μg/mmol creatinine). Receiver operating characteristics (ROC) analysis of urinary Fetuin-A levels for ADPKD rendered an optimum cut-off value of 12.2 μg/mmol creatinine, corresponding to 94% of sensitivity and 60% of specificity (area under the curve 0.74 ; $p = 0.0019$). Furthermore, urinary Fetuin-A levels in ADPKD patients correlated with the degree of renal insufficiency and showed a significant increase in patients with preserved renal function followed for two years.

Conclusions

Our findings establish urinary Fetuin-A as a sensitive biomarker of the progression of ADPKD. Further studies are required to examine the pathogenic mechanisms of elevated renal and urinary Fetuin-A in ADPKD.

Keywords

Fetuin-A, Urine, ADPKD, Biomarker, ELISA

Background

Autosomal dominant polycystic kidney disease (ADPKD) is the most common inherited kidney disease, affecting as many as 1 in 1000 individuals world-wide, but with variable course and prognosis [1-3]. It is caused by mutations in the *polycystic kidney disease (PKD)-1* or less frequently in the *PKD2* gene [4-7]. ADPKD is characterized by the progressive development of numerous large fluid-filled cysts especially in the kidneys over a period of

decades [8]. Cystic growth results in dramatic kidney enlargement, and it induces reactive interstitial inflammation and fibrosis, leading frequently to end stage renal disease (ESRD) [9]. However, important unresolved issues remain in the diagnosis and follow-up of ADPKD. In particular, what determines the rate of cyst progression in patients is unclear, and diagnostic tools to predict disease outcome are elusive. Diagnosis is usually established by renal imaging (ultrasonography, CT-scan or MRI) when there is a positive family history [7]. However, cysts may only appear late in the course of the disease, creating a diagnostic gap. Direct genetic analysis is feasible, but remains challenging owing to the large size, complex genomic structure and allelic heterogeneity of *PKD1* and *PKD2* genes [10,11]. Disease progression is usually assessed by repeated analysis of plasma creatinine levels as readout of glomerular filtration rates (GFR). However, plasma creatinine levels only start rising when the disease is already well advanced. To improve diagnosis and early follow-up of ADPKD, current efforts focus on renal volume assessment by MRI or CT-scan and on non-invasive urine biomarkers. Assessment of renal volume allows an earlier follow-up of the disease and the management of associated symptoms such as hypertension [12]. Only few candidate biomarkers have been identified, including albuminuria, β2-microglobulin [13,14], neutrophil gelatinase-associated lipocalin (NGAL) [15] and monocyte chemotactic protein 1 (MCP-1) [16,17]. With the notable exception of albuminuria [18,19], these remain to be validated.

Future diagnostic and innovative therapeutic approaches may be guided by insights from rodent models of ADPKD with spontaneous or engineered mutations [20]. Among such models, mouse kidneys lacking *Pkd1* are arguably the most disease-relevant since human *PKD1* is mutated in 85% of ADPKD patients [21]. Interestingly, conditional knockout of a targeted *Pkd1* allele (*Pkd1*cKO) in mouse kidneys before or after postnatal day 12–14 revealed that the susceptibility to cystic growth dramatically decreases after day 13, coincident with a metabolic switch and a sudden decline of cell proliferation at this stage of postnatal development [22-25]. Transcriptome profiling of *Pkd1*cKO kidneys revealed that even the aggressive early-onset disease is initiated independently of changes in gene expression levels above 2-fold, and with less than 100 genes de-regulated [24]. Therefore, it may be difficult to identify sensitive markers linked to the etiology of ADPKD that are significantly deregulated at the transcriptional level.

Renal cysts also develop in mice and humans carrying mutations in the *Bicc1* gene that encodes the cytoplasmic RNA-binding protein Bicaudal-C [26-29]. *Bicc1* expression partly depends on *Pkd1* [30] and in turn stimulates the translation of *Pkd2* mRNA [27], indicating that Bicaudal-C mediates critical polycystin functions. A candidate search for direct targets revealed that Bicc1 binds adenylate cyclase-6 (AC6) mRNA and reduces its translation [27]. AC6 is likely a ADPKD-relevant target as it contributes to cyst formation in Pkd1-deficient mouse kidneys [31]. However, since AC6 or other known direct Bicc1 targets cannot be monitored non-invasively, we decided instead to initially screen for candidate biomarkers using gene expression profiling.

Here, we report that polycystic mouse kidneys induced by targeted deletion of *Pkd1* or *Bicc1* as well as the urine of ADPKD patients contain elevated levels of Fetuin-A. Fetuin-A (also known as α2-Heremans Schmid glycoprotein, AHSG, FETUA) is a multifunctional negative acute phase protein in blood plasma that regulates insulin signaling, bone resorption, and the precipitation of calciprotein particles [32]. During development, FETUA is expressed in several tissues and organs, including the brain, liver, bone, kidney, and respiratory and cardiovascular systems [33], whereas in adults, its expression normally is restricted to the liver [34]. Despite the absence of *FETUA* mRNA, the protein has been detected in proximal

tubule epithelial cells of adult rat kidneys by immunostaining, and this staining can be inhibited by blocking megalin-mediated endocytosis [35]. Thus, Fetuin-A may enter proximal tubule cells by reabsorption from the tubule lumen after passing from plasma through the glomerular slit diaphragm [35,36]. We show that Bicc1 mutant cystic kidneys fail to retain the protein and instead release it into urine. We show that urinary Fetuin-A levels are also elevated in patients with ADPKD compared to healthy volunteers. Our findings reveal a new trait shared among ADPKD patients and the *Bicc1* mouse model, and they suggest that Fetuin-A is a promising new disease biomarker that should be considered for further prospective studies and to investigate its potential role in ADPKD pathogenesis.

Results

Upregulation of Fetuin-A in two mouse models of polycystic kidney disease

Insights into disease pathogenesis and identification of biomarkers may be accelerated by genome-wide transcriptome analysis [37]. To this end, total RNA from 3 *Bicc1*KO embryos and 3 wild-type (WT) control littermates was isolated shortly after the onset of cyst formation and subjected to Affymetrix cDNA array hybridization. Array analysis only revealed very few and modest changes at the level of gene transcription (less than 70 genes being changed more than 1.5-fold, data not shown). Among these changes was a 3.5-fold upregulation of the *FETUA* transcript (p = 0.006). Consistently, Western blot analysis of renal extracts at E16.5 (i.e. during onset of cyst formation), P0 and P5 showed increasing expression of Fetuin-A protein with the expected apparent molecular weight of 59 kDa in *Bicc1*KO compared to WT (Figure 1a). While Fetuin-A is mainly synthesized in the liver after birth [34], Western blot analysis of liver extracts at P1 and P3 revealed no difference in its expression in *Bicc1*KO compared to the WT (Figure 1b). This result suggests that Fetuin-A expression is increased in *Bicc1*KO kidneys, rather than systemically.

Figure 1 Expression of Fetuin-A in mouse models of polycystic kidney disease. (a, b) Western blot analysis of Fetuin-A in **(a)** kidney and **(b)** liver extracts of the indicated genotypes. **(c)** Western blots of Fetuin-A in early stages of cyst formation (3 weeks, n = 4 for each genotype) or advanced cystic kidneys (9 weeks, n = 4 for each genotype) of wild-type or KspCad-Cre^{ERT2}; *Pkd1*$^{fl/fl}$ kidneys after tamoxifen administration at postnatal days 10–12. Signal quantification by Image J is shown on the right after normalization to loading control (γ-tubulin). Error bars represent standard deviation. n.s.: non-significant.

To verify whether the increase in renal Fetuin-A was related to cyst formation, we analyzed kidneys carrying a conditional *Pkd1* allele that was deleted by tamoxifen-inducible KspCad-CreERT2 [23,25]. Compared to WT, Fetuin-A was upregulated up to 2.7-fold (p < 0.001) during an early stage of cyst formation, and 7.8-fold (p < 0.001) in animals with advanced cysts (Figure 1c). These results suggest a possible correlation between the level of Fetuin-A and the progression of the disease.

Fetuin-A levels are low in cyst-lining cells, but increase in urine of Bicc1KO mice

To obtain further insight into the regulation of Fetuin-A, we examined its distribution in WT and *Bicc1*KO newborn kidneys by immunostaining. Co-labeling with *Lotus tetragonolobus* lectin, which specifically labels proximal tubules [38] revealed Fetuin-A expression in

cortical epithelial cells of newborn wild-type kidney (Figure 2a). Fetuin-A was neither detected in the medulla nor in the renal pelvis (Additional file 1: Figure S1), concurring with data obtained in rat kidneys [35]. Paradoxically, despite the marked elevation of Fetuin-A in total extracts of *Bicc1*KO newborn kidneys above WT control (Figure 1a), immunolabelling only detected very sparse Fetuin-A staining in few cyst-lining cells in proximal tubules (Figure 2a). To assess whether Fetuin-A accumulates in the urine, we collected urine samples from the bladder at P0 or P3. Compared to heterozygous and WT litter mates, urine from *Bicc1*KO showed an up to 60-fold increase in Fetuin-A levels (n = 5/5, p < 0.005) (Figure 2b). We conclude that cystic *Bicc1*KO kidneys enrich Fetuin-A in the urine.

Figure 2 Localization and excretion of urinary Fetuin-A in newborn kidneys. (a) Frozen sections of WT (n = 2) and *Bicc1*KO newborn kidneys (n = 4) labeled with anti-Fetuin-A antibody (green), and *Lotus tetragonolobus* lectin (LTL, red). *Bicc1* heterozygotes (n = 2) were indistinguishable from WT (not shown). Scale bars: 100 μm. **(b)** Western blot analysis of urinary Fetuin-A excretion of the indicated genotypes at stages P0 and P3. Signal quantification by ImageJ is shown below. Error bars represent standard deviation.

Levels of urinary Fetuin-A correlate with disease progression in ADPKD patients

We therefore evaluated urinary Fetuin-A as a potential ADPKD biomarker in humans. ELISA analysis was conducted on urine samples from 66 ADPKD patients, 17 healthy volunteers and 50 patients with renal diseases of other causes than ADPKD. Clinical characteristics and laboratory variables of patients are reported in Table 1 and Additional file 2: Table S1. Urinary levels of Fetuin-A normalized to creatinine were significantly higher in ADPKD patients (17.5 ± 12. 9 μg/mmol creatinine) compared to healthy volunteers (8.5 ± 3.8 μg/mmol creatinine) and to patients with various renal diseases other than ADPKD (6.2 ± 2.9 μg/mmol creatinine) (Figure 3a). To verify the expression of urinary Fetuin-A in individual urine samples by Western blotting, 11 samples from ADPKD patients and patients with various renal diseases other than ADPKD were randomly selected. The result demonstrated that urinary Fetuin-A levels were significantly augmented in ADPKD group, correlating with the ELISA analysis (Additional file 3: Figure S2). Moreover, consecutive analysis in 6 months intervals during 2 years in 19 patients with early-stage ADPKD (eGFR > 60 ml/min/1.73 m^2) showed that urinary excretion of Fetuin-A increased progressively (p = 0.031, one-way ANOVA) (Figure 3b, Additional file 4: Figure S3a and Table 2). By contrast, eGFR did not significantly change over the same time period (Additional file 4: Figure S3b). This suggests that the levels of Fetuin-A in urine may be a more sensitive marker in determining disease progression than eGFR. Consistently, a significant correlation was found between chronic kidney disease (CKD) stages and the levels of urinary Fetuin-A in ADPKD patients (p = 0.024, one-way ANOVA) (Figure 3c, Additional file 4: Figure S3c and Table 3). To further validate this conclusion, we determined cut-off values discriminating ADPKD patients from normal volunteers using Receiver Operating Characteristics (ROC) curves (Figure 4). All areas under the curves (AUC) were significantly different from chance. Urinary Fetuin-A levels of advanced ADPKD (eGFR < 60 ml/min/1.73 m^2) showed the highest AUC (0.87, p < 0.0001) and that Fetuin-A values at 12.2 μg/mmol creatinine distinguished patients from healthy controls with 94% of sensitivity and 74% of specificity. Fetuin-A values at 12.2 μg/mmol creatinine distinguished patients with early ADPKD (eGFR > 60 ml/min/1.73 m^2) from healthy controls, but the sensitivity and specificity were 94% and 58%, respectively. These analyses yielded optimum cut-off values of 12.2 μg/mmol

creatinine for the establishment of ADPKD diagnosis with a high sensitivity and a reasonable specificity.

Table 1 Clinical characteristics and laboratory variables of patients subjected to ELISA analysis

	Healthy volunteers	Renal diseases other than ADPKD	ADPKD total	early	advanced
Cases (n)	17	50	66	36	30
Age (Years)*	34.9 ± 11.1	65.3 ± 12.6	43.1 ± 17.2	31.9 ± 12.7	56.3 ± 11.5
Gender (n)**					
Male	53 (9)	66 (33)	48 (32)	50 (18)	47 (14)
Female	47 (8)	34 (17)	52 (34)	50 (18)	53 (16)
Pathologies (n)**					
• Diabetes	-	20 (10)	3 (2)	-	6 (2)
• Obesity (BMI > 30 kg/m^2)	-	16 (8)	3 (2)	3 (1)	3 (1)
• Hypercholesterolemia	-	24 (12)	7 (5)	-	16 (5)
eGFR [mL/min/1.73 m^2]*	N.A.	30.0 ± 15.1	71.8 ± 38.8	102.5 ± 20.6	35.4 ± 17.4
Proteinuria [g/ mmol creatinine]*	N.A.	0.621 ± 0.06	0.139 ± 0.05	0.101 ± 0.04	0.215 ± 0.02
High BP, (n)**	-	44 (22)	85 (56)	75 (27)	96 (29)
Fetuin-A (U) [μg/L]*	78.7 ± 39.5	39.2 ± 13.1	104.9 ± 58.7	89.1 ± 48.4	124.1 ± 64.7
Fetuin-A (U) [μg/mmol creatinine]*	8.5 ± 3.8	6.2 ± 2.9	17.5 ± 12.9	13.8 ± 9.6	21.8 ± 14.3

* Data are presented as mean ± SD. ADPKD, autosomal dominant polycystic kidney disease; eGFR, estimated glomerular filtration rate; N.A., not assessed; (U), urine.
** values are in percentage. Absolute numbers are in brackets. High BP is defined as systolic BP >140 and/or diastolic BP >90 mmHg (mean of three measurements) or the need for anti-hypertensive medication.

Figure 3 Evaluation of Fetuin-A as a biomarker for ADPKD. (a) ELISA quantification of Fetuin-A levels normalized to creatinine in urine of ADPKD (n = 66), healthy volunteers (n = 17) and control patients with various renal diseases (n = 50). Solid lines indicate mean. **(b)** Evolution of urinary levels of Fetuin-A normalized to creatinine during 5 visits (V) every 6 months in 19 early ADPKD patients. Average relative change (Δ, %) and p-values are indicated. **(c)** Urinary levels of Fetuin-A normalized to creatinine stratified by CKD stages evaluated based on eGFR values. Stage 1, eGFR = 115 ± 10 ml/min/1.73 m^2 (range, 96–129), n = 23; stage 2, eGFR = 77 ± 8 ml/min/1.73 m^2 (range, 61–89), n = 15; stage 3, eGFR = 45 ± 9 ml/min/1.73 m^2 (range, 31–59), n = 16; stage 4, eGFR = 21 ± 2 ml/min/1.73 m^2 (range, 18–25), n = 7 and stage 5, eGFR = 11 ± 1 ml/min/1.73 m^2 (range, 10–14), n = 5. Solid lines indicate mean. Significance was calculated by one-way ANOVA (p = 0.023).

Table 2 Levels of urinary Fetuin-A correlate with ADPKD progression

Early ADPKD	V_0	V_1	V_2	V_3	V_4
Time (months)	0	6	12	18	24
Cases (n)	19	19	19	19	19
Fetuin-A [μg/L]*	71.6 ± 43.7	95.6 ± 47.8	114.3 ± 65.3	136.1 ± 56.7	150.7 ± 66.4
p-value	n.s.	n.s.	n.s.	0.014	0.0001
Fetuin-A [μg/mmol creatinine]*	13.9 ± 9.6	17.1 ± 13.8	19.6 ± 14.6	24.3 ± 16.3	27.7 ± 16.7
p-value	n.s.	n.s.	n.s.	0.021	0.003

* Data are presented as mean ± SD. One-way ANOVA followed by *Bonferroni's* test was used for comparison (p < 0.05) for both Fetuin-A and Fetuin-A/Creatinine ratio. n.s., not significant.

Table 3 Correlation between levels of urinary Fetuin-A and CKD stage of patients

CKD stage	1	2	3	4	5
Cases (n)	23	15	16	7	5
Fetuin-A [µg/L]*	88.4 ± 42.4	90.6 ± 51.5	113.1 ± 63.7	152.1 ± 64.8	172.4 ± 22.8
p-value		n.s.	0.024	0.003	0.0001
Fetuin-A [µg/mmol creatinine]*	13.4 ± 11.1	14.5 ± 8.8	19.4 ± 12.9	25.1 ± 13.6	30.2 ± 19.3
p-value		n.s.	0.041	0.027	0.012

* Data are presented as mean ± SD. n.s., not significant.
The 66 ADPKD patients were stratified by CKD stages (1 to 5). The stages are based on estimated glomerular filtration rate (eGFR). One-way ANOVA followed by *Bonferroni's* test was used for comparison ($p < 0.05$) for both Fetuin-A and Fetuin-A/creatinine ratio.

Figure 4 Receiver Operating Characteristic (ROC) curves of urinary Fetuin-A as a biomarker for detection of ADPKD. Receiver Operation Characteristic (ROC) curves. The area under the ROC curve was 0.74 (95% CI, 0.6397 to 0.8505, $p < 0.05$) for ADPKD diagnosis, 0.67 (95% CI, 0.5276 to 0.8143, $p < 0.05$) for early ADPKD diagnosis, 0.87 (95% CI, 0.7720 to 0.9692, $p < 0.05$) for advanced ADPKD diagnosis.

Discussion

Improving early diagnosis and follow-up of ADPKD patients remains a major challenge, especially for disease management in the new era of future therapeutic interventions [39]. Ongoing efforts so far have mainly focused on imaging (CRISP consortium) [40] and on new disease biomarkers [41-44]. However, despite intense efforts, the development of non-invasive biomarkers is still in its infancy. Here, we found that two independent mouse models of ADPKD express elevated levels of Fetuin A in the kidney, and that average urinary Fetuin-A levels increase during disease progression in affected ADPKD patients.

Renal Fetuin-A levels increased in the urine of ADPKD patients compared to healthy volunteers, as well as in urine and total kidney extracts of the non-orthologous $Bicc1^{-/-}$ mouse model. In view of the positive data from urine of patients, we did not attempt to extend our study to urine of conditionally *Pkd1*-deleted mutant mice. Nevertheless, analysis of whole kidneys confirmed that Fetuin-A is also upregulated in this orthologous mouse model, in keeping with a role as a disease-relevant marker. Importantly, the levels of urinary Fetuin-A in ADPKD patients correlated with the stage of renal insufficiency during disease progression. In good agreement, Fetuin-A has also been detected within ADPKD kidneys by mass spectrometry analysis of cyst fluid [45]. Together, these observations indicate that Fetuin-A is a sensitive biomarker of disease progression.

Fetuin-A initially attracted our attention because of an apparent upregulation detected by microarray gene expression profiling of embryonic *Bicc1*KO kidneys already at the early onset of cystic disease. However, local transcriptional de-regulation within the kidney could not be confirmed either by Taqman or SYBR Green qRT-PCR due to low baseline expression and substantial variability among samples both in wild-type and cystic newborn kidneys (unpublished observation). Furthermore, immunolabelling detected Fetuin-A in vesicles of wild-type proximal tubules as described previously in the rat [35], and this staining was nearly abolished in *Bicc1*KO, rather than being increased. Nevertheless, the levels of Fetuin-A detected by Western blot clearly increased in *Bicc1*KO compared to wild-type, both in total kidney extracts and in urine. Analysis of livers detected no systemic upregulation or increased hepatic production. Moreover, in a cohort of ADPKD patients that was followed

during 24 months, we found that the levels of urinary Fetuin-A significantly increased without a corresponding increase in eGFR. Taken together, these findings suggest that Fetuin-A specifically accumulates in the urine of cystic kidneys, probably due to impaired renal reabsorption rather than increased filtration or secretion.

Fetuin-A is also secreted in the urine during advanced diabetic nephropathy [46]. However, the levels of urinary Fetuin-A in these patients correlate with microalbuminuria, indicating that Fetuin-A leaked through defective glomeruli and failed to be reabsorbed in proximal tubules. Fetuinuria in diabetic nephropathy thus likely has a different origin than in ADPKD. The levels of Fetuin-A in urine also increase during acute kidney injury (AKI), which can be induced by cisplatin or by ischemia-reperfusion [47]. During AKI, Fetuin-A was enriched both in the cytoplasm of damaged proximal tubule cells and in urine [47], similar to what we observed in cystic kidneys of *Bicc1* KO mice. By contrast, we detected no upregulation of Fetuin-A in the urine of patients with various renal diseases other than ADPKD. Also in urine of patients with kidney stones, a recent study reported a decrease in the levels of Fetuin-A, rather than an increase [48]. Thus, rather than being a general reaction to renal injury, elevated Fetuin-A in adult human kidneys appears to be part of a program that is linked to ADPKD.

Acknowledged limitations of this study include the absence of kidney volume assessment for quantifying the rate of disease progression, and that our patient group has not been stratified by genotype or extrarenal manifestations such as hypertension or liver cysts. Nevertheless, our finding that Fetuin-A is significantly upregulated in a majority of ADPKD patients and in mouse kidneys deficient in *Pkd1* or one of its downstream targets might become clinically useful to aid in diagnosis.

Conclusions

In summary, our findings demonstrate that Fetuin-A production is upregulated in cystic kidneys of two different mouse models of ADPKD and excreted in the urine. In ADPKD patients, urinary Fetuin-A levels were significantly elevated, with a close correlation between fetuinuria and disease progression. While the precise mechanisms underlying the increase of Fetuin-A secretion in the kidney and its role in cystic disease remain to be determined, our findings establish urine Fetuin-A as a novel biomarker of the progression of ADPKD in humans. Further studies are warranted to examine the pathogenic mechanisms of elevated Fetuin-A and its role in the diagnosis of ADPKD.

Methods

Mice and mutant alleles

Mice heterozygous for a targeted null allele of *Bicc1* [29] were maintained on a C57BL/6 genetic background in individually ventilated cages at the EPFL animal facility. To induce a kidney-specific deletion of *Pkd1*, tam-KspCad-CreERT2; Pkd1$^{lox2-11/lox2-11}$ mice orally received tamoxifen by gavage as described [23]. For early stage of cyst formation, mice were sacrificed 3 weeks after administration of 0.5 mg taxomifen at postnatal days 10–12. For late stage of cyst formation, mice were sacrificed 9 weeks after administration of 0.5 mg taxomifen at postnatal days 10–12. All animal experiments were approved by the Animal Care and Use Committee of Leiden University and by the Commission for Biotechnology in

Animals of the Dutch Ministry of Agriculture, or by the Veterinary Service of the Swiss canton of Vaud.

Clinical specimen collection

133 participants (66 ADPKD and 50 patients with various renal diseases and 17 normal volunteers) were enrolled in the ADPKD cohort of the division of Nephrology of the Lausanne University Hospital (CHUV) (Lausanne, Switzerland) prospectively between 2009 and 2014. Clinical data of all participants were collected. All patients were informed about the purpose of the study and gave their informed consent. This study was approved by the local research ethical board and conducted in accordance with the ethical standards of the Helsinki Declaration.

Biochemical assays

Each human urine sample was directly collected into sterile plastic tube and then stored at $-80°C$ for further analysis. Blood samples were immediately processed. Serum creatinine, osmolality, sodium, potassium, calcium, phosphate, BUN, uric acid and urine creatinine, osmolality, sodium, potassium, total proteins were measured at the central lab of the Lausanne University Hospital (Lausanne, Switzerland). Serum creatinine values were used to calculate estimated glomerular filtration rate (eGFR) using the CKD-Epidemiology Collaboration (CKD-EPI) equation [49].

RNA isolation, library preparation and Affymetrix cDNA microarray hybridization

Kidney RNA was extracted using Trizol (Invitrogen) according to the manufacturer instructions. RNA concentration and purity were determined using a Nanodrop (Thermo Fisher, Waltham, MA). RNA integrity was assessed on a Bioanalyzer (Agilent, Santa Clara, CA). High-quality RNA samples (RNA Integrity Number $\geq$ 8) were used for library preparation.

Indirect immunofluorescent labelling

Postnatal mouse kidneys were fixed in 4% paraformaldehyde in PBS for 1.5 hrs, rinsed with PBS, and soaked in 15% sucrose over night at 4°C and embedded in Optimum Cutting Temperature (OCT) compound on dry ice. Cryosections (8 µM) were permeabilised for 10 min with 0.2% Triton X-100 in PBS, blocked with PBS containing 1% BSA and with streptavidin-biotin blocking kit (Vector labs, #SP-2002). Biotinylated LTL (Vector labs, B-1325), 1:200, and goat anti-Fetuin-A antibody (1:300) were added over night at 4°C. Secondary antibody (anti-rabbit Alexa 488, Molecular Probes) and streptavidin pacific blue (Lifetechnologies) were incubated for 1 hr at 25°C at 1:800 and 1:400, respectively, in PBS containing 0.1% Triton X-100. Images were acquired with a 20× objective on a Leica LSM700 confocal microscope.

Western blot analysis

Frozen kidneys were directly lysed in Laemmli buffer by ultrasonication on ice and centrifuged to remove debris while retaining cyst fluids [45] and urine. For Western blot

analysis, urine samples were centrifuged at 3,500 × g for 5 min at 4°C. Proteins were separated by electrophoresis on a 7.5% sodium dodecyl sulfate-polyacrylamide gel and transferred onto nitrocellulose membranes (Amersham-Biosciences). The membranes were blocked for 1 h at 37°C in a solution of PBS containing 5% non-fat milk powder and 0.05% Tween-20 (PBS-T) and then incubated overnight at 4°C with goat polyclonal primary antibody against Fetuin-A (diluted 1:200; Santa Cruz Biotechnology Inc., USA) or mouse anti-γ-tubulin (diluted 1:1000; Sigma). Membranes were washed three times for 10 min in PBS-T and then incubated with the secondary antibodies peroxidase-conjugated anti-mouse or anti-rabbit (GE Healthcare) and anti-goat antibodies (Santa Cruz Biotechnology Inc., USA) at room temperature for 1 h. The proteins were detected using an enhanced chemiluminescence detection system (ECL-Direct systems RPN3000; Pierce Biotechnology, Inc., Rockford, IL, USA). Densitometric analysis of immunoblots and normalization to γ-tubulin expression was performed using Image J software.

Enzyme-linked immunosorbent assay (ELISA)

Urine samples were centrifuged at 3,500 × g for 5 min at 4°C to remove debris prior to ELISA analysis. The concentrations of Fetuin-A in the urine samples were measured with a Fetuin-A (AHSG) Human ELISA kit (Abcam, Cambridge, UK). The assay was performed according to the instructions recommended by the manufacturer. The standard curve was created using lyophilized human Fetuin-A standard preparation supplied with the assay. Following the colorimetric reaction, the optical density was read at 450 nm using a spectrophotometer, and converted to concentrations in μg/L. Urine creatinine levels were measured at the central lab of the Lausanne University hospital using a Cobas-Mira analyzer (Roche). The levels of Fetuin-A were normalized according to urine creatinine concentrations (Fetuin-A: μg/mmol creatinine). Every sample was tested in duplicate.

Statistical analysis

All data were collected and presented as mean ± standard deviation. Normal distribution of the data was assessed using Shapiro-Wilk test. Differences among two groups were compared by unpaired Student's t-test. For comparison among multiple experimental conditions, a nonparametric one-way analysis of variance (ANOVA) followed by *Bonferroni's test* for multiple comparisons was used. $P < 0.05$ was considered a statistically significant difference. Receiving operating curve (ROC) analyses were used to explore the diagnostic performance of urinary Fetuin-A (μg/mmol creatinine) over a range of possible clinical conditions. The best statistical cut-off value of Fetuin-A (μg/mmol creatinine) was defined as the point at which the sum of sensitivity and specificity is more than that at other points. GraphPad Prism v6 was used.

Abbreviations

AC6, Adenylate cyclase-6; ADPKD, Autosomal dominant polycystic kidney disease; AKI, Acute kidney injury; AUC, Area under the curve; BP, Blood pressure; CKD, Chronic kidney disease; CT-scan, Computed tomography scan; eGFR, Estimated glomerular filtration rate; ELISA, Enzyme-linked immunosorbent assay; ESRD, End stage renal disease; kDa, Kilodalton; KO, Knock-out; LTL, *Lotus tetragonolobus* lectin; MRI, Magnetic resonance imaging; N.A., Not assessed; n.s., Not significant; OCT, Optimum cutting temperature; PBS, Phosphate-buffered saline; PBS-T, Phosphate-buffered saline tween-20; ROC, Receiving

operating curve; SDS-PAGE, Sodium dodecyl sulfate polyacrylamide gel electrophoresis; U, Urine; WT, Wild-type.

Competing interests

The authors declare that they have no competing interests.

Authors' contributions

NP, DF, HC, BV, OB and DC participated in the design of the study. NP, FB, LG, WL, SU and SP performed the experiments. NP, DP, OB and DC analyzed the data, and wrote the manuscript. All authors read and approved the final manuscript.
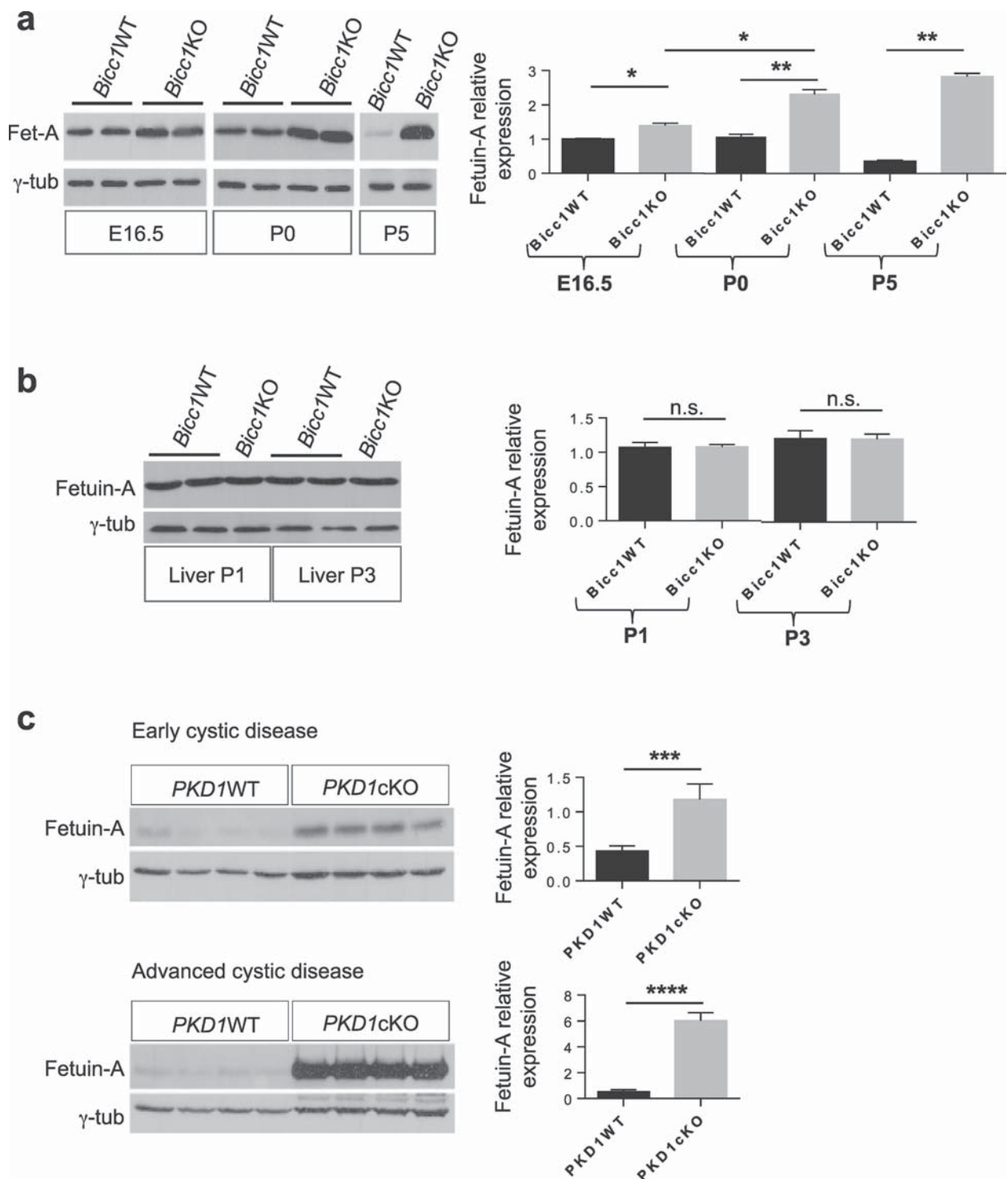
Acknowledgements

References

1. Dalgaard OZ. Bilateral polycystic disease of the kidneys; a follow-up of two hundred and eighty-four patients and their families. Acta Med Scand Suppl. 1957;328:1–255.

2. Iglesias CG, Torres VE, Offord KP, Holley KE, Beard CM, Kurland LT. Epidemiology of adult polycystic kidney disease, Olmsted County, Minnesota: 1935–1980. Am J Kidney Dis. 1983;2:630–9.

3. Dalgaard OZ. Bilateral polycystic disease of the kidneys; a follow-up of 284 patients and their families. Dan Med Bull. 1957;4:128–33.

4. Hughes J, Ward CJ, Peral B, Aspinwall R, Clark K, San Millan JL, et al. The polycystic kidney disease 1 (PKD1) gene encodes a novel protein with multiple cell recognition domains. Nat Genet. 1995;10:151–60.

5. Mochizuki T, Wu G, Hayashi T, Xenophontos SL, Veldhuisen B, Saris JJ, et al. PKD2, a gene for polycystic kidney disease that encodes an integral membrane protein. Science. 1996;272:1339–42.

6. Qian F, Watnick TJ, Onuchic LF, Germino GG. The molecular basis of focal cyst formation in human autosomal dominant polycystic kidney disease type I. Cell. 1996;87:979–87.
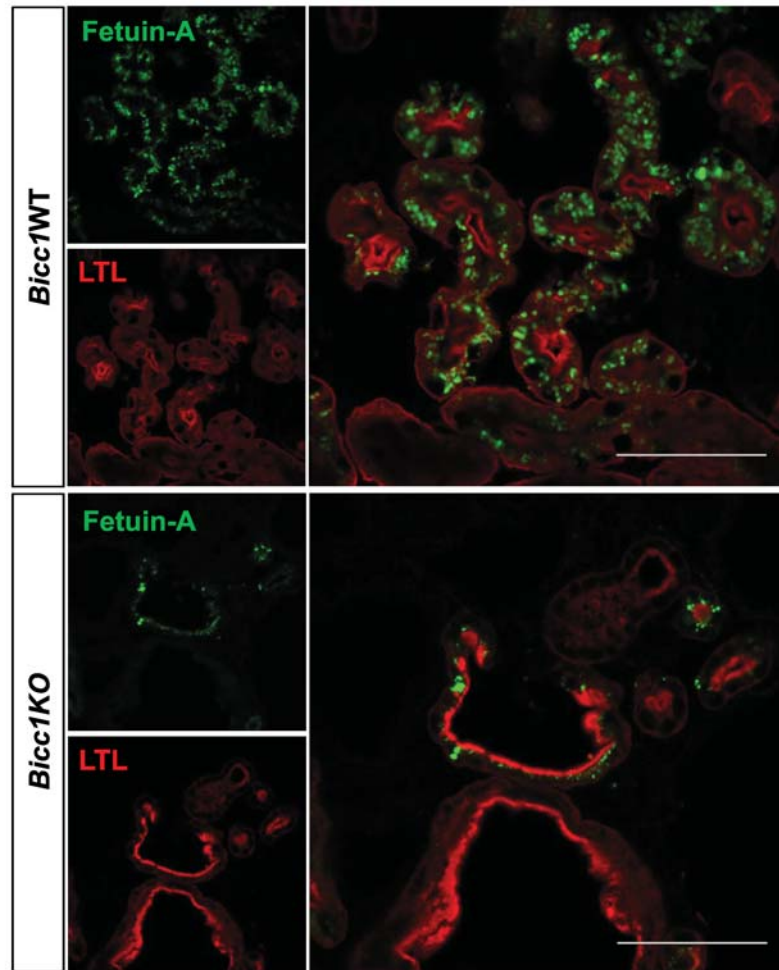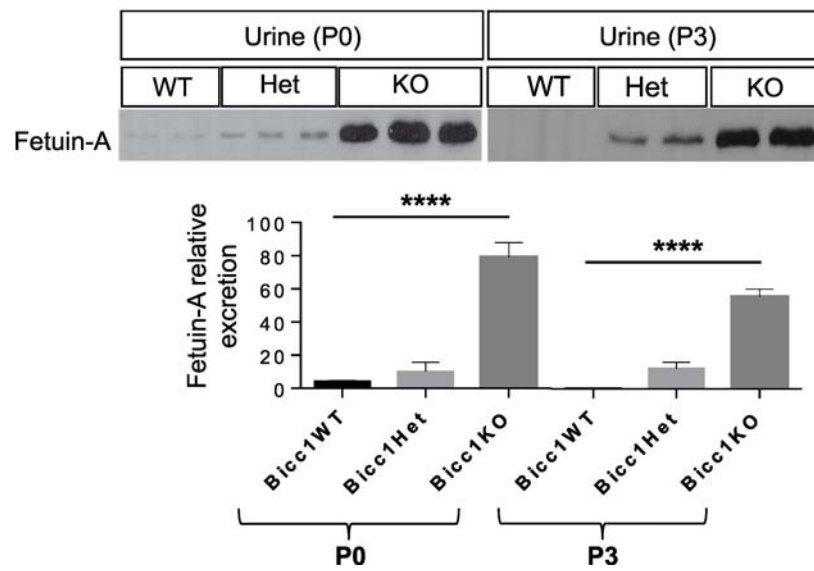
7. Harris PC, Rossetti S. Molecular diagnostics for autosomal dominant polycystic kidney disease. Nat Rev Nephrol. 2010;6:197–206.

8. Torres VE. Treatment strategies and clinical trial design in ADPKD. Adv Chronic Kidney Dis. 2010;17:190–204.

9. Chang MY, Ong AC. Autosomal dominant polycystic kidney disease: recent advances in pathogenesis and treatment. Nephron Physiol. 2008;108:p1–7.

10. Rossetti S, Chauveau D, Walker D, Saggar-Malik A, Winearls CG, Torres VE, et al. A complete mutation screen of the ADPKD genes by DHPLC. Kidney Int. 2002;61:1588–99.

11. Rossetti S, Hopp K, Sikkink RA, Sundsbak JL, Lee YK, Kubly V, et al. Identification of gene mutations in autosomal dominant polycystic kidney disease through targeted resequencing. J Am Soc Nephrol. 2012;23:915–33.

12. Grantham JJ, Chapman AB, Torres VE. Volume progression in autosomal dominant polycystic kidney disease: the major factor determining clinical outcomes. Clin J Am Soc Nephrol. 2006;1:148–57.

13. Dimitrakov D, Kumchev E, Lyutakova E, Grigorov L. Glomerular hyperfiltration and serum beta 2-microglobulin used as early markers in diagnosis of autosomal dominant polycystic kidney disease. Folia Med (Plovdiv). 1993;35:59–62.

14. Birenboim N, Donoso VS, Huseman RA, Grantham JJ. Renal excretion and cyst accumulation of beta 2microglobulin in polycystic kidney disease. Kidney Int. 1987;31:85–92.

15. Bolignano D, Coppolino G, Campo S, Aloisi C, Nicocia G, Frisina N, et al. Neutrophil gelatinase-associated lipocalin in patients with autosomal-dominant polycystic kidney disease. Am J Nephrol. 2007;27:373–8.

16. Zheng D, Wolfe M, Cowley Jr BD, Wallace DP, Yamaguchi T, Grantham JJ. Urinary excretion of monocyte chemoattractant protein-1 in autosomal dominant polycystic kidney disease. J Am Soc Nephrol. 2003;14:2588–95.

17. Azurmendi PJ, Fraga AR, Galan FM, Kotliar C, Arrizurieta EE, Valdez MG, et al. Early renal and vascular changes in ADPKD patients with low-grade albumin excretion and normal renal function. Nephrol Dial Transplant. 2009;24:2458–63.

18. Parikh CR, Dahl NK, Chapman AB, Bost JE, Edelstein CL, Comer DM, et al. Evaluation of urine biomarkers of kidney injury in polycystic kidney disease. Kidney Int. 2012;81:784–90.

19. Meijer E, Boertien WE, Nauta FL, Bakker SJ, van Oeveren W, Rook M, et al. Association of urinary biomarkers with disease severity in patients with autosomal dominant polycystic kidney disease: a cross-sectional analysis. Am J Kidney Dis. 2010;56:883–95.

20. Wilson PD. Mouse models of polycystic kidney disease. Curr Top Dev Biol. 2008;84:311–50.
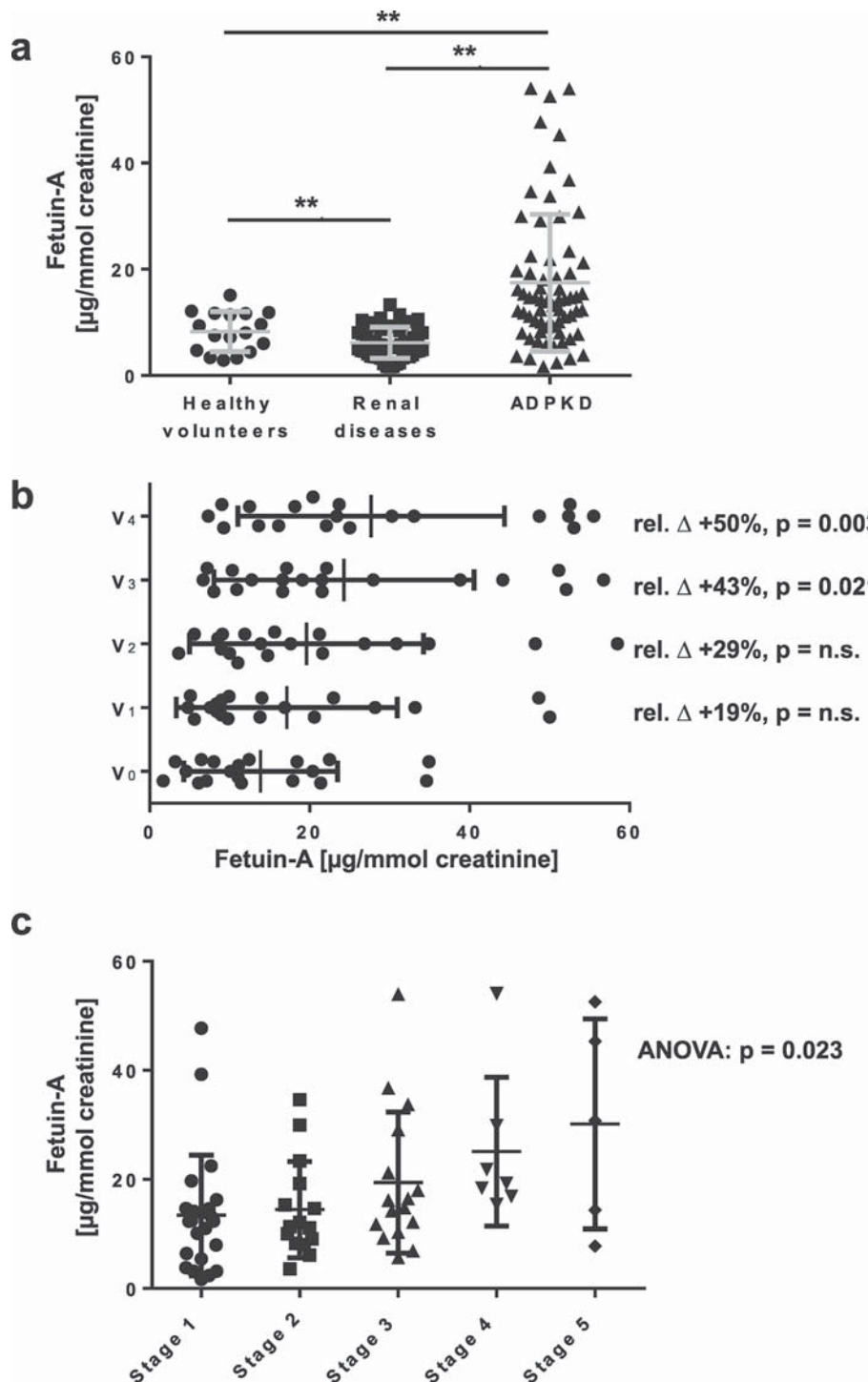
21. Rossetti S, Consugar MB, Chapman AB, Torres VE, Guay-Woodford LM, Grantham JJ, et al. Comprehensive molecular diagnostics in autosomal dominant polycystic kidney disease. J Am Soc Nephrol. 2007;18:2143–60.

22. Piontek K, Menezes LF, Garcia-Gonzalez MA, Huso DL, Germino GG. A critical developmental switch defines the kinetics of kidney cyst formation after loss of Pkd1. Nat Med. 2007;13:1490–5.

23. Leonhard WN, van der Wal A, Novalic Z, Kunnen SJ, Gansevoort RT, Breuning MH, et al. Curcumin inhibits cystogenesis by simultaneous interference of multiple signaling pathways: in vivo evidence from a Pkd1-deletion model. Am J Physiol Renal Physiol. 2011;300:F1193–202.

24. Menezes LF, Zhou F, Patterson AD, Piontek KB, Krausz KW, Gonzalez FJ, et al. Network analysis of a Pkd1-mouse model of autosomal dominant polycystic kidney disease identifies HNF4alpha as a disease modifier. PLoS Genet. 2012;8:e1003053.

25. Lantinga-van Leeuwen IS, Leonhard WN, van der Wal A, Breuning MH, de Heer E, Peters DJ. Kidney-specific inactivation of the Pkd1 gene induces rapid cyst formation in developing kidneys and a slow onset of disease in adult mice. Hum Mol Genet. 2007;16:3188–96.

26. Cogswell C, Price SJ, Hou X, Guay-Woodford LM, Flaherty L, Bryda EC. Positional cloning of jcpk/bpk locus of the mouse. Mamm Genome. 2003;14:242–9.

27. Piazzon N, Maisonneuve C, Guilleret I, Rotman S, Constam DB. Bicc1 links the regulation of cAMP signaling in polycystic kidneys to microRNA-induced gene silencing. J Mol Cell Biol. 2012;4:398–408.

28. Tran U, Zakin L, Schweickert A, Agrawal R, Doger R, Blum M, et al. The RNA-binding protein bicaudal C regulates polycystin 2 in the kidney by antagonizing miR-17 activity. Development. 2010;137:1107–16.

29. Maisonneuve C, Guilleret I, Vick P, Weber T, Andre P, Beyer T, et al. Bicaudal C, a novel regulator of Dvl signaling abutting RNA-processing bodies, controls cilia orientation and leftward flow. Development. 2009;136:3019–30.

30. Lian P, Li A, Li Y, Liu H, Liang D, Hu B, et al. Loss of Polycystin-1 Inhibits Bicc1 Expression during Mouse Development. PLoS One. 2014;9:e88816.

31. Rees S, Kittikulsuth W, Roos K, Strait KA, Van Hoek A, Kohan DE. Adenylyl cyclase 6 deficiency ameliorates polycystic kidney disease. J Am Soc Nephrol. 2013;25:232–7.

32. Mori K, Emoto M, Inaba M. Fetuin-A: a multifunctional protein. Recent Pat Endocr Metab Immune Drug Discov. 2011;5:124–46.

33. Dziegielewska KM, Mollgard K, Reynolds ML, Saunders NR. A fetuin-related glycoprotein (alpha 2HS) in human embryonic and fetal development. Cell Tissue Res. 1987;248:33–41.
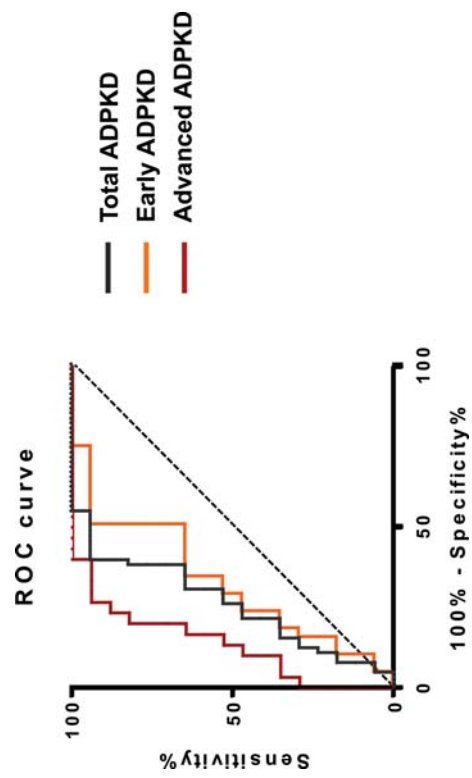
34. Denecke B, Graber S, Schafer C, Heiss A, Woltje M, Jahnen-Dechent W. Tissue distribution and activity testing suggest a similar but not identical function of fetuin-B and fetuin-A. Biochem J. 2003;376:135–45.

35. Matsui I, Hamano T, Mikami S, Inoue K, Shimomura A, Nagasawa Y, et al. Retention of fetuin-A in renal tubular lumen protects the kidney from nephrocalcinosis in rats. Am J Physiol Renal Physiol. 2013;304:F751–60.

36. Matsui I, Hamano T, Mikami S, Fujii N, Takabatake Y, Nagasawa Y, et al. Fully phosphorylated fetuin-A forms a mineral complex in the serum of rats with adenine-induced renal failure. Kidney Int. 2009;75:915–28.

37. He JC, Chuang PY, Ma'ayan A, Iyengar R. Systems biology of kidney diseases. Kidney Int. 2012;81:22–39.

38. Terada N, Ohno N, Yamakawa H, Seki G, Fujii Y, Baba T, et al. Immunoelectron microscopic localization of protein 4.1B in proximal S1 and S2 tubules of rodent kidneys. Med Electron Microsc. 2004;37:45–51.

39. Torres VE, Chapman AB, Perrone RD, Bae KT, Abebe KZ, Bost JE, et al. Analysis of baseline parameters in the HALT polycystic kidney disease trials. Kidney Int. 2012;81:577–85.

40. Grantham JJ, Torres VE, Chapman AB, Guay-Woodford LM, Bae KT, King Jr BF, et al. Volume progression in polycystic kidney disease. N Engl J Med. 2006;354:2122–30.

41. Kistler AD, Mischak H, Poster D, Dakna M, Wuthrich RP, Serra AL. Identification of a unique urinary biomarker profile in patients with autosomal dominant polycystic kidney disease. Kidney Int. 2009;76:89–96.

42. Kistler AD, Serra AL, Siwy J, Poster D, Krauer F, Torres VE, et al. Urinary proteomic biomarkers for diagnosis and risk stratification of autosomal dominant polycystic kidney disease: a multicentric study. PLoS One. 2013;8:e53016.

43. Boertien WE, Meijer E, Li J, Bost JE, Struck J, Flessner MF, et al. Relationship of copeptin, a surrogate marker for arginine vasopressin, with change in total kidney volume and GFR decline in autosomal dominant polycystic kidney disease: results from the CRISP cohort. Am J Kidney Dis. 2013;61:420–9.

44. Ben-Dov IZ, Tan YC, Morozov P, Wilson PD, Rennert H, Blumenfeld JD, et al. Urine MicroRNA as potential biomarkers of autosomal dominant polycystic kidney disease progression: description of miRNA profiles at baseline. PLoS One. 2014;9:e86856.

45. Lai X, Bacallao RL, Blazer-Yost BL, Hong D, Mason SB, Witzmann FA. Characterization of the renal cyst fluid proteome in autosomal dominant polycystic kidney disease (ADPKD) patients. Proteomics Clin Appl. 2008;2:1140–52.

46. Inoue K, Wada J, Eguchi J, Nakatsuka A, Teshigawara S, Murakami K, et al. Urinary fetuin-A is a novel marker for diabetic nephropathy in type 2 diabetes identified by lectin microarray. PLoS One. 2013;8:e77118.

47. Zhou H, Pisitkun T, Aponte A, Yuen PS, Hoffert JD, Yasuda H, et al. Exosomal Fetuin-A identified by proteomics: a novel urinary biomarker for detecting acute kidney injury. Kidney Int. 2006;70:1847–57.

48. Wu YX, Li CY, Deng YL. Patients with nephrolithiasis had lower fetuin-A protein level in urine and renal tissue. Urolithiasis. 2014;42:29–37.

49. Florkowski CM, Chew-Harris JS. Methods of estimating GFR - different equations including CKD-EPI. Clin Biochem Rev. 2011;32:75–9.
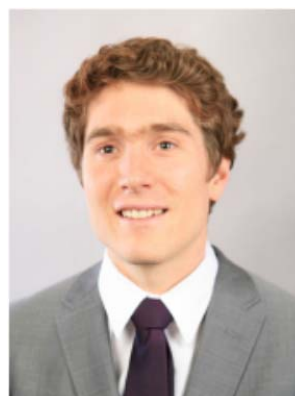
rel. Δ +50%, p = 0.003
rel. Δ +43%, p = 0.021
rel. Δ +29%, p = n.s.
rel. Δ +19%, p = n.s.

ANOVA: p = 0.023

ROC curve

Total ADPKD
Early ADPKD
Advanced ADPKD

Avenue de la Chablière 22
CH-1004 Lausanne
E-Mail: florian.bernet@alumni.ethz.ch
Date of birth: 10th of April 1982
Swiss

Curriculum Vitae

FLORIAN BERNET

EDUCATION

2010 – 2015	PhD in Molecular Biology, EPF Lausanne (CH) *Topic: Regulation of the mRNA silencing activity of Bicaudal-C*
2007 – 2009	MSc in Microbiology and Immunology, ETH Zurich (CH) Master thesis at University of Queensland (AU) *Topic: Structural and functional analysis of the Staphylococcus aureus histidine kinase YycG*
2003 – 2007	BSc in Biochemistry, ETH Zurich (CH)
2002	Matura Kantonschule Oerlikon (CH)

WORK EXPERIENCE

2008 – 2009	Scientific assistant, Group of Prof. Dr. Hardt, ETH Zurich (CH)
2007	Teaching assistant, ETH Zurich (CH) *Organization of an introductory molecular biology laboratory course for first year students*

PUBLICATIONS

Piazzon N, Bernet F, Guihard L, Wouter LN, Urfer S, Firsov D, Chehade H, Vogt B, Piergiovanni S, Peters DJ, Bonny O and Constam DB.
Urine Fetuin-A is a biomarker of Autosomal Dominant Polycystic Kidney Disease progression. Journal of Translational medicine (2015) 13:103

Stecher B, Denzler R, Maier L, Bernet F, Sanders MJ, Pickard DJ, Barthel M, Westendorf AM, Krogfelt KA, Walker AW, Ackermann M, Dobrindt U, Thomson NR, Hardt WD
Gut inflammation can boost horizontal gene transfer between pathogenic and commensal Enterobacteriaceae. Proc Natl Acad Sci U S A (2012) 109: 1269-1274.

CONFERENCE ATTENDENCE

Keystone symposia 2014, 'Cilia, Development and Human Disease'
Tahoe City, USA, February 2014, Poster presentation

Swiss RNA Workshop 2014,
Bern, CH, January 2014, Poster presentation

Life science symposium by doctoral students 2011,
Lausanne, CH, July 2011

Life science symposium 2010, 'Engineering Life'
Lausanne, CH, September 2010

LANGUAGE SKILLS

German	Mother tongue
English	Good knowledge written and spoken
French	Fair knowledge written and spoken